INFORMATION TO USERS

This dissertation was produced from a microfilm copy of the original document. While the most advanced technological means to photograph and reproduce this document have been used, the quality is heavily dependent upon the quality of the original submitted.

The following explanation of techniques is provided to help you understand markings or patterns which may appear on this reproduction.

1. The sign or "target" for pages apparently lacking from the document photographed is "Missing Page(s)". If it was possible to obtain the missing page(s) or section, they are spliced into the film along with adjacent pages. This may have necessitated cutting thru an image and duplicating adjacent pages to insure you complete continuity.

2. When an image on the film is obliterated with a large round black mark, it is an indication that the photographer suspected that the copy may have moved during exposure and thus cause a blurred image. You will find a good image of the page in the adjacent frame.

3. When a map, drawing or chart, etc., was part of the material being photographed the photographer followed a definite method in "sectioning" the material. It is customary to begin photoing at the upper left hand corner of a large sheet and to continue photoing from left to right in equal sections with a small overlap. If necessary, sectioning is continued again — beginning below the first row and continuing on until complete.

4. The majority of users indicate that the textual content is of greatest value, however, a somewhat higher quality reproduction could be made from "photographs" if essential to the understanding of the dissertation. Silver prints of "photographs" may be ordered at additional charge by writing the Order Department, giving the catalog number, title, author and specific pages you wish reproduced.

University Microfilms

300 North Zeeb Road
Ann Arbor, Michigan 48106

A Xerox Education Company

Downloaded from SHAREOK. Persistent Handle URL: https://hdl.handle.net/11244/3301

72-23,096

GARRISON, Charles Michael, 1945-
THE MECHANISM FOR THE SLOW OXIDATION OF METHANE AT ELEVATED PRESSURES.

The University of Oklahoma, Ph.D., 1972
Engineering, chemical

University Microfilms, A XEROX Company, Ann Arbor, Michigan

THIS DISSERTATION HAS BEEN MICROFILMED EXACTLY AS RECEIVED.

THE UNIVERSITY OF OKLAHOMA

GRADUATE COLLEGE

THE MECHANISM FOR THE SLOW OXIDATION OF METHANE AT ELEVATED PRESSURES

A DISSERTATION

SUBMITTED TO THE GRADUATE FACULTY

in partial fulfillment of the requirements for the

degree of

DOCTOR OF PHILOSOPHY

BY

CHARLES MICHAEL GARRISON

Norman, Oklahoma

1972

THE MECHANISM FOR THE SLOW OXIDATION OF METHANE

AT ELEVATED PRESSURES

APPROVED BY

C. M. Sliepcevich

Sherrill D. Elrington

Arthur Wm Adey

F M Townsend

Jerry L Lott

DISSERTATION COMMITTEE

PLEASE NOTE:

Some pages may have

indistinct print.

Filmed as received.

University Microfilms, A Xerox Education Company

THE MECHANISM FOR THE SLOW OXIDATION OF METHANE AT ELEVATED PRESSURES

ABSTRACT

Although the mechanism for the slow oxidation of methane at low pressures is fairly well established, much remains to be learned about the mechanism at high pressure. The purpose of this study was to clarify the high pressure mechanism.

Oxidation experiments were conducted using a nominal 10:1 methane to oxygen molar ratio feed at 2000 atmospheres pressure in the temperature range of 270° to 310°C; limited data were taken at 7000 atmospheres in the temperature range of 230° to 282°C. The experimental program had to be terminated prematurely due to a failure in the reactor.

A numerical technique was developed to simulate the oxidation reaction. The results of the simulation were compared with results obtained by compiling experimental data from previous investigations conducted at pressures from 150 to 6800 atmospheres and temperatures between 272° and 362°C. This simulation showed that reaction mechanisms proposed by previous investigators were inadequate for predicting the

formation of several of the major products in concentrations as large as those measured experimentally.

A high pressure oxidation mechanism was proposed to modify these previous mechanisms. A reaction simulation based on this high pressure mechanism gave results that were generally in agreement with experimental data.

ACKNOWLEDGMENTS

The author gratefully acknowledges the continued interest and guidance of the members of his committee, Dr. C. M. Sliepcevich, Dr. J. L. Lott, Dr. A. W. Aldag, Dr. S. D. Christian, and Dr. F. M. Townsend. Dr. S. E. Babb, Jr., also made helpful suggestions.

I wish to thank Dr. N. Tripathy who assisted with the experimental work.

I am grateful to Messrs. G. J. Scott and W. F. Porter of the Physics Shop and Messrs. F. A. Wallace, J. C. Higginbottom, and P. E. Miller of the Central Research Shop for equipment maintenance.

The efforts of Mrs. Barbara Everidge who typed the manuscript, Mr. G. L. Puckett who assisted with the drafting, and Mrs. Joyce Gerald who handled the graphical work and gave many helpful suggestions during the course of my graduate studies are greatly appreciated.

This work was sponsored by the National Science Foundation. The Phillips Petroleum Company also provided a fellowship during the early part of my studies.

I also gratefully acknowledge the support and assistance of my wife through these many years of graduate school.

TABLE OF CONTENTS

		Page
LIST OF TABLES		viii
LIST OF ILLUSTRATIONS		ix
Chapter		
I.	INTRODUCTION	1
II.	REVIEW OF PREVIOUS WORK	3
	Experimental Work	4
	Oxidation Studies at Elevated Pressures	9
	Previous Mechanisms and Kinetic Studies	11
III.	THEORY OF A RADICAL REACTION	21
	Formation of Radicals	22
	Termination of Radicals	23
	Propagation of Radicals	24
	Branching Reactions	27
IV.	EXPERIMENTAL EQUIPMENT	29
	Feed Preparation and Storage System	29
	Compression System	34
	High Pressure System	36
	Product Receiver System	44
	Auxiliaries	45
V.	EXPERIMENTAL PROCEDURE	47
	Feed Preparation and Storage	47
	Prior to Reaction	50
	During a Run	52
	Sample Collection	53
VI.	ANALYTICAL EQUIPMENT AND PROCEDURE	55
	Analytical Equipment	55
	Analytical Procedure	62
	Calibration	65

Chapter		Page
VII.	PROPOSED HIGH PRESSURE MECHANISM FOR METHANE OXIDATION	68
VIII.	METHOD OF MECHANISM ANALYSIS	79
	General	80
	Analysis	82
IX.	RESULTS AND DISCUSSION	103
	Results of Experimental Work	103
	Discussion of the Mechanism Development	123
	Discussion of the Mechanism Analysis	133
X.	CONCLUSIONS	162
NOMENCLATURE		165
BIBLIOGRAPHY		168
APPENDICES		178
A.	CALIBRATION OF MANGANIN CELL AND DYNALOG RECORDER	179
B.	CALIBRATION OF GAS CHROMATOGRAPH	181
C.	EQUATIONS FOR COMPUTER ANALYSIS	191
D.	REACTOR DESIGN	195
E.	SUMMARY OF EXPERIMENTAL DATA	220

LIST OF TABLES

Table		Page
1.	Reaction Pre-Exponential Factors	91
2.	Terms Used in Estimating Rate Constants	93
3A.	Literature Values of Rate Constant Factors . . .	96
3B.	Literature Values of Relationships Between Rate Rate Constant Terms	98
4.	Stoichiometric Oxygen Consumption to Form Reaction Products	116
5.	Density of Methane at Extreme Pressures	119
6.	Simulated versus Calculated Ignition Delay . . .	152
7.	Physical Properties of Construction Materials . .	200
8.	Summary of Data for Figures 44 and 45	214
9.	Experimental Parameters	221
10.	Total Outlet Composition, Mole Percent	222
11.	Yield as Percent of Reacted Methane	223

LIST OF ILLUSTRATIONS

Figure		Page
1.	Floor Plan of High Pressure Cell	30
2.	Flow Diagram of Feed Preparation and Storage System	31
3.	Feed Storage Vessels	32
4.	Flow Diagram of Compression System	35
5.	Flow Diagram of Reaction and Product Receiver Systems	37
6.	13,600 atm Compression Cylinder	38
7.	13,600 atm Reactor	40
8.	Internal Heater Attached to Top Cover	42
9.	Chromatographic Equipment Used for Analyses	57
10.	The Effect of Pressure and Temperature on the Region of Slow Oxidation for a Nominal 10:1 Methane-Oxygen Mixture	99
11.	The Effect of Pressure on the Observed Formaldehyde Concentration	107
12.	The Effect of Pressure on the Observed Methanol Concentration	108
13.	The Effect of Pressure on the Observed Formic Acid Concentration	109
14.	The Effect of Pressure on the Observed Carbon Monoxide Concentration	110
15.	The Effect of Pressure on the Observed Carbon Dioxide Concentration	111

Figure Page

16. The Effect of Pressure and Temperature on the Methane Percent Conversion at Ten Minute Residence Time for a Nominal 10:1 Methane-Oxygen Feed Mixture 117

17. The Comparison Between Observed and Simulated Liquid Concentrations at 375 atm and 326°C . . 134

18. The Comparison Between Observed and Simulated Gaseous Concentrations at 375 atm and 326°C . 135

19. The Comparison Between Observed and Simulated Liquid Concentrations at 475 atm and 320°C . . 136

20. The Comparison Between Observed and Simulated Gaseous Concentrations at 475 atm and 320°C . 137

21. The Comparison Between Observed and Simulated Liquid Concentrations at 680 atm and 306°C . . 138

22. The Comparison Between Observed and Simulated Gaseous Concentrations at 680 atm and 306°C . 139

23. The Comparison Between Observed and Simulated Liquid Concentrations at 1020 atm and 304°C . 140

24. The Comparison Between Observed and Simulated Gaseous Concentrations at 1020 atm and 304°C . 141

25. The Comparison Between Observed and Simulated Liquid Concentrations at 3400 atm and 290°C . 142

26. The Comparison Between Observed and Simulated Gaseous Concentrations at 3400 atm and 290°C . 143

27. The Effect of Residence Time on the Simulated Radical Concentrations at 375 atm and 326°C . 149

28. The Comparison of the Concentration of Methanol and Water as Observed Experimentally with the Predictions of Two Simulation Runs at 375 atm and 326°C 156

29. A Comparison of Gaseous Products from Two Simulated Runs at 375 atm and 326°C 159

30. A Comparison of Liquid Products from Two Simulated Runs at 375 atm and 326°C 160

Figure		Page
31.	Manganin Cell and Foxboro Recorder Calibration .	180
32.	Chromatographic Calibration Curve for Methanol .	182
33.	Chromatographic Calibration Curve for Formaldehyde	183
34.	Chromatographic Calibration Curve for Ethanol .	184
35.	Chromatographic Calibration Curve for Acetone .	185
36.	Chromatographic Calibration Curve for Formic Acid	186
37.	Chromatographic Calibration Curve for Oxygen . .	187
38.	Chromatographic Calibration Curve for Nitrogen .	188
39.	Chromatographic Calibration Curve for Carbon Monoxide	189
40.	Chromatographic Calibration Curve for Carbon Dioxide	190
41.	The Sideport Opening with Double Cone	196
42.	Details of 200,000 psi Reactor	198
43.	The Sideport Opening with the New Inner Liner .	201
44.	The Shear Stress Distribution in the Completed Vessel	215
45.	The Reduced Shear Stress Distribution in the Completed Vessel	216
46.	The Tangential Stress Distribution in the Completed Vessel	217
47.	The Reduced Tangential Stress Distribution in the Completed Vessel	218

CHAPTER I

INTRODUCTION

Hydrocarbons are one of the largest sources of power and organic raw materials presently known. One particularly important member of this class of compounds is methane, the chief constituent of natural gas. However, despite its common use as a fuel and starting material for petrochemical synthesis, much still remains to be learned about the relatively common reactions involving methane, even oxidation, which constitutes the basis for this study. In this dissertation the term oxidation shall refer to the process of slow oxidation as contrasted to combustion or rapid oxidation.

The process of methane oxidation has been actively studied since the 1890's. As early as the 1930's, it was shown that elevated pressures affected the reaction rate and the reaction products, but relatively little explanation was advanced. However, these early studies at elevated pressure did show that previously postulated reaction mechanisms were unsatisfactory.

Most of the experimental work at elevated pressure prior to 1960 was limited to less than a few hundred

atmospheres. Since then studies at the University of Oklahoma have reached 13,600 atmospheres.

The effects of temperature, residence time, and reaction surface have been studied primarily at pressures below 1000 atmospheres and to a much lesser extent to 6800 atmospheres. Since only a few experimental data points were available at pressures above 6800 atmospheres, it was originally contemplated that this study would concentrate on the pressure range of 6800 to 13,600 atmospheres. However, early in this study it became evident that equipment problems would limit the pressure to a few thousand atmospheres. For this reason, it was decided to concentrate on pressures up to 2000 atmospheres (although some measurements were made up to 7000 atmospheres). Temperatures were varied between 230°C and 310°C at residence times of zero to sixty minutes. The initial charge composition was maintained essentially constant at 8.2 mole percent oxygen and 91.8 mole percent methane.

The results from this and previous studies were combined to develop a reaction mechanism for the slow oxidation. The ability of the mechanism to predict observed behavior was tested using a numerical technique for the simulation developed in this study.

CHAPTER II

REVIEW OF PREVIOUS WORK

At temperatures above 600°C the oxidation of methane takes place virtually instantaneously in flames. At temperatures between about 200° and 600°C, slow oxidation occurs. This study is limited to the slow oxidation of methane.

Up until the end of the nineteenth century, the investigation of hydrocarbon oxidation had been limited to the study of flames. According to Shtern (85), it was generally thought that the fuel molecule decomposed to carbon and hydrogen, which then reacted with oxygen. His monograph is an excellent survey of the field of gas phase hydrocarbon oxidation. Shtern divided the studies into three general time periods. The first, from the end of the 1890's to the end of the 1920's, consisted mainly of experimental studies to determine intermediates and products, with reaction mechanisms characterized as non-chain theories. From the end of the 1920's to the middle of the 1930's, work was concentrated on explaining the mechanism of gas phase hydrocarbon oxidation in terms of the chain theory. The third period, from the mid-thirties until the early sixties, was characterized by studies to determine the exact mechanism.

Experimental Work

After Bone (16, 57) had reestablished Dalton's finding (26) that hydrocarbons oxidized explosively in a limited amount of oxygen to produce carbon monoxide and hydrogen, he started his analysis of the slow oxidation of hydrocarbons. Bone and Wheeler (18) showed that the fastest reacting mixture for methane oxidation contained two moles of methane for every mole of oxygen instead of an equimolar mixture. In all of their experiments, they found neither free hydrogen nor carbon, although both of these had been found in explosive studies.

Several factors were found that affected the reaction rate. Fort and Hinshelwood (33) noted a marked induction period for methane oxidation during which no appreciable reaction took place. Bone (15, 17) found that introducing small concentrations of "foreign vapours," such as water, formaldehyde, methanol and nitrogen dioxide, eliminated the reaction induction period. Newitt and Haffner (67) used reaction mixtures of

$$2\ CH_4 + O_2 + 6.5\ x$$

where x = carbon dioxide, water, or nitrogen, at fifty atmospheres pressure and found that the diluents slowed the reaction rate so much that it was necessary to increase the reaction temperature by 20°C to obtain reaction times similar to the undiluted mixture.

Many investigations have been made on the effect of the surface exposed to the reaction. Norrish and Foord (70) found that allowing air into the reaction vessel slowed the rate while Hoare (48) showed that the rate decreased with the age of the vessel. Norrish and Reagh (71) found that the reaction rate could be slowed and finally stopped by decreasing the diameter of the reaction vessel. Several observers (33, 48, 70) noted that packing the reaction vessel decreased the rate of reaction while others (17, 42, 48) noted that glass or silica surfaces often caused nonreproducible results, possibly through devitrification of the surface.

Although Fort and Hinshelwood (33) showed the existence of an induction period in methane oxidation, little was known about it. It was generally assumed that during the induction period an active intermediate was being formed which was necessary to carry on the oxidation process, but the identity of the intermediate was unknown. Shtern (84) showed that the intermediate products formed were stable by interrupting a reaction and then restarting it. He interrupted the reaction by dumping the mixture into a vessel containing mercury; he then restarted it by transferring the mixture to another reaction vessel and heating. Even after the mixture had remained in a cold mercury vessel for as long as twenty hours, the reaction was restarted with a maximum induction period of about 16 percent of normal.

Bone and his school (15, 17) postulated that the first product was methanol, which was rapidly converted to formaldehyde. The methanol conversion theory was given strength by Bone and Gardner's finding (17) that methanol is oxidized faster than methane. Methanol, however, was not found in the reaction products until 1932 when Newitt and Haffner (67) reported finding it in oxidation experiments run at 50 to 150 atmospheres pressure.

Following Newitt and Haffner's discovery (67) of methanol at elevated pressure, other investigators reported finding it, such as Newitt and Szego (68) and Newitt and Gardner (66). Newitt and Gardner reported finding equal amounts of methanol and formaldehyde during the induction period of atmospheric reactions. Newitt and Szego reported that increasing the contact time decreased both formaldehyde and methanol concentrations in elevated pressure reactions. However, contrary to Bone's theory, Shtern (74, 86) found that less than 5 percent of the formaldehyde formed in the reaction came from methanol.

Much evidence was amassed to indicate that formaldehyde was the intermediate responsible for the postulated branching reaction. It was shown (33, 67) that the formaldehyde concentration normally reached a maximum about the end of the induction period. Norrish (69) used 3500-3800 A light to photo-initiate the reaction in an attempt to prove that

formaldehyde was the branching agent. He stated that formaldehyde was responsible for branching since peroxides could not adsorb light of that wavelength. Norrish also showed that addition of formaldehyde in a greater amount than found in the reaction caused the reaction to start immediately and to proceed at a faster rate than normal. In this case, however, the formaldehyde concentration and the reaction rate rapidly dropped to normal values.

A school of thought opposing Bone's theory of the aldehyde intermediate was Bach's peroxide theory (5), which postulated that an aklyl hydroperoxide, ROOH, was the first intermediate of the reaction. The studies of Bone (15, 17) and Newitt (66, 67, 68) discounted this theory because they did not find peroxides. However, Minkoff (64) reported finding hydrogen peroxide during atmospheric pressure studies. Minkoff did not find any aklyl hydroperoxide, but he suspected its presence early in the reaction due to an immediate pressure drop. Karmilova (54) reported finding equal concentrations of formaldehyde and hydrogen peroxide, with both reaching a maximum at the same time. Fok (32) and Fisher (31) reported finding methyl hydroperoxide at temperatures below 100°C in photoinitiated reactions. Fisher found that adding large amounts of formaldehyde dropped both methyl hydroperoxide and hydrogen peroxide concentrations below detection limits.

Another possible branching intermediate was a peroxy acid, particularly peroxyformic acid for methane oxidation.

Bone and Gardner (17) found relatively large amounts of peroxyformic acid when they reacted 2:1 and 1:1 formaldehyde-oxygen mixtures. Similar results were found by Harding and Norrish (41). Enikolopyan (28) found peroxyacetic acid in the oxidation of acetaldehyde.

There seemed to be general agreement (2, 14, 49) that all of the carbon monoxide was produced from formaldehyde, but there were conflicting opinions on the formation of carbon dioxide. Studies by Karmilova (55) and by Hoare and Milne (49) showed that carbon dioxide was formed only from carbon monoxide while, on the other hand, Bone and Wheeler (18) and Lukovnikov and Neiman (62) found that carbon dioxide must come from other sources. Lukovnikov postulated that carbon dioxide is formed from decomposing radicals. Data from several studies, particularly those of Newitt and Haffner (67), Lott (60), Hardwicke (42), and Bauerle (9), have shown that the carbon monoxide to carbon dioxide ratio decreases with both increasing pressure and increasing residence time. Lott also found that the ratio increases with increasing temperature.

Several minor products have been reported in the oxidation reactions, particularly in the high pressure reactions. Among these products are formic acid, methyl formate, ethanol, acetic acid, and acetone.

Most hydrocarbons when oxidized exhibit an unusual phenomenon called a cool flame. A cool flame is seen as a bluish glow that may traverse a reaction mixture several times

and is characterized by a sudden pressure pulse and a temperature rise of about 100°C, rather than the 1000°C rise found in true ignition (24). Methane was not thought to exhibit this phenomenon until one was observed by Vanpee (93), and later by Lott (60). Several theories have been proposed to explain the occurance of cool flames, but none of these have been widely accepted.

The phenomenon of a negative temperature coefficient is also observed in the oxidation of most hydrocarbons. This negative temperature coefficient refers to a temperature range in which the reaction rate decreases with increasing temperature. Ridge (80) suggested that the negative temperature coefficient region is situated in the transition zone between a high temperature and a low temperature mechanism. He states that the reduction in rate is due to the thermal destruction of the intermediates of the low temperature mechanism. Then, as the temperature is raised further, the high temperature mechanism becomes controlling.

Oxidation Studies at Elevated Pressures

Only a limited number of investigations have been carried out to study the slow oxidation of methane at elevated pressures. The work that has been done can be divided according to whether the overall objectives were economic or theoretical.

Economically oriented investigations were conducted by Paris (73), Wiezevich (99), Boomer (19, 20, 21), and Furman (35, 36). Their objective was to develop the most profitable process for oxidizing methane into marketable products. Paris found that the optimum conversion to methanol and formaldehyde was obtained with a low conversion per pass and a high recycle. Wiezevich found that methanol yield increased with pressure to 135 atm while overall conversion fell with increasing pressure. Boomer found that the concentration of useful products--methanol, formaldehyde, and formic acid--increased with increasing oxygen concentration to a maximum at 6 percent oxygen, and then decreased linearly with increasing oxygen. Boomer also studied the catalytic activity of silver, copper and glass surfaces.

The theoretical studies, made by Townsend and Chamberlain (89), Newitt and Haffner (67), Newitt and Szego (68), Lott (60), Hardwicke (42), and Bauerle (9), were done primarily to define the reaction mechanism and reaction kinetics. Townsend studied the spontaneous ignition temperature of methane and found that the ignition temperature decreased with both increasing pressure and increasing methane concentration. Townsend also found that ignition occurred at a temperature 20° to 30°C lower if a silica surface, rather than a steel surface, was used. Newitt studied the effect of pressure, temperature, residence time, and diluents on the reaction

products at pressures to 150 atm. Lott studied the effect of temperature and residence time at pressures to 13,600 atm. Hardwicke similarly studied the reaction using two different reaction surfaces at pressures to 6800 atm. Bauerle studied the effect of the surface to volume ratio of different catalysts on the ignition delay of the reaction at pressures to 680 atm.

Previous Mechanisms and Kinetics Studies

The papers published from the 1890's to the early 1930's on the mechanism of hydrocarbon oxidation were mainly non-chain theories. The hydroxylation theory of Bone and his school (15, 17, 67, 68) is probably the best example. This theory stated that the hydrocarbon was slowly hydroxylated by introduction of oxygen between a hydrogen atom and the carbon skeleton of the molecule. For methane the mechanism was

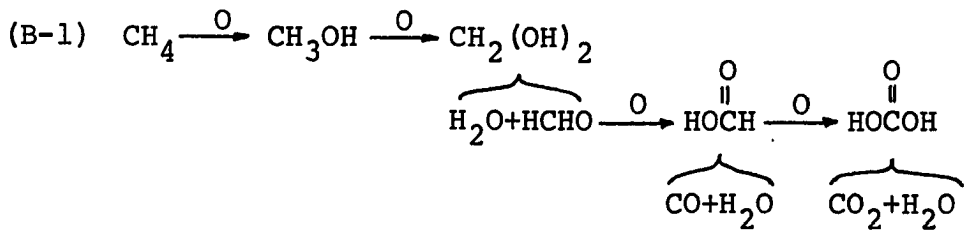

Bone recognized many problems arising from his theory, particularly that methanol had never been found as a reaction product. The discovery by Newitt and Haffner (67) of methanol in their

*In this text, mechanism steps will be identified by a letter prefix denoting the author and a step number.

elevated pressure studies in 1932 revived interest in the hydroxylation theory.

Several other non-chain theories were postulated in this time period. In a work that was forgotten until the 1920's, Bach (5) put forth a peroxidation scheme with the basic structure

(Ba-1) $CH_4 + O_2 \rightarrow CH_3OOH$

(Ba-2) $2\ CH_3OOH \rightarrow 2\ HCHO + 2\ H_2O$

Lewis (58) thought that higher hydrocarbons could be dehydrogenated to olefins, with the olefins being oxidized. Pope, Dykstra, and Edgar (76) postulated a degradative aldehyde scheme in which a higher aldehyde forms a lower aldehyde, carbon monoxide, and water, as in

(P-1) $C_8H_{18} + O_2 \rightarrow C_7H_{15}CHO + H_2O$

(P-2) $C_7H_{15}CHO + O_2 \rightarrow C_6H_{13}CHO + CO + H_2O$

$\vdots$

(P-3) $CH_3CHO + O_2 \rightarrow HCHO + CO + H_2O$

Each of these postulated mechanisms, however, was at variance with at least some aspect of known behavior (85).

In the late 1920's the idea of a radical-propagated branching chain reaction was developed and later proved. Semenov (82) suggested in his original mechanism that the following steps took place:

(NS-1) $:O + CH_4 \rightarrow :CH_2 + H_2O$

(NS-2) $:CH_2 + O_2 \rightarrow HCHO + :O$

(NS-3) $HCHO + O_2 \rightarrow H_2O + CO_2$

(NS-4) $2\ HCHO + O_2 \rightarrow 2\ H_2O + 2\ CO$

(NS-5) $HCHO + O_2 \rightarrow :O + HCOOH \rightarrow H_2O + CO$

(NS-6) $:O \xrightarrow{wall} 1/2\ O_2$

Norrish (70, 72) developed a slightly different mechanism.

(N-1) $CH_4 + O_2 \rightarrow HCHO + H_2O$

(N-2) $HCHO + O_2 \rightarrow :O + HCOOH \rightarrow H_2O + CO$

(N-3) $:O + CH_4 \rightarrow :CH_2 + H_2O$

(N-4) $:CH_2 + O_2 \rightarrow HCHO + :O$

(N-5) $HCHO \xrightarrow{oxidation} CO + H_2O$

(N-6) $HCHO + :O \rightarrow X (\rightarrow CO + H_2O)$

(N-7) $:O \xrightarrow{wall} 1/2\ O_2$

(N-8) $:O + CH_4 + M \rightarrow CH_3OH + M$

Both Semenov and Norrish considered the :O and $:CH_2$ diradicals to be the active centers.

Norrish and Foord (70) used the idea of a quasi-stationary state to develop an expression describing the reaction. The theory of the quasi-stationary state assumes that the radical concentrations are constant since the rate of change of the radical concentration is much smaller than the rate of change of the molecule concentrations. Norrish and

Foord calculated that the reaction rate for methane consumption should be

$$\frac{-d[CH_4]}{dt} = \frac{k_2 k_3^{\,2} [CH_4]^2 [O_2] Pd}{k_6 (k_7 S + k_8 [CH_4]^2 P^2 d)} \qquad (2\text{-}1)$$

where the k's are the rate constants for the reactions in Norrish's mechanism, where the brackets denote molecule concentration, and where d, S, and P are respectively the vessel diameter, the surface area, and the total pressure.

Semenov (83) later discounted the possibility of diradicals being the main reaction carrier. He stated that excessive amounts of energy would be necessary to form diradicals and that they would be too easily destroyed while monoradicals, on the other hand, would perpetuate themselves. Cvetanovic (25) showed that reacting ethylene with atomic oxygen did not yield formaldehyde even though formaldehyde was formed when ethylene reacted with molecular oxygen. This observation meant that the radical chain probably proceeded without oxygen atoms.

On the basis of all information then available, Semenov (83) proposed the following mechanism in 1958:

(S-0) $CH_4 + O_2 \rightarrow CH_3\cdot + HO_2\cdot$

(S-1) $CH_3\cdot + O_2 \rightarrow HCHO + \cdot OH$

(S-2) $\cdot OH + CH_4 \rightarrow CH_3\cdot + H_2O$

(S-2') $\cdot OH + HCHO \rightarrow HCO\cdot + H_2O$

(S-3) $HCHO + O_2 \rightarrow HCO\cdot + HO_2\cdot$

(S-4) $HCO\cdot + O_2 \rightarrow HO_2\cdot + CO$

(S-5) $HO_2\cdot + CH_4 \rightarrow CH_3\cdot + H_2O_2$

(S-5') $HO_2\cdot + HCHO \rightarrow HCO\cdot + H_2O_2$

(S-6) $\cdot OH \xrightarrow{wall}$ chain breaking

(S-7) $HO_2\cdot \xrightarrow{wall}$ chain breaking

(S-8) $HCHO \xrightarrow{wall}$ chain breaking

Semenov used the quasi-stationary state idea to develop the following rate equation from his mechanism

$$\frac{-d[CH_4]}{dt} = \frac{2k_2k_3}{k_6}\left(\frac{k_2\ k_5}{k_2'\ k_5'}\right)^{1/2}[CH_4]^2[O_2] \qquad (2\text{-}2)$$

which was similar in form to Norrish's result in Equation 2-1. At the same time, Enikolopyan (29) found experimentally that the maximum rate of methane consumption was

$$\left(\frac{-d[CH_4]}{dt}\right)_{max} = k[CH_4]^{1.62}[O_2]^{0.96} \qquad (2\text{-}3)$$

which approximated both Semenov's and Norrish's results.

Semenov's mechanism (83) contained a major feature different from the previous mechanisms. Reaction S-3 was a degenerate branching reaction in which two molecules reacted to form radicals. Semenov stated that this type of endothermic reaction explained the slow increase in reaction rate as the reaction proceeded. He justified step S-0 as the initiation

reaction since it required less energy than an initiation reaction based on molecular decomposition.

Enikolopyan (30) wrote a generalized mechanism for the oxidation of hydrocarbon RH; he then used the quasi-stationary state theory to derive the overall rate equations from the mechanism. He postulated that in different temperature ranges certain reactions could be ignored. In this way, he calculated that the rate would be independent of oxygen concentration in low temperature liquid-phase reaction. He also concluded that the rate should be second order with respect to oxygen in gas phase reactions above 500°C, with transitions in the rate equation in the intermediate temperature ranges between these two extremes. This calculation fitted some of the experimental data then available.

Hoare and Milne (49) added several steps to Semenov's second mechanism (83) to explain formation of carbon dioxide and destruction of hydrogen peroxide. The steps that were not included in Semenov's mechanism are:

(HM-1) $CO + \cdot OH \rightarrow CO_2 + H\cdot$

(HM-2) $CO + HO_2\cdot \rightarrow CO_2 + \cdot OH$

(HM-3) $HCHO + \_\_ \xrightarrow{\text{wall}} CO_2 + \_\_$

(HM-4) $H\cdot + O_2 + M \rightarrow HO_2\cdot + M$

(HM-5) $H_2O_2 + M \rightarrow 2\ \cdot OH + M$

(HM-6) $\cdot OH + H_2O_2 \rightarrow H_2O + HO_2\cdot$

Hoare and Milne concluded that over 80 percent of the carbon dioxide formed comes from step HM-2. They also stated that both formaldehyde and hydrogen peroxide must be considered as intermediates since hydrogen peroxide must be present to regenerate the formaldehyde. This statement would explain the fact that while addition of formaldehyde eliminated the induction period for the reaction, the addition of hydrogen peroxide only shortened it (49).

The possibility of alkyl hydroperoxides ROOH playing an important part in oxidation reactions has also been studied. Blundell (14) found that the reaction

(R-1)* $CH_3^{\cdot} + O_2 \rightarrow CH_3OO^{\cdot}$

does occur and is a two body reaction. Fisher and Tipper (31) suggested the following reaction mechanism based on methyl hydroperoxide

(FT-1) $^{\cdot}OH(HO_2^{\cdot}) + CH_4 \rightarrow CH_3^{\cdot} + H_2O\ (H_2O_2)$

(FT-2) $CH_3^{\cdot} + O_2 + M \rightarrow CH_3O_2^{\cdot} + M$

(FT-3) $CH_3O_2^{\cdot} \rightarrow HCHO + {}^{\cdot}OH$

(FT-4) $CH_3O_2^{\cdot} + HCHO \rightarrow CH_3OOH + HCO^{\cdot}$ (in latter stage of reaction)

(FT-5) $^{\cdot}OH(HO_2^{\cdot}) + HCHO \rightarrow HCO^{\cdot} + H_2O(H_2O_2)$

(FT-6) $HCHO + O_2 \rightarrow HCO^{\cdot} + HO_2^{\cdot}$

(FT-7) $HCO^{\cdot} + O_2 \rightarrow HO_2^{\cdot} + CO$

---

*In this text, general reaction steps will be identified by the prefix R followed by the reaction number, with the numbers continuing through the text.

(FT-8) $H_2O_2 \xrightarrow{wall} H_2O + 1/2\ O_2$

(FT-9) $CH_3OOH \xrightarrow{wall} HCHO + H_2O$ or $CH_3OH + 1/2\ O_2$

(FT-10) $H_2O_2 + M \rightarrow 2\ \cdot OH + M$

(FT-11) $CH_3OOH \rightarrow CH_3O\cdot + \cdot OH$

(FT-12) $CH_3O\cdot + HCHO \rightarrow CH_3OH + HCO\cdot$

(FT-13) $CH_3O\cdot + O_2 \rightarrow HCHO + HO_2\cdot$

Fisher and Tipper also discussed another possible reaction that they neglected

(FT-14) $CH_3OO\cdot + CH_4 \rightarrow CH_3OOH + CH_3\cdot$

They stated that the difference in activation energies for FT-3 and FT-14 is 8.5 kcal/mole. However, they neglected reaction FT-14 in favor of FT-4, as a source for methyl hydroperoxide, and (indirectly) for methanol since most of the methanol is formed only after HCHO is in the system. Fisher also stated that reactions FT-12 and FT-13 are in strong competition for the $CH_3O\cdot$ radical.

Hardwicke, Lott, and Sliepcevich (43) developed the following reaction mechanism based on the high pressure oxidation reaction:

(HLS-0) $CH_4 + O_2 \rightarrow CH_3\cdot + HO_2\cdot$

(HLS-1) $CH_3\cdot + O_2 \rightarrow CH_3OO\cdot$

(HLS-2) $CH_3OO\cdot \rightarrow HCHO + \cdot OH$

(HLS-3) $CH_3OO\cdot + CH_4 \rightarrow CH_3OOH + CH_3\cdot$

(HLS-4) $CH_3OOH \rightarrow CH_3O\cdot + \cdot OH$

(HLS-5) $CH_3O\cdot + CH_4 \rightarrow CH_3OH + CH_3\cdot$

(HLS-6) $CH_4 + \cdot OH \rightarrow CH_3\cdot + H_2O$

(HLS-7) $CH_4 + HO_2\cdot \rightarrow CH_3\cdot + H_2O_2$

(HLS-8) $HCHO + \cdot OH \rightarrow HCO\cdot + H_2O$

(HLS-9) $HCHO + HO_2\cdot \rightarrow HCO\cdot + H_2O_2$

(HLS-10) $HCHO + O_2 \rightarrow CO_2 + H_2O$

(HLS-11) $HCO\cdot + O_2 \rightarrow CO + HO_2\cdot$

(HLS-12) $CO + HO_2\cdot \rightarrow CO_2 + \cdot OH$

(HLS-13) $2\ H_2O_2 \rightarrow 2\ H_2O + O_2$

(HLS-14) $CH_3\cdot + \cdot OH \rightarrow CH_3OH$

(HLS-15) $HCO\cdot + \cdot OH \rightarrow HCOOH$

(HLS-16) $HCO\cdot + CH_3O\cdot \rightarrow HCOOCH_3$

(HLS-17) $CH_3OO\cdot \rightarrow$ termination

(HLS-18) $CH_3\cdot \rightarrow$ termination

(HLS-19) $HO_2\cdot \rightarrow$ termination

(HLS-20) $\cdot OH \rightarrow$ termination

(HLS-21) $HCO\cdot \rightarrow$ termination

Even after the mechanism of slow oxidation is specified, an accurate overall kinetic expression will be needed before the process can be used commercially. Widely varying results, however, have been reported for the kinetics of the overall reaction of methane oxidation. Much of the variation can be attributed to different temperature ranges, pressure

ranges, reactant concentrations, and reaction surfaces. Results of many studies previous to 1969 were tabulated by Bauerle (9). Most values found for the overall activation energy range between 40 and 60 kcal/mole. Most studies have found that the reaction rate is approximately second order with respect to methane. Less agreement is found in the reported values of the order with respect to oxygen, with most values falling between 0.5 and 2.5. An unusual case was reported by Hardwicke (44) for extreme pressures, with the rate equation for oxygen consumption in the methane-rich reaction being

$$\frac{-d[O_2]}{dt} = k\ [O_2]^{-2}\ P^{2.34}$$

with an activation energy of 42.9 kcal/mole. The negative order for oxygen was due to the autocatalytic behavior of the reaction. The reason for the difference between Hardwicke's negative order with respect to oxygen and the previously reported positive values is that Hardwicke correlated his data over the entire time period of the reaction while the earlier investigators reported a value based on the slope of the oxygen curve at the point of maximum consumption.

CHAPTER III

THEORY OF A RADICAL REACTION

A chemical bond consisting of a pair of electrons can be broken in one of two ways.

(R-2a) $A - B \rightarrow A\cdot + B\cdot$

(R-2b) $A - B \rightarrow A^{+} + B:^{-}$

In the first case, the bond is broken symmetrically, resulting in two uncharged fragments, each having a single unpaired electron. In the second case, the bond is broken unsymmetrically, leaving two oppositely charged fragments: one being deficient an electron, the other having an extra electron. The fragments in the latter case are ions; the fragments in the former case are radicals, which are also called free radicals. As the gas phase oxidation of methane is a free radical process, only the chemistry of free radicals will be discussed.

The average lifetime for a radical is very short, usually much less than one second. Also, the concentration of radicals in a reaction is usually quite small, often on the order of 10^{-8} moles per liter or less (77). Then for a radical to have an appreciable effect, it must be very reactive.

High reactivity is one of the main characteristics of free radicals.

The following discussion of free radical chemistry is only a brief survey of the field. For more detailed information on the subject of free radical chemistry, the reader is directed to any of a number of texts, particularly those of Pryor (77), Trotman-Dickenson (90), Steacie (88) and Walling (96).

Free radicals have three principal classes of reactions: formation or initiation, termination, and propagation. A fourth type, branching, is similar to some types of initiation and propagation steps, but it will be considered separately. The following sections discuss the characteristics of these reactions.

Formation of Radicals

Although a radical reaction usually requires a low concentration of radicals, some method of producing even this low concentration is necessary. The three main techniques for producing radicals are irradiation, thermal homolysis, and oxidation-reduction reactions.

Irradiation techniques can use either electromagnetic radiation, including visible light, ultraviolet, etc., or corpuscular radiation of high energy electrons, neutrons, etc. Electromagnetic radiation, however, is the more common. As an example, methyl radicals are often generated by a photo-induced decomposition of acetone.

A similar method for generating radicals is thermal homolysis. It requires a temperature of 350° to 550°C to break a carbon-carbon sigma bond, which has a bond energy of about 90 kcal per mole. Likewise, a peroxidic oxygen-oxygen bond requires an operating temperature of 50° to 150°C to break the 25-35 kcal per mole bond (77).

A third method for generating radicals is oxidation-reduction reactions. Reactions of this type are especially important where low temperatures are needed, on the order of 0° to 50°C.

Termination of Radicals

Similar to radical formation, in which radicals are formed in pairs, radicals are also destroyed in pairs. These unpaired electrons eventually become part of a chemical bond in a stable product. There are two major methods of radical destruction, combination and disproportionation.

In a radical combination, two radicals of any type combine to form a single molecule in the reaction

(R-3) $$R\cdot + S\cdot \rightarrow R\text{-}S^{*} \rightarrow R\text{-}S$$

where R-S* is an activated transition state and R-S is the stable molecule. Bond making is an exothermic reaction, so the activated specie usually must collide with a third body to lose its excess energy. If such a collision does not occur rapidly, the activated complex will decompose, although the

radicals formed do not necessarily have to be the same R· and S· radicals. A third body is not needed if the molecule is large enough so that it can distribute the activation energy among its vibrational modes and form a stable product (45).

Disproportionation is different from combination in that the two radicals collide and form two stable products, one of them often an olefin. An example of this reaction is

$$\text{(R-4)} \qquad R^{\cdot} + R_2\overset{H}{C}-CR_2^{\cdot} \rightarrow RH + R_2C{=}CR_2$$

In disproportionation, when a hydrogen atom is abstracted, it is usually removed from a position β to the radical center as shown above (77).

Propagation of Radicals

With the exception of termination reactions, one of the chief characteristics of radical reactions is that usually a radical is formed for every radical that is destroyed. This process is referred to as radical propagation. Propagation can take one of three main forms: radical transfer, radical isomerization, or radical decomposition.

Radical Transfer

A transfer reaction is a reaction in which the reactive center moves, usually by abstracting an atom or functional group from a molecule. Probably the most common radical transfer reaction is hydrogen transfer, of the type

(R-5) $R\cdot + SH \rightarrow [R\text{--}H\text{--}S] \rightarrow RH + S\cdot$

Since the breaking of the SH bond requires a large amount of energy, some amount of bond making between R and H undoubtedly has taken place in the transition state. This bond making is part of the driving force for the reaction. The fact that the S-H bond is highly stretched in the transition state has been shown by primary isotope effects using deuterium in place of the hydrogen atom (77).

Hydrogen atoms can be abstracted by radicals from any hydrogen donor in the system. A tertiary hydrogen is easier to remove than a secondary, and both are easier to remove than primary hydrogen. Due to the many variables in reacting systems, the only transfer reaction whose reaction rate has been measured directly is the hydrogen reaction (90)

(R-6) $H\cdot + H_2 \rightarrow H_2 + H\cdot$

where the hydrogens can be deuterium, tritium, and ortho or para hydrogen.

A specific type of reaction in the category of transfer reactions is radical addition. Radical addition refers to a reaction in which a radical attacks a double bond, such as in an olefin or a carbonyl, to form a larger radical. An example of this type of reaction is a radical polymerization chain

(R-7) $B\cdot + C{=}C \rightarrow B\text{-}C\text{-}C\cdot \xrightarrow{C=C} B\text{-}C\text{-}C\text{-}C\text{-}C\cdot \rightarrow \ldots$

The radical formed can continue to react until it terminates with another radical or until the reactive center is transferred.

Radical Isomerization

Radicals have the ability to rearrange their structure by shifting atoms or groups of atoms from one location to another. The driving force for such a reaction is related to the energy released in going from a primary to a more stable secondary or tertiary radical.

The simplest isomerization reaction is the transfer of a unit, such as a hydrogen atom, from its parent atom to another location four or five atoms down the chain, such as

(R-8) 

This isomerization uses a relatively unstrained five or six member ring transition state. Four-membered rings have also been postulated for some reactions, although they are strained structures. A 1,2-hydrogen transfer with a three membered ring transition state, such as

(R-9) 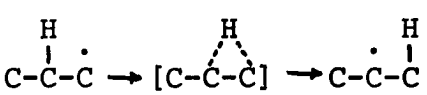

is not likely, but it is not considered impossible (77).

Radical Decomposition

Free radicals can also decompose to form a smaller radical and a stable product. This decomposition can be considered to be the reverse of radical addition. This type of reaction can compete with other reactions, such as propagation, as in

(R-10) 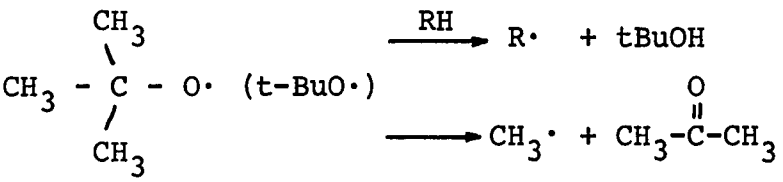

depending on the reaction conditions. The difference between radical decomposition and radical isomerization is that an atom or a group of atoms migrates with its bonding electron in isomerization while only an electron migrates in decomposition reactions.

Branching Reactions

A branching reaction is generally a reaction in which more radicals are produced than are used. This self accelerating reaction can cause chain explosions if it proceeds fast enough.

Branching reactions have been considered since early in the development of radical mechanisms. In this type of reaction, a radical reacts with a molecule in a manner similar to a propagation step. However, a branching step rapidly forms two or more separate radicals, all of which can propagate chains or cause branching themselves. A reaction of this

type is

(R-11) $H\cdot + O_2 \rightarrow \cdot OH + O:$

In 1935, Semenov (82) discussed the existence of another type of self-accelerating branching reaction, which he referred to as degenerate branching. Degenerate branching was a reaction with one or more molecules reacting to form two or more radicals. The difference between this reaction and normal initiation reactions is that the reacting molecule is a relatively unstable product of the overall reaction. Reactions of the form

(R-12a) $ROOH \rightarrow RO\cdot + \cdot OH$

or (R-12b) $RCH(=O) + O_2 \rightarrow HO_2\cdot + RC(=O)\cdot$

both satisfy the criterion of a degenerate branching reaction.

Degenerate branching reactions are much slower then branching reactions, due to the large activation energy barrier. This slowness was the basis for the theory of degenerate branching. Radicals react too fast and their average lifetime is too short to use the mechanism of branching to explain the slowly accelerating rate of many reactions. A slower reaction step, degenerate branching, is needed. In several applications a degenerate branching mechanism has definitely been proven.

CHAPTER IV

EXPERIMENTAL EQUIPMENT

The equipment used in this study was basically the same as that described by Hardwicke (42) who gave a detailed description of the individual components. A floor plan of the major pieces of equipment is shown in Figure 1.

This chapter has been divided into the following categories: Feed Preparation and Storage System, Compression System, High Pressure System, Product Receiver System, and Auxiliaries.

Feed Preparation and Storage System

A schematic drawing of the Feed Preparation and Storage System is shown in Figure 2. A photograph showing the storage tanks is shown in Figure 3.

The feed gas was mixed in a 295-liter feed mixing tank, T1, having a pressure rating of 27 atm. This tank was built for the military to contain breathing oxygen. The inlet and outlet lines, a pressure gauge, and a vent line were connected to the top opening of the tank. A water drain line and a water inlet from a Sprague, air-driven pump were attached to the bottom of the tank. A 165 atm, size 12-R-12, sight

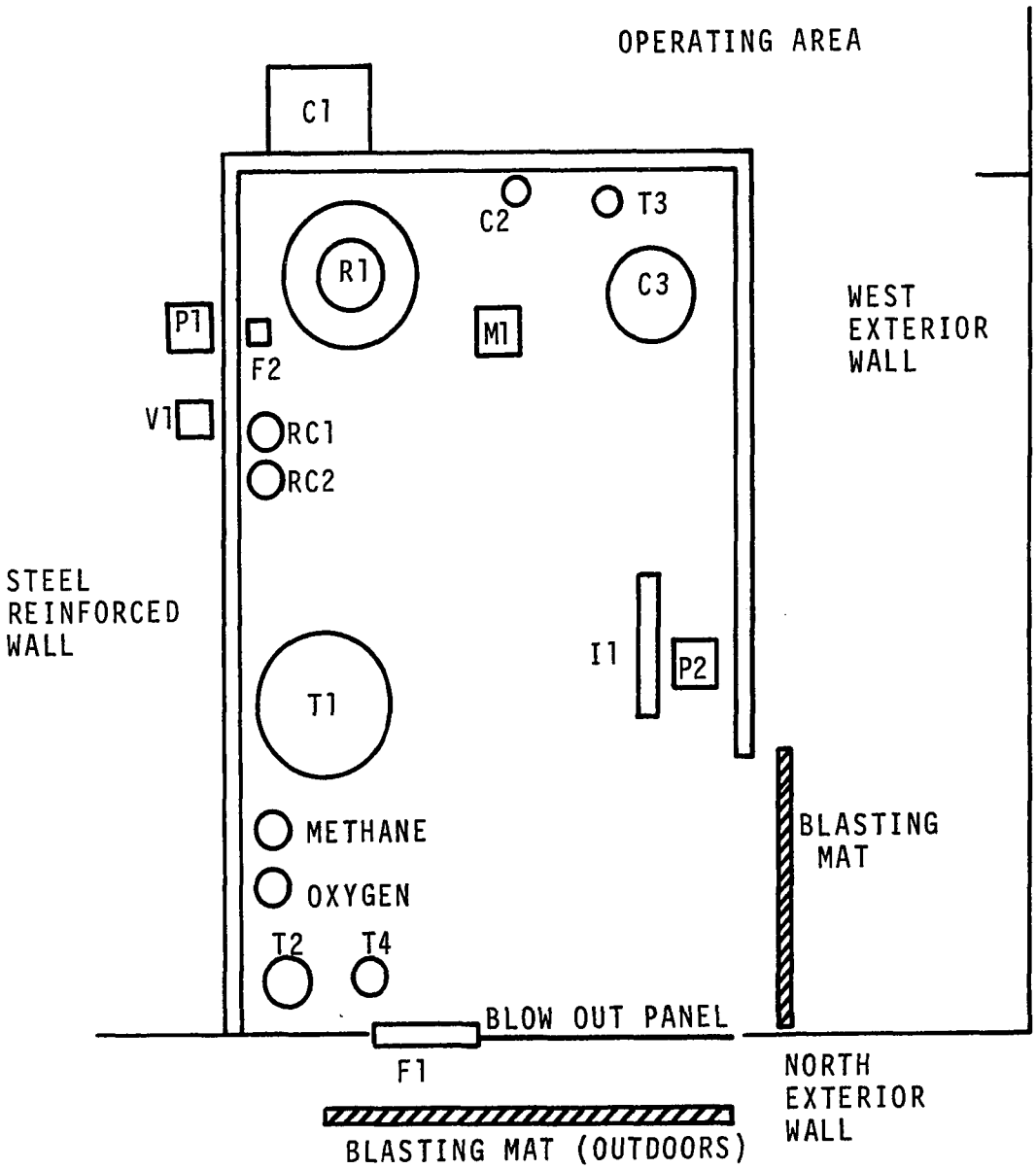

Figure 1. Floor Plan of High Pressure Cell.

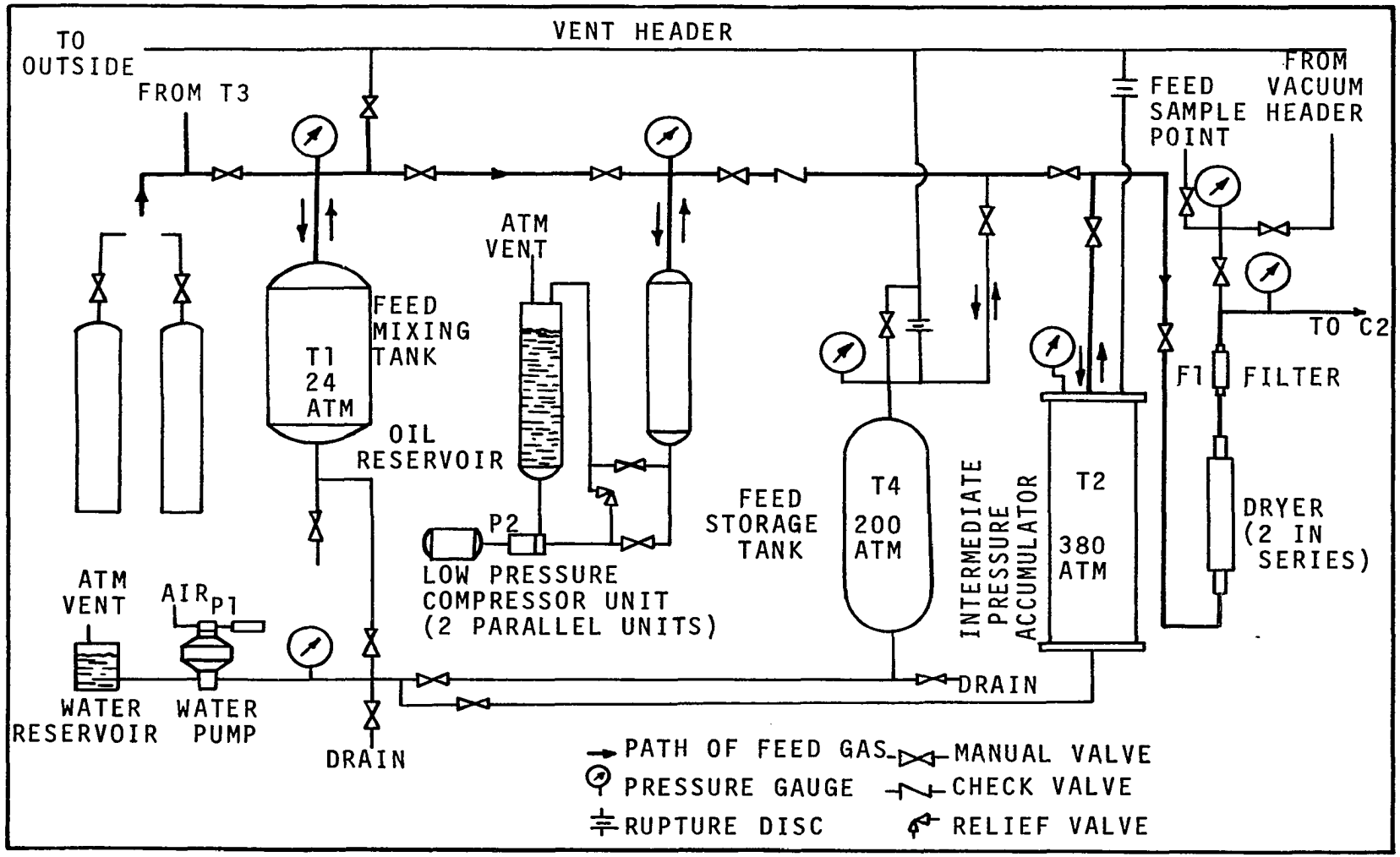

Figure 2. Flow Diagram of Feed Preparation and Storage System.

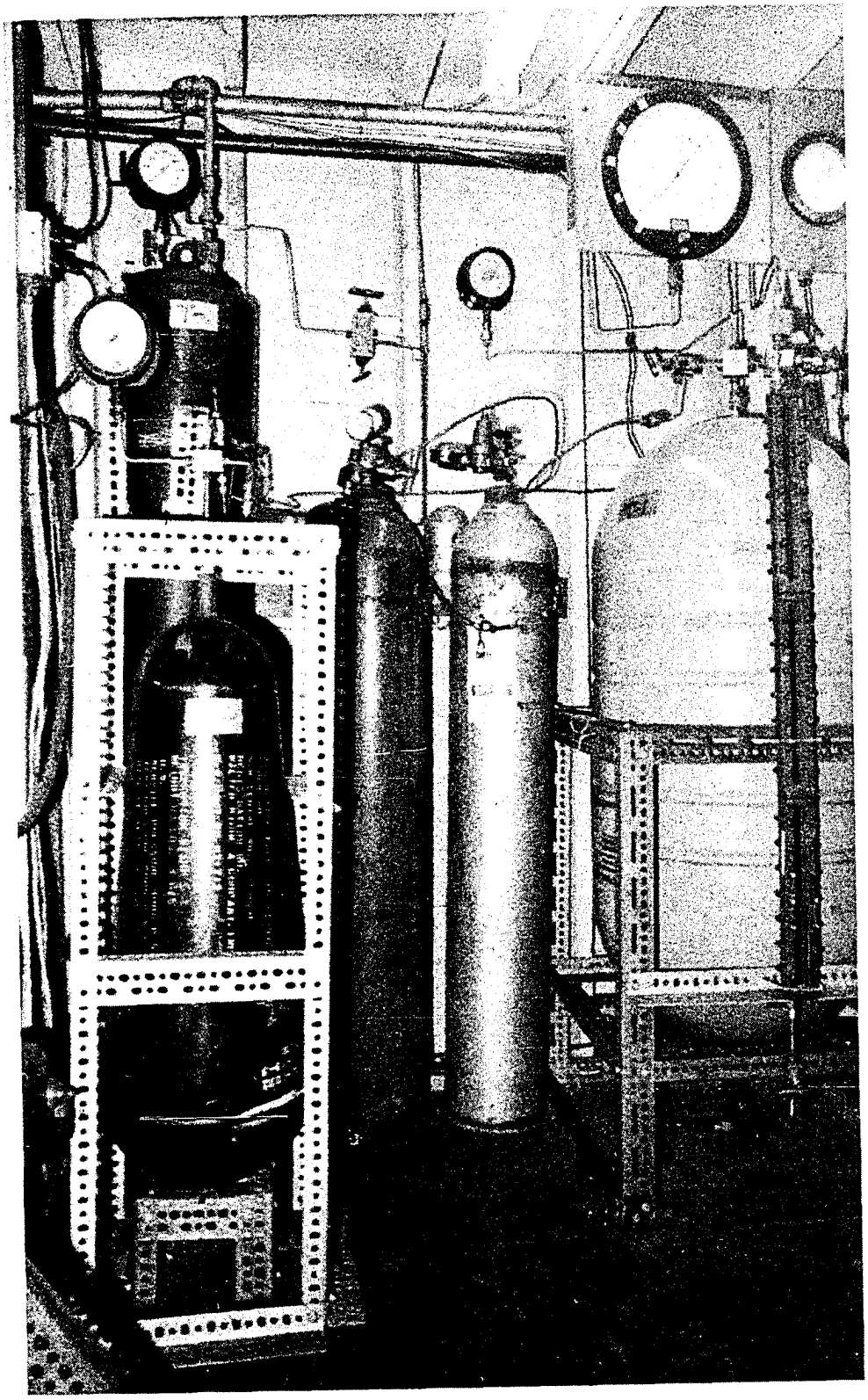

Figure 3. Feed Storage Vessels.

glass built by the Jerguson Gage and Valve Company, was attached to determine the water level in the tank.

The Sprague air driven pump, P1, Model 2-216-C-100, was connected to the feed storage tank, the intermediate pressure accumulator, and the mixing tank. Appropriate valves were used to pump water to each tank separately. The pump could develop 600 atm pressure by using air at 6.8 atm.

The feed was transferred from the mixing tank to the feed storage tank by the low pressure compressor, C1, rated at 680 atm. This unit consisted of two oil reservoirs, connected to a Seco high pressure pump P2, Model No. 20LAH-3, and two high pressure cylinders.

The feed storage tank, T4, was a pear-shaped vessel with a pressure rating of 340 atm and a volume of 48.9 liters. The steel storage tank, originally a military air starter bottle, had a single inlet-outlet line with a safety head assembly, a dump valve, a pressure gauge connected to the top opening and water inlet and outlet lines connected to the bottom opening.

The intermediate pressure accumulator, T2, was made by Autoclave Engineers (AE) from 4340 alloy steel. The 43-liter tank was closed with a self-sealing O-ring seal. Although T2 had a pressure rating of 1500 atm at 25°C and a rupture disc rated at 1360 atm, the pressure never exceeded 380 atm. The tank had a gas inlet-outlet line and a pressure

gauge on the top and a water inlet-outlet line at the bottom. Openings on top and bottom were standard AE fittings.

To prevent contamination of the feed mixture with a reaction product, it was necessary to remove any water vapor that had been adsorbed by the feed gas. The feed gas was passed through two driers and a filter. The driers were Autoclave Engineers Kuentzel bombs, with an indicated working pressure of 680 atm at 350°C, which were filled with Drierite. The filter consisted of two sintered metal discs inside a standard Autoclave Engineers filter, No. 5C-A.

Compression System

A schematic drawing of the compression system is shown in Figure 4.

The feed gas was pumped from the intermediate pressure accumulator to the high pressure accumulator using the intermediate pressure compression cylinder, C2. The cylinder was a heat-treated 400 series stainless steel cylinder with an aluminum piston. The bottom of the compression cylinder was sealed with an O-ring closure. The compressor, rated at 1700 atm, was originally used at the University of Michigan.

The intermediate pressure compression cylinder was activated by an air driven, SC Corporation oil pump, P3, Model No. 100-600-30, which was also connected to the high pressure compression cylinder and the high pressure intensifier. The pressure medium for the pump was Plexol 201 hydraulic oil made by the Rohm and Haas Company.

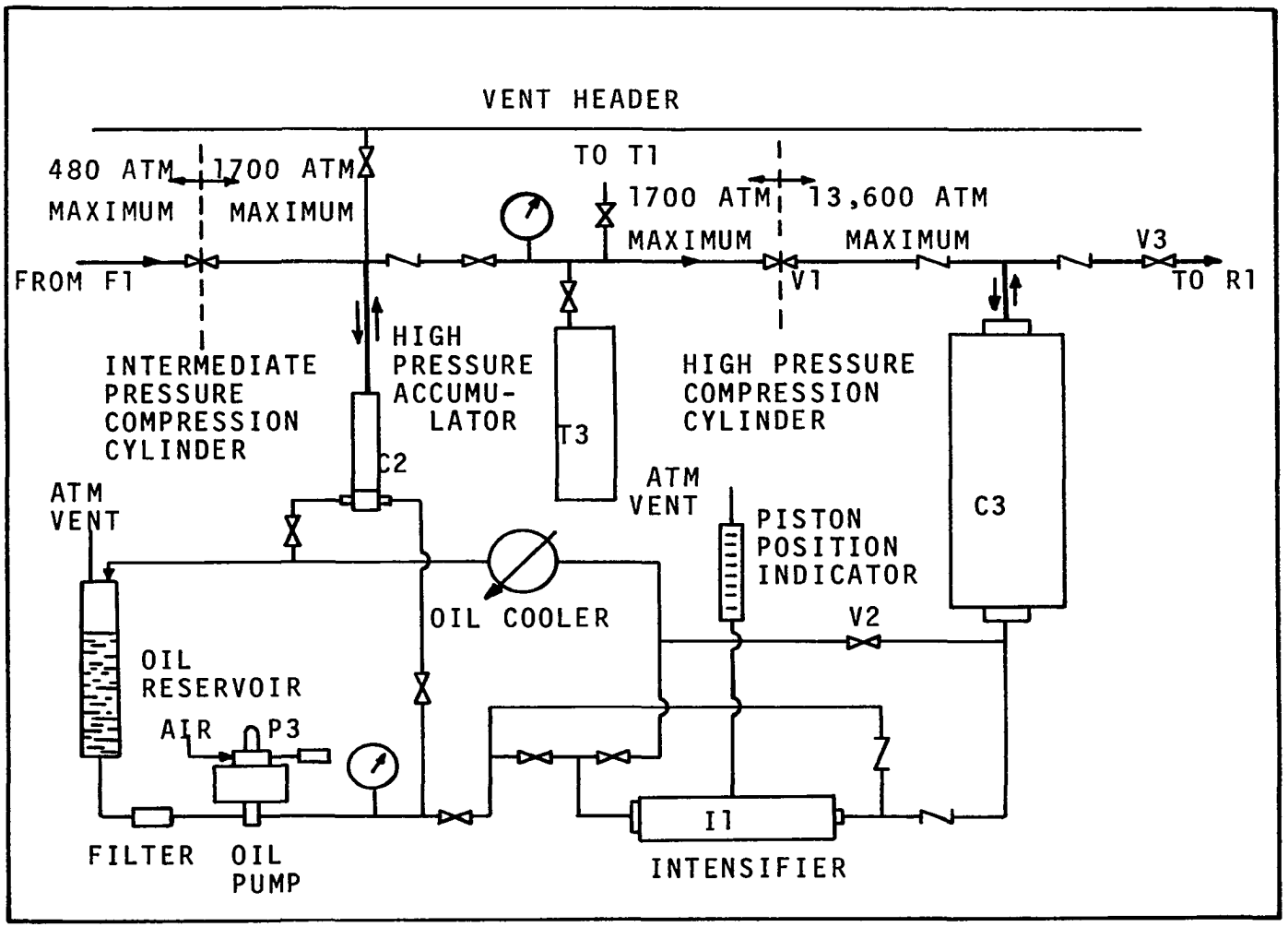

Figure 4. Flow Diagram of Compression System.

The high pressure accumulator, T3, which had been obtained from the University of Michigan, was a 75 mm gun barrel with plugs welded into the bore. An AE cone seat had been cut into the top for the inlet-outlet line. The tank had a working pressure of 1700 atm.

High Pressure System

A schematic drawing of the high pressure system is shown in Figures 4 and 5. Lott (60) has presented the design equations, and a description of the fabrication of the individual vessels.

Feed gas was transferred from the high pressure accumulator to the high pressure compression cylinder, C3, shown in Figure 6. This triplex cylinder was made by Autoclave Engineers from 4340 gun steel for a working pressure of 13,600 atm at 150°C. Hydraulic oil was separated from the feed gas by a free piston with sliding O-ring seals. The ends of the cylinder were sealed with Bridgman, unsupported-area closures. The top of the cylinder was connected to the reactor, while the bottom was attached to the high pressure intensifier and the SC oil pump. Standard duplex tubing, 19 mm by 1.59 mm i.d., was used on all high pressure lines.

The high pressure intensifier, I1, was built by Autoclave Engineers for a working pressure of 13,600 atm. The piston, with a stroke of 184 mm, had a 10:1 area ratio with a 25.4-mm diameter shaft on the high pressure end. The

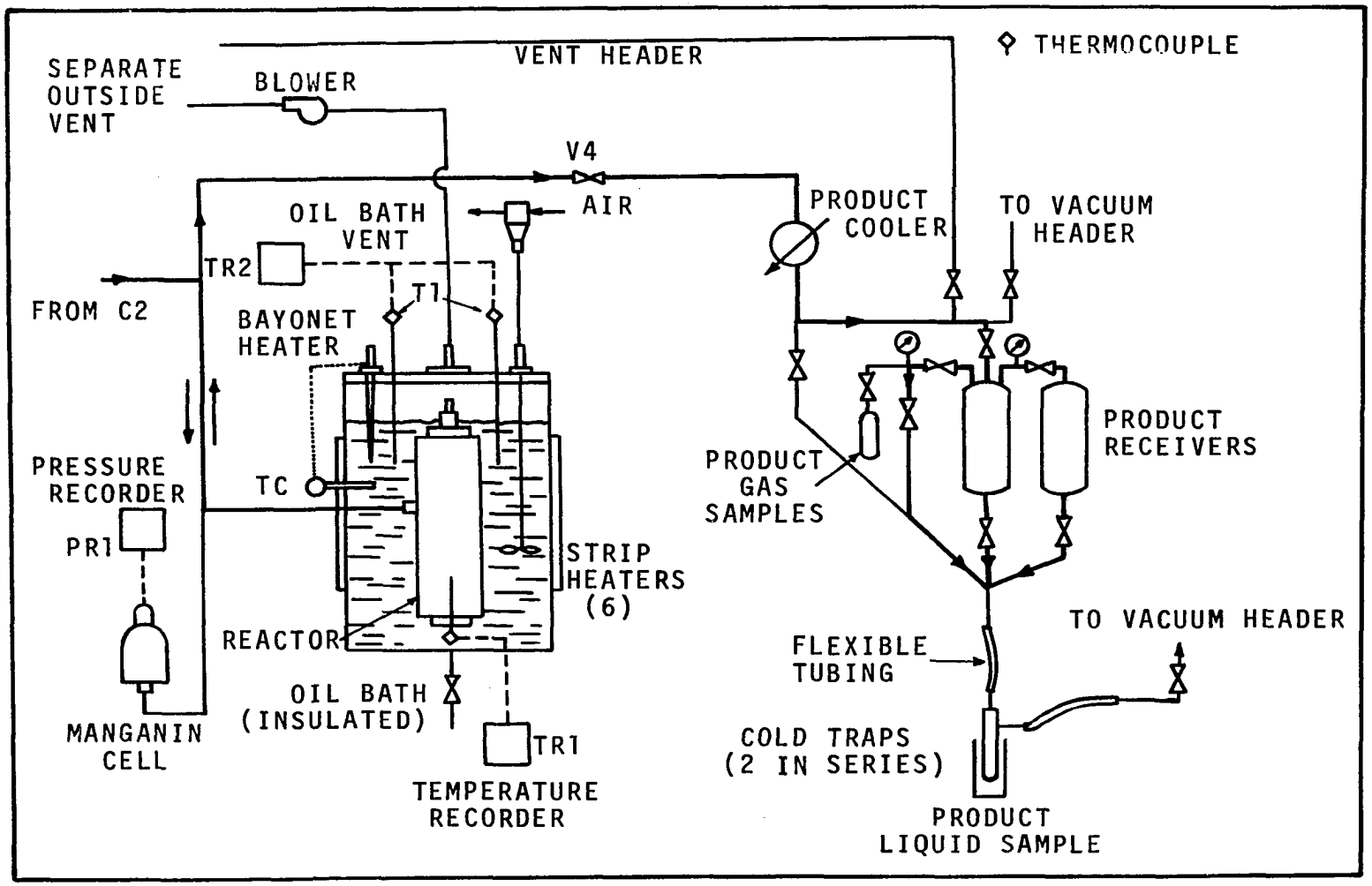

Figure 5. Flow Diagram of the Reaction and Product Receiver Systems.

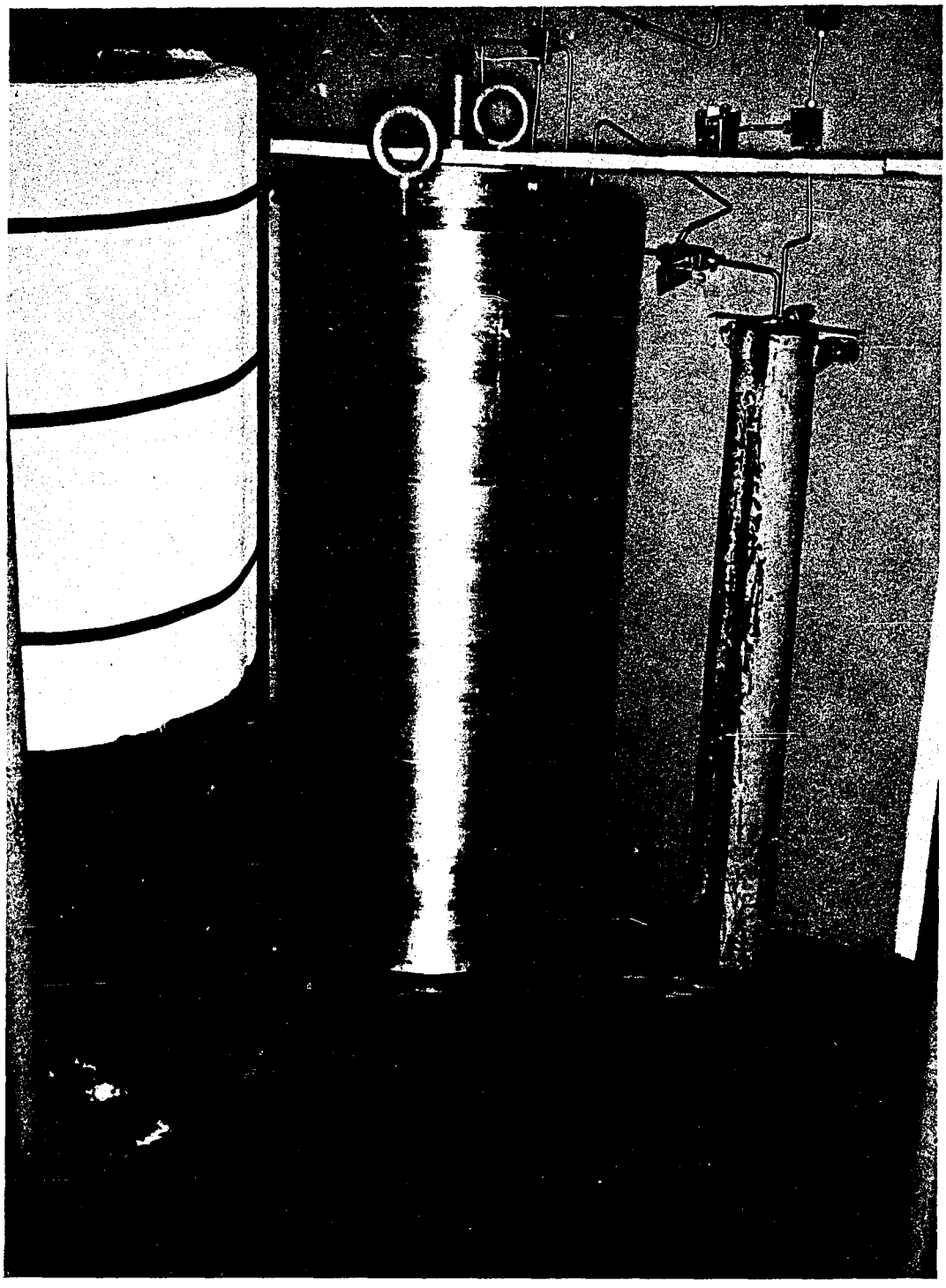

Figure 6. 13,600 atm Compression Cylinder [from Lott (60) reproduced by permission].

intensifier cavity was connected to a graduated cylinder, used to measure the piston displacement. Valves and check valves were added to enable the intensifier piston to be reversed without loss of pressure in the high pressure compression cylinder.

The reactor, R1, also built by Autoclave Engineers, was of duplex construction from 18 percent nickel maraging steel; it is shown in Figure 7. The top and bottom reactor plugs and the electrode were also built of 18 percent nickel maraging steel, while the main nuts and other pieces were constructed from 4340 steel. The reactor was designed for a working pressure of 13,600 atm at 425°C; its dimensions are 50.8 mm i.d., 305 mm o.d., 254 mm internal length, and 813 mm external length, and it has an inlet-outlet port in the side for a 19 mm double cone connection. The top and bottom closures were sealed with Bridgman, unsupported-area seals.

The pressure in the reactor was measured by a Harwood Engineering Company manganin cell, M1. The pressure cell consisted of an active coil and a compensating coil, both of manganin wire; each coil had a resistance of about 120 ohms. The cell readings were recorded by a Foxboro Dynalog Recorder, Model 9410HC, on a one hour circular chart. The recorder had three ranges, capable of measuring nominal pressures of 3,400 atm, 6,800 atm, and 13,600 atm, respectively. The manganin cell calibration chart is shown in Appendix A.

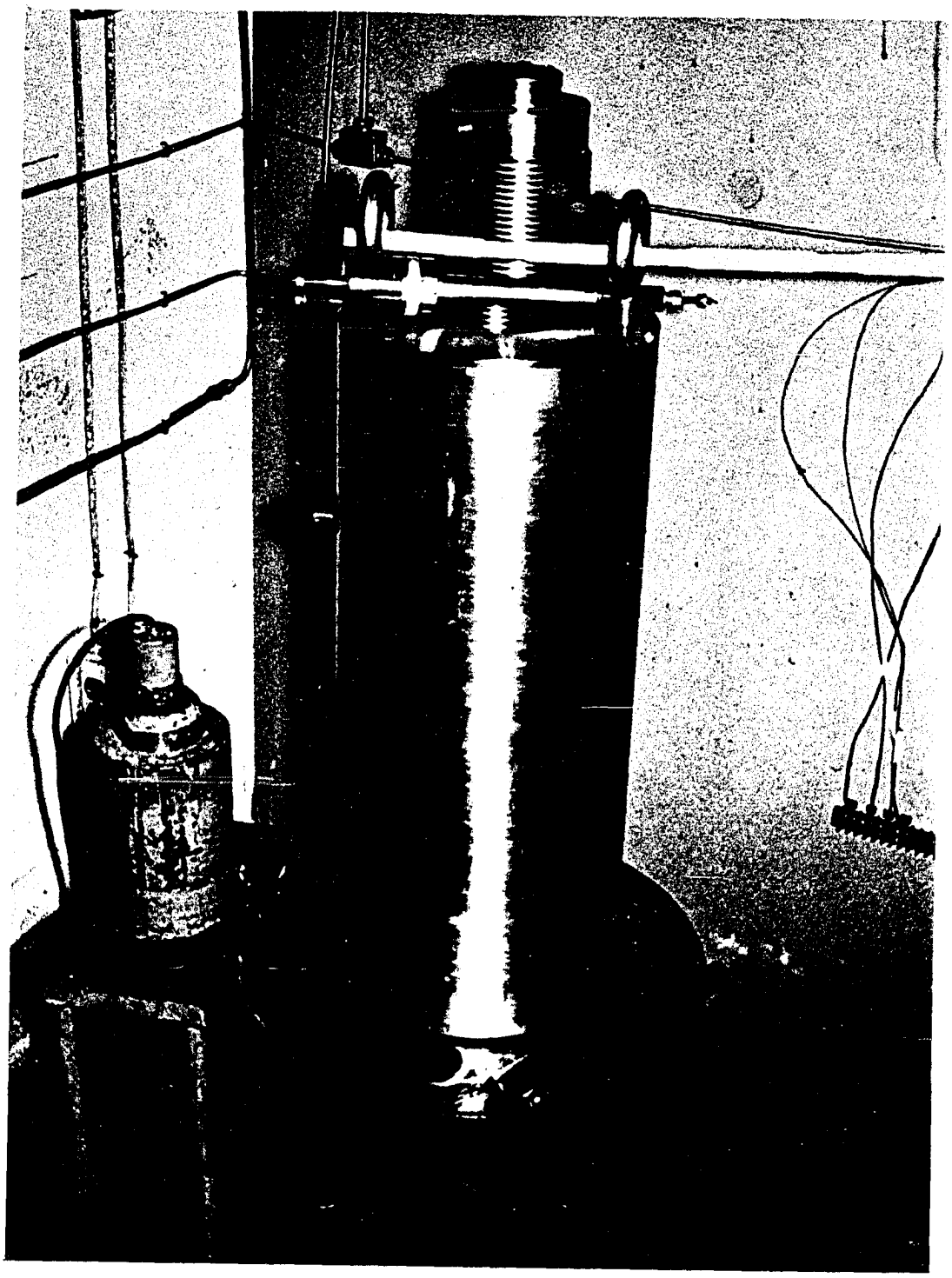

Figure 7. 13,600 atm Reactor [from Lott (60) reproduced by permission].

The reaction vessel contained an internal resistance heater. This heater consisted of 9.0 m of #18 nickel-chromium wire, with a resistance of 1.35 ohm per meter, wound around an alumina core. The core, built by the Norton Company for a previous oxidation study, was 39.7 mm o.d., 28.6 mm i.d., and 210 mm long with a 1.59-mm groove spiraling down the cylinder at 4 grooves per cm. After the core was wound with the wire, the outer surface was coated with alumina, Norton Company Alumdum #RA 1139, and was baked. Both lead wires to the heater were strung with porcelain beads to prevent an electrical short to the thermowell in the reactor or to each other. The heater, with the attached end plug, is shown in Figure 8.

The electrical current for the heater was transmitted through the electrode inside the closure plug in the top of the reactor. The electrode was insulated from the plug with heat-shrinkable Teflon tubing and with alumina rings. These alumina rings, made by Coors Porcelain Company, were part of another Bridgman seal. The reactor body served to complete the electrical circuit. The current was controlled by a 240 volt powerstat, Model 8P57515, made by the Superior Electric Company.

The temperature inside the reactor was monitored with an iron-constantan thermocouple in a thermowell that extended through the plug in the bottom cover. The thermocouple was connected to a Bristol strip chart recorder, Model 1PH560-51-T46.

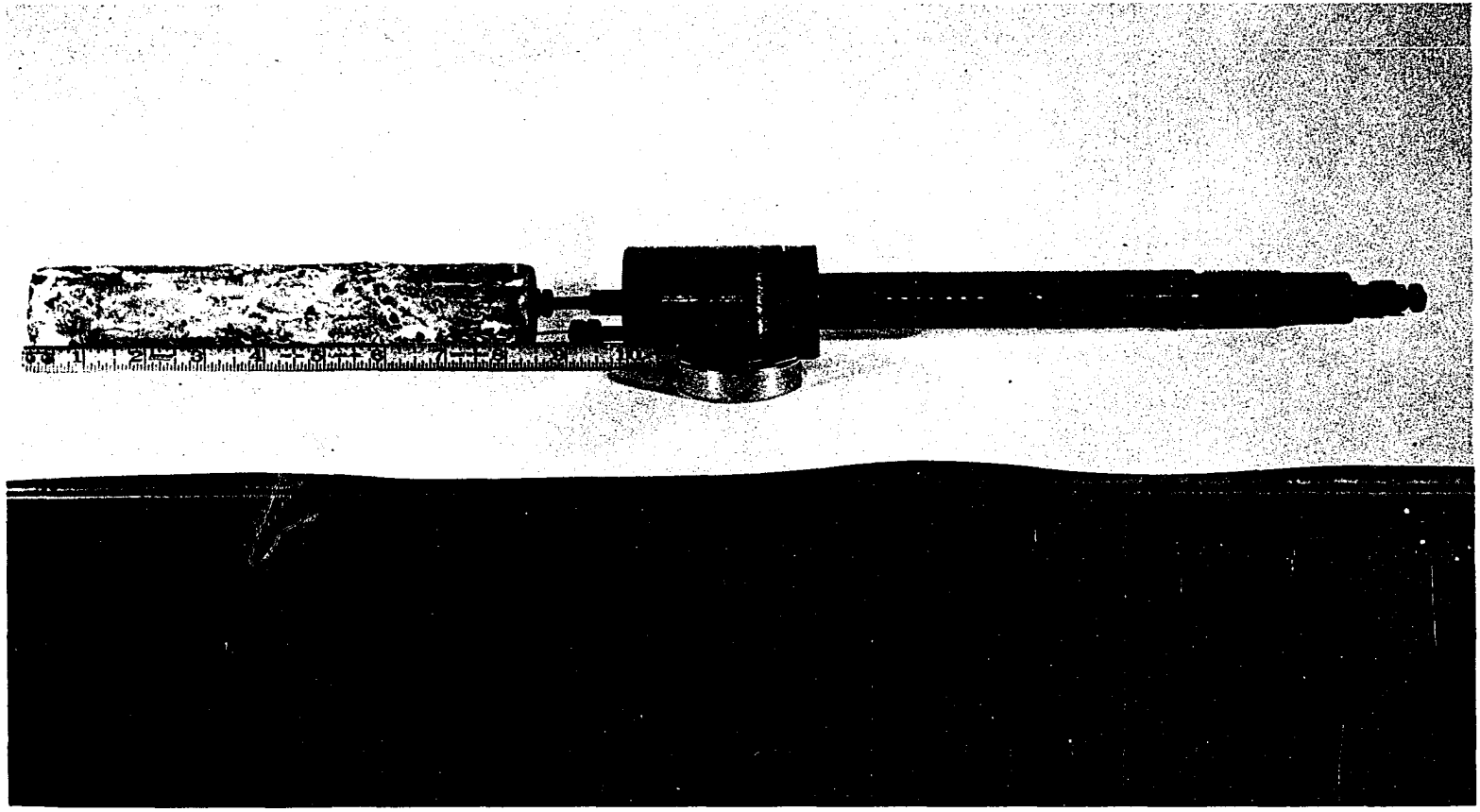

Figure 8. Internal Heater Attached to Top Cover [from Hardwicke (42) reproduced by permission].

Between and during runs the reactor temperature was maintained at a level below normal reaction temperatures with an oil bath. The bath, made of steel plate, was 0.6 m in diameter and 0.9 m tall. The bath was mounted on four pipe legs, welded to a 13-mm steel plate. The reactor was positioned inside the bath by a steel support ring. The oil bath had a sealed opening in the wall for the inlet-outlet pipe to the reactor. The heating oil was Mobiltherm 600, purchased from the Mobil Oil Company.

The oil bath was heated by six, 1000-watt strip heaters connected in parallel on the outside wall. The heaters were embedded in Thermon T-3 heat-conducting cement, made by the Thermon Manufacturing Company, and covered with Kaylo pipe insulation. The gaps in the insulation were filled with a paste made from asbestos powder. The bottom of the oil bath was insulated with the same asbestos paste, with chicken wire embedded in it for added strength. The heaters were connected to a 220-volt line through a powerstat with a 30-amp ammeter and fuse.

Fine adjustment of the oil bath temperature was made by a 750-watt Chromalox bayonet heater, which was connected to a 300°C Fenwall thermoswitch, Model 18002-0. The thermoswitch extended through the oil bath wall into the oil.

The top cover of the oil bath rested on the rim of the oil bath. The cover had openings for the shaft of a Mixing Equipment Company air driven mixer and for a vent pipe.

The vent pipe was connected to a blower to exhaust the oil fumes to a vent header. The cover also had a heating well for the bayonet heater and two thermowells for iron-constantan thermocouples, used to measure the oil temperature. These thermocouples were connected to a Brown Company strip chart recorder Model 153X60P12.

Product Receiver System

The product receiver system is shown in Figure 5.

The product gas from the reactor passed into the receiver system. The gas first passed through a water-cooled coil of 6.4-mm, 304 stainless steel high pressure tubing, and then into the two receivers. The first receiver, RC1, with a volume of 6.02 liters, was made from a piece of schedule 40 pipe with pipe caps welded to each end. The other receiver, RC2, with a 8.20-liter volume, was a stainless steel cylinder (originally built to hold breathing oxygen for the military). The receivers were connected to a 68-atm USG pressure gauge with an included vacuum scale.

Liquid samples were taken using two cold finger condensers, connected in series in a dry ice-acetone bath. Each condenser was made from a 25-mm test tube, 150 mm long, with a ground glass joint connected to a head with an overhead inlet tube and a side exit port. Gas samples were taken in steel cylinders with a volume of 0.4 liter and a pressure rating of 140 atm.

Auxiliaries

Dry air was available in the cell at 9.5 atm to power the Sprague pump, the SC Company pump, and the air driven mixer. Vacuum was supplied from a Welch Duo-Seal Vacuum Pump, V1, Model R-1400, located outside the cell. Vent headers were installed on two sides of the cell to remove purged gas and oil fumes.

The barricaded cell, 4 m by 2.3 m by 2.3 m tall, consisted of a 50 mm tongue-and-groove wood construction, covered with steel plate on three sides and on the top. The outside wall was a 2 by 2.3-m plywood blowout panel held in place with wood screws. It was calculated that a pressure differential of 0.1 atm across the wall would blow out the panel. A 2 by 3-m reinforced Manila rope blast mat hung across the doorway to the cell and another lay on the roof of the cell. A third blast mat hung outside the blowout panel, as shown in Figure 1. The floor below the high pressure system had been previously reinforced to support the weight of the equipment.

A high capacity Westinghouse explosion-proof fan, F1, Model FH, was installed in the blowout panel to remove oil bath fumes and dissipate any gas resulting from leaks. A Times Facsimile Corporation blower, F2, Model 34B-50, was installed between the oil bath lid and the vent header to reduce the amount of oil vapor escaping into the cell.

All valves operating at a pressure above 680 atm had valve handle extensions that passed through the cell wall.

All of the 13,600-atm valves had flared extensions that would not be blown through the wall if a valve gland nut failed.

CHAPTER V

EXPERIMENTAL PROCEDURE

Feed Preparation and Storage

The two components of the feed gas mixture were purchased in standard 1-A cylinders. Pure grade methane, 99 mole percent, was purchased from Phillips Petroleum Company. Linde pure grade oxygen, 99.5 mole percent, was purchased locally.

Methane was charged to the feed mixing tank, T1, through clean copper tubing. The inlet line was purged with methane by loosening the fitting at the inlet and bleeding methane through the line. After the fitting was tightened, the inlet valve was opened, and methane was added to the tank until the tank pressure reached 6.1 atm. The valve was closed and the copper tubing was removed. The copper tubing was then attached to the oxygen cylinder regulator and the filling procedure repeated. Oxygen was added until the total pressure reached 6.8 atm, resulting in a gas mixture containing about 8.2 mole percent oxygen.

A fixed inlet header, permanently connecting both cylinders to the feed tank, was not used because of possible leakage which could contaminate either cylinder. Methane was

always added to the mixing tank first so that the methane composition remained well above the explosive limits. The explosive limits lie between 0.25 and 0.72 mole of methane per mole of oxygen at atmospheric pressure and between 0.15 and 2.84 moles methane per mole oxygen at 200 atm (59). In the event that the tank had been vented to the atmosphere, vacuum was pulled on the system for several hours before refilling.

After the feed mixing tank was pressurized with feed gas, water was pumped into the bottom of T1 using the Sprague air pump. The water level in the tank was monitored by the sight glass.

When the pressure in T1 reached 24 atm, feed gas was transferred to the feed storage tank, T4, using the low pressure compressor. After charging one of the high pressure cylinders in the low pressure compressors with feed gas, hydraulic oil was pumped into it until the pressure in the cylinder reached 170 atm. This maximum compressor outlet pressure was specified to prevent bursting the 240-atm rupture disc on T4. The compressor pump was then stopped and the gas was expanded into T4. Afterwards, the oil was transferred to the oil reservoir using new feed gas. Since the time required to pressurize the cylinder approximately equaled the time to drain the oil, the two units of the low pressure compressor were used alternately. Feed gas was compressed until the pressure in T4 reached about 140 atm. During the transfer

operation, the water pump maintained the pressure in T1 at 24 atm.

The feed storage tank was installed during this study to eliminate lengthy time delays. In earlier studies all runs had to be stopped when the feed gas in the intermediate pressure accumulator, T2, was depleted. The procedure to refill T2 took approximately three days. In this study, feed gas was pumped into the feed storage tank during any free time. When the feed gas in T2 was depleted, the gas could be transferred to it from the feed storage tank in about two hours by using the Sprague air driven pump.

When the feed gas in T2 was depleted, the water in T2 was drained. The valve connecting T4 to T2 was opened, forcing the water from T2. After the pressure in the two tanks had equalized, T4 was filled with water by the Sprague air pump, forcing all the feed gas into T2. Tank T4 was then isolated, drained, and repressurized with feed gas from T1.

At the end of the gas transfer operation, the pressure in T2 was approximately 140 atm. Water was then pumped into T2 until the pressure reached 375 atm. As feed gas was used from T2, more water was pumped into it to maintain the pressure level. A feed sample was taken each time tank T2 was refilled.

Since the feed gas had been stored over water in the three low pressure tanks, T1, T4, and T2, the gas had to be

dried before it was used. The feed gas leaving T2 passed through two drying cylinders filled with Drierite and then through a filter to remove particulates.

The gas from T2 was used to pressurize either the high pressure accumulator, T3, or the reactor system. For either usage, feed gas was withdrawn from tank T2 to pressurize the intermediate pressure compression cylinder, C2. The SC Company air driven oil pump was used to pump hydraulic oil into C2, compressing the gas to a maximum pressure of 1500 atm.

Prior to Reaction

About fifteen hours prior to the start of an experimental run, the coarse adjustment for the oil bath strip heaters was set to give an oil bath temperature 40° to 60°C cooler than the desired run temperature. The exhaust fan, F1, was turned on to remove oil fumes from the building. The oil bath stirring motor was started to help maintain a uniform temperature distribution in the oil bath. Final adjustment of the oil bath temperature was made prior to starting the run.

Although normally both the reactor and the receivers remained under vacuum from the previous run, they were again evacuated for at least another fifteen minutes. The vacuum scale on the receiver pressure gauge was watched to determine if gas was leaking into the combined reactor and receiver system. The reactor dump valve, V4, was then closed, and the pressure in the receiver section again was observed.

Spot checks were made of the reactor heating system to make certain that an electrical short was not present. The liquid sample condensers were then prepared by placing the condensers, acetone, and dry ice into a Dewar flask. The condensers and an evacuated gas sample collection bottle were attached to the receivers. The Foxboro pressure recorder was zeroed. The oil bath vent blower was turned on to reduce further the amount of oil vapor in the pressure cell.

The reactor was slowly filled with feed gas, care being taken that the rate of pressure rise in the reactor did not exceed the limit of 100 atm per minute found by Lott (60). The controlled rate of pressure rise was necessary to prevent premature ignition of the feed gas by adiabatic compression. With the valve to T3 closed, the high pressure inlet valve, V1, was opened to fill the high pressure compression cylinder, C3, with gas from T2, to a pressure of about 340 atm. Valve V3, between C3 and the reactor, was then opened slightly to pressurize the reactor slowly. The rate of pressure rise in the reactor was observed on the Foxboro recorder and by way of mirrors showing the pressure gauge on C3.

This procedure was repeated until the pressure in the reactor reached 270 atm. The reactor pressure was then slowly raised to 1300 atm using the same procedure with gas from T3.

At this point, valve V1 was closed, isolating the high pressure system. Hydraulic oil was pumped by the SC pump to the low pressure end of the intensifier, I1, forcing high

pressure oil into the bottom of C3. Valve V3 was left open during this pumping operation since the slow pressure rise would not cause ignition. Pumping continued until the desired pressure was reached or until the oil in the intensifier piston indicator showed that the piston had traveled the full stroke. The piston was reversed by diverting oil from the low pressure end of I1 to the high pressure end.

If additional pressure was desired, the intensifier cycle could be repeated until C3 was filled with oil. Once C3 was full, valve V3 was closed, and the oil drained. Valve V1 was opened and C3 was repressurized from T3 and C2. This entire procedure was repeated until the reactor reached the desired pressure. A pressure of 3400 atm could normally be reached by starting at a pressure of 1300 atm in the reactor and using the intensifier once. A pressure of 6800 atm required using the intensifier three times. Pressures higher than 6800 atm required draining the oil from C3 and refilling it with feed gas.

During a Run

The reactor was pressurized to a point below the desired operating pressure and isolated. The additional pressure was generated by rapidly heating the gas to the reaction temperature with the internal heater. The temperature was maintained at the desired level by watching the internal temperature reading on the Bristol strip chart recorder and

adjusting the powerstat to the internal heater. After a predetermined time, the pressure was released by opening the dump valve, V4, and turning off the internal heater.

Sample Collection

The reaction products passed through a water-cooled coil and into the receivers. After the gas in the receivers and in the reactor had time to return to thermal equilibrium, the open system pressure and the temperatures in the reactor and in the receivers were recorded. A gas sample was collected after purging the sample collection bottle twice with gas products. The sample bomb was then pressurized to about 3.5 atm with the gas sample.

The purged gas and the remainder of the reaction products in the reactor and in the receivers were slowly passed through the two cold trap condensers with the gas flow regulated by a needle valve. The non-condensable gases passed to the vent header and escaped to the atmosphere. The condensable products were frozen out in the dry ice bath.

After passing all of the reaction products through the cold trap, the condensers were removed. The sample was then melted and transferred to a collection bottle. The cold traps were then returned to the system, and vacuum was pulled for thirty minutes to assure that all condensable products were removed from the reactor and receivers. The remaining liquid products were added to the first, and the total weight was recorded.

The gas sample bottle was plugged and set aside for future analysis. The liquid sample bottle was sealed and placed in a freezer until the analysis could be made.

CHAPTER VI

ANALYTICAL EQUIPMENT AND PROCEDURE

The products of each experimental run were collected in two ways. A small gas sample was taken directly from the receivers. The rest of the reaction products were passed through a dry ice-acetone cold trap to collect a sample containing all components that were condensable at -78°C. These two samples were then analyzed separately using gas chromatography. Most of the analytical equipment and procedures used are the same as described by Bauerle (9).

Analytical Equipment

The chromatographic analyses were done on a F & M Scientific 700 Laboratory Chromatograph made by the Hewlett Packard Company. The main body of the assembly consisted of the oven cabinet and the control cabinet. A Hewlett Packard F & M Scientific 240 Temperature Programmer was connected to the oven cabinet to control the heating rate of the oven. The detector sub-unit in the oven cabinet was connected to a Hewlett Packard F & M Scientific 50B Automatic Attenuator, which controlled the attenuation of the output peak. The detector output was recorded continuously on a Moseley Strip Chart Recorder, Model

7127A, with a Model 229 Disc Instrument Company integrator as part of the recorder. A photograph of the system is shown in Figure 9.

Equipment Description

The oven cabinet contained the entire gas system and the main power controls. The carrier gas flow was controlled by two rotameters. Liquid samples were injected with a syringe through a rubber septum into either the upper or lower column injection ports. Gas samples were injected into the chromatograph by a sliding sampling valve. The chromatograph columns were heated by an oven equipped with a 1050 watt heating element and blower. The detector consisted of a heated thermal conductivity cell for measuring the presence and relative concentrations of unknown substances. The main power switch, the subsidiary power switches and potentiometers for controlling the temperature of the column oven, the injection ports, and the detector filaments were all housed in the oven cabinet. A gauge showed the measured temperatures in the injection ports, the oven, and the detector block.

The control cabinet contained the components for the detector and the detector output. The bridge switch and the filament current dial controlled the current flowing through the arms of the detector bridge. The manual attenuator dial divided the detector output voltage by powers of two to keep the recorder pen on chart. The coarse and fine adjustment

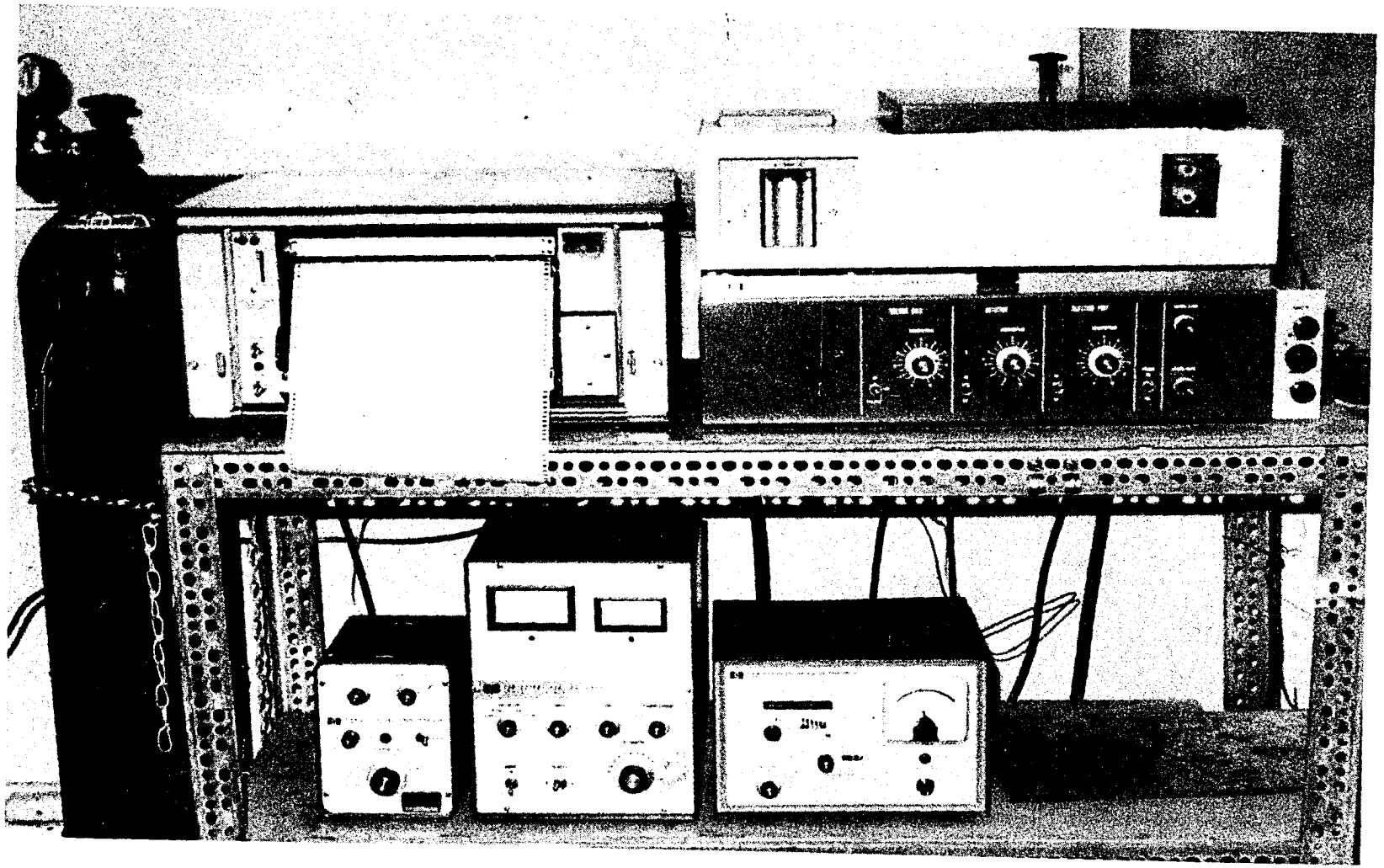

Figure 9. Chromatographic Equipment Used for Analyses.

knobs zeroed the chart pen by balancing the detector bridge. The polarity switch reversed the polarity of the detector output voltage so that, if desired, the detection and reference columns could be reversed. This switch could also be used to convert a negative output signal into a positive peak.

The temperature programmer cabinet contained the controls to vary the oven temperature linearly with time. A selector switch allowed twelve different heating rates, from 0.5° to 30°C per minute, plus an isothermal setting. A dial permitted the selection of the initial temperature. A limit switch stopped the heating rate and held the temperature constant at the desired temperature.

The automatic attenuator cabinet enabled the selection of either automatic or manual attenuation of the detector output signal. A selector dial reduced the output signal by powers of two, with attenuation ranging from 1 to 1024. The minimum attenuation dial was used in automatic operation, permitting the selection of values other than unity for a minimum attenuation.

The output signal was recorded on the strip chart recorder. The area under the output curve was calculated continuously by the integrator and recorded by a second pen. The chart drive had a selector switch to specify the chart speed, which could be set at four values between 0.25 and 2 inches per minute.

Equipment Function

The helium carrier gas was delivered from the gas regulator to the back of the oven cabinet. The flow was split in half, with each stream being fed to the inlet of a flow control rotameter. From the rotameter outlet, each stream was delivered to a heated chamber directly behind the injection port assembly. Upon injection, the sample was swept into the primary chromatograph column by the carrier gas, while the carrier gas flowed through the secondary column as a reference. After traversing the columns, both gas streams passed through the detector assembly and were then vented to the atmosphere.

Each column consisted of a tube packed with a uniform-particle substance, or support, which could be coated with a non-volatile liquid, or substrate. The different components in the sample undergoing analysis had different affinities towards the substrate and support, thus separating the sample into a series of bands which were eluted down the column. As each band left the column, it entered the detector.

The detector, or heated thermal conductivity cell, contained a Wheatstone bridge, with one arm in the reference stream and one arm in the detection stream. The bridge was balanced so that a voltage was not produced when pure carrier gas passed across the filaments. A sample component with a thermal conductivity different from the carrier gas changed the temperature of the filament in the primary detection stream. This temperature variation caused a change in the

resistance of the detection arm, producing a voltage across the terminals of the bridge proportional to the amount of sample passing through the detector. This voltage actuated the pen on the strip chart recorder.

Since the recorder had a full scale response of 1 mv DC, the problem of possibly driving the pen off scale existed. This problem was eliminated by using the automatic attenuator. Each time the output voltage increased to a value of 95 percent of full scale deflection, the automatic attenuator cut the signal in half. After the signal maxima was reached, the pen output signal was doubled each time the pen dropped to 32 percent of full scale, until the minimum attenuation value was reached. The integrator in the recorder cabinet operated as a function of the pen displacement only; it did not detect a change in attenuation. Therefore, the integrator could not be used simultaneously with the automatic attenuator.

Columns

The column packing for the gas columns was activated Linde Type 5A molecular sieve, 60-80 mesh, made by the Matheson Company. The liquid column packing was 50-80 mesh Porapak T made by Waters Associates, Inc.

Molecular sieve packings are not usually used to separate gas mixtures containing carbon dioxide because the carbon dioxide is irreversibly absorbed on the packing at low temperatures. Carbon dioxide can be driven off the molecular

sieve at a temperature of about 225°C (9). However, the separation of the major components in the gas mixture, oxygen, nitrogen, and methane, requires a low temperature for good separation. The solution to this problem was temperature programming the column oven from 25°C to 250°C. The oxygen, nitrogen, and methane eluted through the column first, followed by carbon monoxide and ethane, with carbon dioxide last.

The Porapak T packing for the liquid column consisted of porous polymer beads that are not usually coated with a substrate. Therefore, at high temperatures, there was no column bleeding or vaporization of the packing substrate. Although the packing has a very large surface area, approximately 50 square meters per gram, there was no adsorption with polar compounds. No damage occurred if the column was overloaded with sample.

The chromatography columns were specifically constructed for this study. The gas columns were made from 0.91 meters of 6.4 mm diameter stainless steel tubing, bent in a 16 cm diameter loop. The liquid columns were made from 2.44 meters of 3.2 mm stainless steel tubing, coiled in a 22 cm diameter loop. The packings were prepared by drying them for 24 hours previous to packing: the molecular sieve at 270°C, the Porapak T at 180°C. In packing both sets of columns, one end of each tube was plugged with fiberglass wool. Vacuum was then pulled on the plugged end of each tube while the packing was slowly added. When each column was filled, the open end was

filled, the open end was plugged with more fiberglass and the column was sealed with Swagelok plugs. An additional set of commercially built Porapak T columns were purchased from Hewlett Packard and compared to the hand packed set. No difference in operating performance was found between the two sets.

Analytical Procedure

The gas analyses were done using the following operating conditions:

Columns	0.91 meters of 5A molecular sieve
Regulator pressure	6.8 atm
Helium flow rate	60 ml/minute
Injection port temp.	260°C
Detector temp.	260°C
Detector filament current	150 ma
Oven temp.	35°C - programmed to 250°C at 20°C per minute
Approx. sample size	5.0 ml

The liquid analyses were done using the following conditions:

Columns	2.44 meters of Porapak T
Regulator pressure	6.8 atm
Helium flow rate	130 ml/minute
Injection port temp.	260°C
Detector temp.	260°C
Detector filament current	150 ma
Approx. sample size	1 µl

The separation of the water-methanol peaks required an oven temperature of 85°C. The separation of the other components in the liquid sample was accomplished in a second analysis using an oven temperature of 140°C, stepped to 165°C four minutes after the water peak.

The retention times for the components in the three analyses are listed below, with time in minutes.

Gas Component	Time
Oxygen	1.5
Nitrogen	2.4
Methane	3.4
Carbon monoxide	5.8
Ethane	11
Carbon dioxide	16

Liquid Components	Time at 85°C	Time at 140-165°C
Formaldehyde	3.0	1.0
Water	9.6	2.1
Methanol	16.5	2.7
Methyl formate	20.	3.0
Ethanol		5.2
Acetone		8.0
Formic acid		12.8

Procedure for Gas Analysis

The gas sample was obtained by bubbling the gas through the sample loop and into a beaker of distilled water to prevent atmospheric back-contamination. The sample loop was made from 230 cm of 3.2 mm diameter copper tubing wrapped in a 5.5 cm diameter coil. After the loop was sufficiently purged, the flow was stopped. The gas was allowed to keep bubbling until the loop pressure dropped to atmospheric pressure at which time the sample loop was isolated.

To start the analysis, the gas sample was injected into the chromatograph using a sliding sampling valve. The carrier gas flow in the upper column was diverted through the sampling loop, sweeping the sample into the column. The gas analysis

was started at a temperature of 35°C with a programmed temperature rise of 20°C per minute starting one minute after injection. The shut off switch was set at 250°C.

The first analysis for each gas sample was made on automatic attenuation with a minimum attenuation of four. It was necessary to mark on the chart paper the maximum attenuation that each component peak required. After this analysis was completed, it was necessary to make at least two additional analyses of the same sample, using manual attenuation and the integrator. The attenuation dial was adjusted for each peak so that the entire peak stayed on scale at one attenuation. An attempt was also made to keep each peak as large as possible to reduce the percentage error caused by reading small values of the integrator area.

Procedure for Liquid Analysis

Liquid samples were obtained by flushing the 1 µl syringe several times with sample and then drawing some sample into the syringe. The sample was injected into the upper chromatograph column through the rubber septum in the injection port. The hot injection port immediately vaporized the sample, which was swept into the column by the carrier gas.

Separation of all components, except methanol, was accomplished at 140°C, with the temperature being stepped to 165°C four minutes after the water peak. This temperature jump speeded the analysis for formic acid, which still

required almost 13 minutes. To separate the water and methanol peaks, it was necessary to run the analysis again at a lower temperature, 85°C.

In a manner similar to the gas analyses, the first run of each of the two liquid analyses was made on automatic attenuation. At least two additional runs were made at each temperature level on manual attenuation.

Calibration

Gas sample calibration samples were made manometrically in 4.6 liter steel bottles. Measured amounts of the different gases were mixed to a maximum pressure of 3.2 atmospheres. Liquid calibration samples, with a total mass of up to 42 grams, were measured gravimetrically on an Ainsworth Type 10 single pan balance.

It was attempted originally to calibrate the chromatograph by using either peak heights or the product of the peak height and the peak half-width for each peak. Either method would have made the analyses much easier, since the automatic attenuator could be used for all runs with the first method and for most of the runs using the second. However, there was enough variation in calibration for successive runs on the same sample that both methods were discarded.

Reproducible results were obtained, though, when the Disc integrator was used. All samples were run a minimum of three times each to determine the area ratio of each peak to

that of the major peak in the sample. All calibration samples were made so that the major component was methane for the gas samples and water for the liquid samples, as would be found in the actual analyses. The calibration curves are shown in Appendix B.

Identification of the component peaks was made by comparing the elution time to the known sample elution time. If, during one of the liquid analyses, the identity of a peak was not certain, a small amount of the component in question was added to the next injection to see if a new peak was added or the questionable peak was enlarged. Known samples were analyzed occasionally to determine if the column retention times had changed and to check calibration.

The chemicals used for calibration and for feed preparation were as follows:

Oxygen: Linde Division of Union Carbide, 99.5 mole percent minimum purity

Methane: Phillips Petroleum Company, pure grade, 99 mole percent minimum

Nitrogen: Linde Division of Union Carbide, dry grade, 99.7 mole percent minimum

Carbon Dioxide: Matheson Company, Coleman instrument grade, 99.99 percent

Carbon Monoxide: Matheson Company, C.P. grade, 99.5 percent

Dimethyl Ether: Matheson Company, 99.87 percent typical purity

Ethane: Matheson Company, C.P. grade, 99.0 percent minimum

Hydrogen: Linde Division of Union Carbide, 99.5 percent

Methanol: J. T. Baker Chemical Corp., Absolute, 99.8 percent

Formaldehyde: Baker Chemical Campany, 36.2 percent, (12 percent methanol preservative in water)

Formic Acid: Mallinckrodt Chemical Works, 88.0 percent minimum in water

Ethyl Alcohol: U.S. Industrial Chemicals Company, U.S.P. grade, absolute

Methyl Formate: Matheson, Coleman, and Bell, practical grade

Acetone: Baker and Adamson, 99.5 percent minimum

Acetic Acid: Fisher Scientific Company, 80-82 percent solution in water

The Chromatograph carrier gas was:

Helium: Linde Division of Union Carbide, 99.99 percent pure.

CHAPTER VII

PROPOSED HIGH PRESSURE MECHANISM FOR METHANE OXIDATION

The kinetics and mechanism of methane oxidation have been studied since the late nineteenth century. Originally, the reason for establishing any mechanism was to determine how the reaction proceeded. Later, more utilitarian motives developed, such as using a "proven" mechanism for one reaction to predict how another reaction should occur or to find ways to alter the course of a reaction to obtain specific products.

A complete mechanism must show a chemically logical sequence of steps to form intermediate and final products. Thus, it can be used to determine the relative amounts of each of the products. Other distinctive aspects of the kinetic study can be explained from the mechanism, such as the cool flame phenomena, wall effects, and the negative temperature coefficients for hydrocarbon oxidation.

An almost unlimited number of mechanistic theories are possible for a reaction when there are little or no accurate kinetic data available. Obtaining "accurate" kinetic data for a reaction can be much more difficult than it might seem, depending on the reaction being studied. According to

Trotman-Dickenson (91) the following features are desirable for an accurate study of a gas phase reaction:

1. The reaction should be clean and free from chain reactions and side reactions at all pressures.
2. The reaction should be studied over a wide pressure range.
3. No heterogeneous reactions should take place as such reactions mask energy transfer at low pressure.
4. The products of the reaction should be detectable, even in trace concentrations.

Thus, the study must determine the effect of reactant concentration, diluent concentration, temperature, and time.

Unfortunately, the oxidation of methane meets only one of the four requirements for a good kinetic study, i.e., the reaction can be studied over a wide pressure range. It is known that the reaction has a free radical mechanism, which indicates that heterogeneous reactions can be controlling. Also, for most radical reactions, the concentration of the radicals is so minute that they may not be detected. Depending on the relative concentrations of the reactants, side reactions may confuse the determination of which specie is produced first.

An additional complication was explained by Johnston (53) in what he referred to as the Uncertainty Principle of Reaction Mechanisms. This principle states that, if there are more than two free radicals formed in a reaction, the mechanism

cannot be determined by analyzing only the reactants and products since there would be more elementary reactions than can be observed from the products. However, for reactions that do have more than two free radicals, much can be done to clarify the reaction mechanism (53), including:

1. Spectroscopic observation of the intermediate free radicals.
2. Separate study of some of the elementary reactions in simpler systems.
3. Evaluation of thermodynamic properties of the intermediates.
4. Quantitative application of gas phase reaction rate theories.

It is not unusual for reaction mechanisms to have several different radicals postulated. Semenov's low pressure mechanism for methane oxidation (83) included four different radicals. Ingold and Bryce (52) experimentally detected seven different free radicals in a low pressure methane oxidation study.

Even though it is desirable to write a complete description of the oxidation process, such a complete answer could be very cumbersome for general hydrocarbon oxidation. Provision must be made for low pressure formation of hydrogen, while no hydrogen is found at high pressures. At high temperatures, olefins are formed; they are not produced at low temperatures. The mechanism needs to show a change from peroxide formation to aldehyde formation with increasing temperature

in the middle temperature range. It must also explain the carbon dioxide paradox for methane oxidation, in that at low pressure carbon dioxide is not found or is only formed long after carbon monoxide, while at high pressure it is found earlier than carbon monoxide.

This present study has been limited to a kinetic description of uncatalyzed methane oxidation by molecular oxygen at elevated pressures. An attempt has been made to describe the formation of all oxygenated compounds containing a single carbon-atom chain found in the reaction products at these pressures. More work needs to be done to describe the formation of compounds containing carbon chains of two or more atoms. As neither hydrogen nor olefins have been found in the high pressure studies, provision for these products has not been included in this study.

The proposed high pressure mechanism for methane oxidation is listed below. With the exception of reactions forming hydrogen, this mechanism also encompasses the reaction at low pressures.

G-0 $CH_4 + O_2 \leftrightarrow CH_3\cdot + HO_2\cdot$

G-1 $O_2 + CH_3\cdot \leftrightarrow CH_3OO\cdot$

G-2 $CH_3OO\cdot \leftrightarrow [\cdot CH_2OOH] \leftrightarrow HCHO + \cdot OH$

G-3 $CH_4 + CH_3OO\cdot \leftrightarrow CH_3\cdot + CH_3OOH$

3a $HCHO + CH_3OO\cdot \leftrightarrow HCO\cdot + CH_3OOH$

G-4 $CH_3OOH \leftrightarrow CH_3O\cdot + \cdot OH$

4a $HCHO + O_2 \leftrightarrow HCO\cdot + HO_2\cdot$

4b $H_2O_2 \leftrightarrow \cdot OH + \cdot OH$

G-5 $CH_4 + CH_3O\cdot \leftrightarrow CH_3\cdot + CH_3OH$

5a $CH_4 + \cdot OH \leftrightarrow CH_3\cdot + H_2O$

5b $CH_4 + HO_2\cdot \leftrightarrow CH_3\cdot + H_2O_2$

5c $CH_4 + HCO\cdot \leftrightarrow CH_3\cdot + HCHO$

5d $CH_4 + \cdot COOH \leftrightarrow CH_3\cdot + HCOOH$

G-6 $O_2 + CH_3O\cdot \leftrightarrow HO_2\cdot + HCHO$

6a $O_2 + HCO\cdot \leftrightarrow HO_2\cdot + CO$

6b $O_2 + HCO\cdot \longleftrightarrow [HC(=O)OO\cdot \leftrightarrow \cdot OC(=O)OH] \longleftrightarrow CO_2 + \cdot OH$

G-7 $HCHO + CH_3O\cdot \leftrightarrow HCO\cdot + CH_3OH$

7a $HCHO + \cdot OH \leftrightarrow HCO\cdot + H_2O$

7b $HCHO + HO_2\cdot \leftrightarrow HCO\cdot + H_2O_2$

7c $HCHO + \cdot COOH \leftrightarrow HCO\cdot + HCOOH$

G-8 $CO + HO_2\cdot \leftrightarrow CO_2 + \cdot OH$

8a $CO + \cdot OH \leftrightarrow \cdot COOH$

G-9 $CH_3OH + \cdot OH \leftrightarrow CH_3O\cdot + H_2O$

9a $CH_3OH + HO_2\cdot \leftrightarrow CH_3O\cdot + H_2O_2$

G-10 $H_2O_2 + \cdot OH \leftrightarrow HO_2\cdot + H_2O$

10a $H_2O_2 + CH_3\cdot \leftrightarrow \cdot OH + CH_3OH$

G-11 $HCO\cdot + HO_2\cdot \leftrightarrow CO + H_2O_2$

11a $CH_3O\cdot + HCO\cdot \leftrightarrow HCHO + HCHO$

11b $CH_3O\cdot + CH_3O\cdot \leftrightarrow CH_3OH + HCHO$

11c $HO_2\cdot + HO_2\cdot \leftrightarrow H_2O_2 + O_2$

11d $CH_3O\cdot + HO_2\cdot \leftrightarrow HCHO + H_2O_2$

G-12 $CH_3\cdot + \cdot OH \longleftrightarrow CH_3OH$

12a $HCO\cdot + \cdot OH \longleftrightarrow HCOOH$

12b $HCO\cdot + CH_3O\cdot \longleftrightarrow CH_3OOCH$ (MF)

12c $CH_3\cdot + CH_3\cdot \longleftrightarrow C_2H_6$

G-13 Radical $\xrightarrow{\text{wall}}$ Termination

(In the body of this paper, the reverse reaction of Reaction G-1 shall be referred to as G-M1. Similar nomenclature shall apply to the other reactions.)

The proposed mechanism appears to be very unwieldy at first glance. However, the equations listed actually belong to a relatively small number of reaction types in which the reactions are generally grouped. The mechanism starts with an initiation reaction, G-0, which initially produces all of the free radicals. There is a series of reactions, G-1, G-2, G-3, and G-3a, necessary to build up the concentration of intermediate molecules and radicals during the induction period. Reactions G-4, G-4a, and G-4b are degenerate branching reactions which increase the radical concentration during the main part of the reaction. There are several groups of propagation reactions, Groups G-5 through G-10, between a molecule and a radical with each group containing a different parent molecule. There are several groups of radical destruction reactions, Groups G-11, G-12, and G-13, to show radical disproportionation, termination, and wall capture.

There are significant differences between this mechanism and the low pressure mechanism presented by Semenov (83). The foregoing high pressure mechanism assumes the formation of methyl hydroperoxide, CH_3OOH, in addition to formaldehyde, HCHO, as a degenerate branching intermediate. Reactions are necessary to show the formation of products not considered by Semenov, particularly methanol, formic acid, and methyl formate. The possibility of gas phase radical combinations and disproportionations not covered by the low pressure mechanism are discussed.

Semenov (83), in discussing his reaction S-1

$$\text{(S-1)} \qquad CH_3\cdot + O_2 \rightarrow HCHO + OH\cdot$$

observed that the reaction was too complicated to be an elementary reaction and must be made up of at least two reactions, such as Reactions G-1 and G-2 shown above in the proposed high pressure mechanism. However, he calculated that at the high temperatures necessary for oxidation at atmospheric pressure, about 700°K, Reaction G-2 followed Reaction G-1 so rapidly that the methyl hydroperoxide radical disappeared as fast as it was formed. This conclusion explained the fact that formaldehyde was the only intermediate found in atmospheric pressure reactions. At lower temperatures, however, the rate constant for Reaction G-2 is much smaller due to a large activation energy for isomerization. It is then possible that the hydroperoxide radical will exist long enough to

react with other molecules. Reactions G-3 and G-3a are likely examples of such a reaction.

It has been postulated (31, 81, 94) that hydroperoxide molecules, instead of aldehyde molecules, are controlling in low temperature gas phase or liquid phase hydrocarbon oxidations. Since the oxidation temperatures and densities in high pressure studies are about midway between the high temperature, atmospheric pressure gas phase studies and the liquid phase studies, one might expect that the reactions in the high pressure studies might consist of a mixture of the extreme cases, so that Reactions G-2, G-3, and G-3a may occur simultaneously. This assumption does explain the reaction products found at high pressures.

All of the reactions in Groups G-5 to G-10 are propagation reactions of radicals grouped with one of the major molecules. It can be seen, however, that several of the reactions at the first of the mechanism and several of the reverse reactions could be associated with these groups. It can also be seen that there are several sets of reactions with competing transition states from the collision of the same two reactants, such as Reactions (1) G-M6, G-7b; (2) G-7a, G-M2; (3) G-6a, G-6b; and (4) G-M5b, G-10a. For each of these sets, the competing transition states would be

(1) 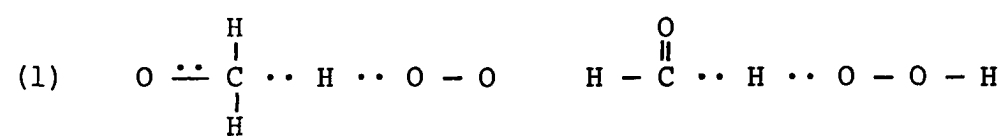

(2) 

(3) 

(4) 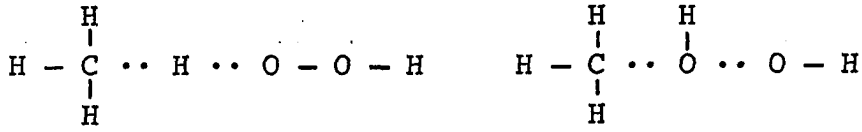

The dominating transition state is determined mainly by the energetics of the reaction, but the probability of the proper orientation and other outside effects also influence the result.

Although several mechanisms have shown the formation of hydrogen peroxide (43, 49, 83), and its existence has been proven (52, 85), it has seldom been reported as a reaction product. Since hydrogen peroxide is known to be relatively unstable, it is logical to assume that at reaction temperatures, it reacts to form other products. The early mechanisms either ignored hydrogen peroxide destruction or lumped it into a reaction of the type

(R-13) $H_2O_2 \xrightarrow{\text{surface}}$ chain breaking

Hardwicke (42), in trying to keep the reaction stoichiometrically simple, described this reaction as

(R-14) $2\ H_2O_2 \xrightarrow{\text{wall}} 2\ H_2O + O_2$

while Hardwicke, Lott, and Sliepcevich (43) considered the

same type equation to be a gas phase reaction. None of these approaches should control the destruction of the peroxide at extreme pressures as wall reactions should be minimal and the postulated gas phase reaction is too complicated to be considered elementary.

Hoare and his co-workers (49, 50) have shown that homogeneous decomposition of hydrogen peroxide predominates at low pressure and high temperatures, above 420°C. Their conclusions for this decomposition is shown in the present mechanism as Reactions G-4b, G-10 and G-11c. These reactions, when added together, yield the same overall result as shown in Reaction HLS-13. The possibility also exists that hydrogen peroxide can react similar to other molecules to form products other than water and oxygen. Reactions G-10a and G-M9a show examples of this type of reaction to form methanol.

Once a radical is formed, some method must exist for it to terminate. Reaction Groups G-11, G-12 and G-13 show equations for such reaction types as disproportionations, terminations, and wall capture. Again, orientation and other effects may determine which of the two gas phase reactions take place. Since the activation energy of either reaction type is low and the radicals are very reactive, radical destruction takes place at almost every collision between two radicals (10). Neither Group G-11 nor G-12 is an exhaustive list of the possible reactions. Only those reactions which explain formation of known products have been included above.

As will be shown later, however, addition of these radical destruction reactions does not change most calculated molecular concentrations appreciably. Even though the rate constants for these reactions are much larger than the constants for propagation reactions, the number of molecules formed by termination reactions is small in comparison, due to the low radical concentration. These radical destruction equations are important, however, to show that the radical concentration does not continually increase.

Equation Group G-13 is put forward with little clarification. This equation describes the generally accepted method of radical termination at low pressures or at high surface to volume ratios. The reactant can be any radical in the system. Little can be said about the stable products of a wall termination due to the many factors involved.

CHAPTER VIII

METHOD OF MECHANISM ANALYSIS

The earliest explanation of oxidation mechanisms were qualitative attempts to determine at least one equation to show the formation of each product. Little kinetic data were available to check these theories. Later experimenters, notably Norrish (70) and Semenov (83), mathematically solved their mechanism equations to find reaction rates and compared their results to experimental behavior. In most cases, however, many overly simplifying assumptions were necessary and the only rate that was analyzed was that of the chief constituent, methane.

Several problems arose from this simplified treatment. Semenov (83) assumed that the formaldehyde concentration was constant, although his graphical results showed the concentration decreasing with time after the maximum. Several terms were eliminated from the analysis based on the assumption that the different radical concentrations were within an order of magnitude of each other, thus some terms were smaller than others in the methane equation. These assumptions were necessary to arrive at a simplified answer.

Another of the limitations of Semenov's analysis (83) was that all of the reactions were considered to be nonreversible. This assumption was necessary in his analysis to allow all of the radical concentration equations to be solved independently of each other, even though many of the reactions are now known to be reversible.

Semenov's mechanism (83) satisfactorily described methane consumption for a low pressure reaction, but it does not apply to high pressure studies where additional products are formed. Also, the methane consumption equation, Equation 2-2, is not particularly important in methane rich reaction mixtures since the methane concentration hardly changes. While many of the reactions in Semenov's analysis could be neglected to obtain a reasonable equation for methane consumption, these same reactions are essential to account for the formation of other products.

General

The first step in any analysis consists of writing the equations for all possible reactions that could apply to the mechanism. All varieties of elementary reactions should be considered, such as radical initiation, transfer, isomerization, disproportionation, decomposition, termination, and molecular reactions. Previous studies can be very useful as a starting point for this step.

The elementary reactions postulated should be at least chemically feasible and should be considered to be reversible unless known otherwise. One helpful rule of thumb for elementary reactions is that the most complicated reaction consists of a maximum of two bonds breaking and two bonds forming, as in a four-center reaction (22). Another aspect to be considered is the Rice-Teller Principle of Least Motion (79), which states that for the activation energy of a reaction to be as low as possible, the atoms must not move about any more than necessary.

Rate constants for the elementary reactions can be a problem for reactions other than low pressure gas phase reactions. For gas phase reactions, order of magnitude estimates are possible. Ideal gas phase reactions, approximated by low pressure reactions, can be controlled only by concentration effects. However, the rate constant for non-ideal reactions, particularly high density reactions, is much more difficult to determine because the reaction can be controlled by molecular interaction, rather than reactant concentrations.

If the reaction being analyzed is considered to be isothermal and at constant volume, the problem can be solved directly. Otherwise, equations for pressure and temperature must be included. If the reaction is such that transport needs to be considered, the system can be divided and considered as many small reactors, with interaction between them.

This modification greatly magnifies the problem, and in all but extremely simple cases, makes a solution almost impossible.

For constant volume, isothermal reactions with no transport, all that is necessary are the simultaneous, first order partial differential equations describing the formation and consumption of each specie with the appropriate initial concentrations of the reactants. There are many computational schemes to solve such problems, but most of them require a prohibitively large amount of computer time and are also unstable when used with kinetic studies (27). For precise work Edelson (27) recommended using a modification of Nordsieck's predictor-corrector technique, as described by Gear (37). For initial work a much simplier technique is preferred, such as the rectangular integration (51) used in this paper.

A numerical analysis similar to that used in this study was made by Allara (1) for oxidation of butane, isobutane, and isopentane in vapor and liquid phases and at temperatures of 100° to 155°C. Allara considered a simplified mechanism with irreversible reactions. Unfortunately the integration technique used was not discussed in the paper.

Analysis

Differential equations describing the formation and destruction of each chemical specie with respect to time were obtained from the mechanism by using the traditional kinetic definition of the Law of Mass Action, that of the rate of

formation of a product equalling the product of the concentrations of the reactants multiplied by a rate constant for the reaction. The differential equations are listed below. The terms, Kx and KMx, in the equations refer to the rate constants for a forward reaction and a reverse reaction respectively, where x represents the number of the reaction being considered.

The following partial differential equations describe the formation and destruction of each molecular specie:

$$\frac{\partial(CH_4)}{\partial t} = (CH_3\cdot)[KM0(HO_2\cdot) + KM3(CH_3OOH) + KM5(CH_3OH) + KM5a(H_2O) + KM5b(H_2O_2) + KM5c(HCHO) + + KM5d(HCOOH)] - (CH_4)[K0(O_2) + K3(CH_3OO\cdot) + K5(CH_3O\cdot) + K5a(\cdot OH) + K5b(HO_2\cdot) + K5c(HCO\cdot) + K5d(\cdot COOH)] \quad (8\text{-}1)$$

$$\frac{\partial(O_2)}{\partial t} = (HO_2\cdot)[KM0(CH_3\cdot) + KM4a(HCO\cdot) + KM6(HCHO) + KM6a(CO) + KM11c(HO_2\cdot)] + KM1(CH_3OO\cdot) + KM6b(CO_2)(\cdot OH) - (O_2)[K0(CH_4) + K1(CH_3\cdot) + K4a(HCHO) + K6(CH_3O\cdot) + (HCO\cdot)(K6a + K6b) + KM11c(H_2O_2)] \quad (8\text{-}2)$$

$$\frac{\partial(CH_3OOH)}{\partial t} = (CH_3OO\cdot)[K3(CH_4) + K3a(HCHO)] + KM4(CH_3O\cdot)(\cdot OH) - (CH_3OOH)[KM3(CH_3\cdot) + KM3a(HCO\cdot) + K4] \quad (8\text{-}3)$$

$$\frac{\partial(HCHO)}{\partial t} = (HCO\cdot)[KM3a(CH_3OOH) + KM4a(HO_2\cdot) + K5c(CH_4) + KM7(CH_3OH) + KM7a(H_2O) + KM7b(H_2O_2) + KM7c(HCOOH)] + K2(CH_3OO\cdot) + (CH_3O\cdot)[K6(O_2) + 2(K11a)(HCO\cdot) + K11b(CH_3O\cdot) + K11d(HO_2\cdot) - (HCHO)[(\cdot OH)(KM2 + K7a) + K3a(CH_3OO\cdot) + K4a(O_2) + KM5c(CH_3\cdot) + (HO_2\cdot)(KM6 + K7b) + K7(CH_3O\cdot) + K7c(\cdot COOH) + 2(KM11a)(HCHO) + KM11b(CH_3OH) + KM11d(H_2O_2)] \quad (8\text{-}4)$$

$$\frac{\partial(H_2O_2)}{\partial t} = (\cdot OH)[KM4b(\cdot OH) + KM10a(CH_3OH)] + (HO_2\cdot)[K5b(CH_4) + K7b(HCHO) + K9a(CH_3OH) + KM10(H_2O) + K11(HCO\cdot) + K11c(HO_2\cdot) + K11d(CH_3O\cdot)] - (H_2O_2)[K4b + (CH_3\cdot)(KM5b + K10a) + KM7b(HCO\cdot) + KM9a(CH_3O\cdot) + K10(\cdot OH) + KM11(CO) + KM11c(O_2) + KM11d(HCHO)] \quad (8\text{-}5)$$

$$\frac{\partial(CO)}{\partial t} = (HCO\cdot)[K6a(O_2) + K11(HO_2\cdot)] + KM8(CO_2)(\cdot OH) + KM8a(\cdot COOH) - (CO)[(HO_2\cdot)(KM6a + K8) + K8a(\cdot OH) + KM11(H_2O_2)] \quad (8\text{-}6)$$

$$\frac{\partial(CO_2)}{\partial t} = K6b(HCO\cdot)(O_2) + K8(CO)(HO_2\cdot) - (CO_2)(\cdot OH)(KM6b + KM8) \quad (8\text{-}7)$$

$$\frac{\partial(HCOOH)}{\partial t} = (\cdot COOH)[K5d(CH_4) + K7c(HCHO)] + K12a(HCO\cdot)(\cdot OH) - (HCOOH)[KM5d(CH_3\cdot) + KM7c(HCO\cdot) + KM12a] \quad (8\text{-}8)$$

$$\frac{\partial(CH_3OH)}{\partial t} = (CH_3O\cdot)[K5(CH_4) + K7(HCHO) + KM9(H_2O) + KM9a(H_2O_2) + K11b(CH_3O\cdot)] + (CH_3\cdot)[K10a(H_2O_2) + K12(\cdot OH)] - (CH_3OH)[KM5(CH_3\cdot) + KM7(HCO\cdot) + (\cdot OH)(K9+KM10a) + K9a(HO_2\cdot) + KM11b(HCHO) + KM12] \quad (8-9)$$

$$\frac{\partial(MF)}{\partial t} = K12b(HCO\cdot)(CH_3O\cdot) - KM12b(MF) \quad (8-10)$$

$$\frac{\partial(C_2H_6)}{\partial t} = K12c(CH_3\cdot)(CH_3\cdot) - KM12c(C_2H_6) \quad (8-11)$$

$$\frac{\partial(H_2O)}{\partial t} = (\cdot OH)[K5a(CH_4) + K7a(HCHO) + K9(CH_3OH) + K10(H_2O_2)] - (H_2O)[KM5a(CH_3\cdot) + KM7a(HCO\cdot) + KM9(CH_3O\cdot) + KM10(HO_2\cdot)] \quad (8-12)$$

The following partial differential equations describe the formation and destruction of each different radical specie:

$$\frac{\partial(CH_3\cdot)}{\partial t} = A - (CH_3\cdot)B \quad (8-13)$$

where $A = (CH_4)[K0(O_2) + K3(CH_3OO\cdot) + K5(CH_3O\cdot) + K5a(\cdot OH) + K5b(HO_2\cdot) + K5c(HCO\cdot) + K5d(\cdot COOH)] + + KM1(CH_3OO\cdot) + KM10a(CH_3OH)(\cdot OH) + KM12(CH_3OH) + 2(KM12c)(C_2H_6)$

$B = KM0(HO_2\cdot) + K1(O_2) + KM3(CH_3OOH) + KM5(CH_3OH) + KM5a(H_2O) + (H_2O_2)(KM5b + K10a) + KM5c(HCHO) + KM5d(HCOOH) + K12(\cdot OH) + 2(K12c)(CH_3\cdot)$

$$\frac{\partial (CH_3O\cdot)}{\partial t} = C - (CH_3O\cdot)D \qquad (8\text{-}14)$$

where $C = K4(CH_3OOH) + (CH_3OH)[KM5(CH_3\cdot) + KM7(HCO\cdot) + K9(\cdot OH) + K9a(HO_2\cdot)] + (HCHO)[KM6(HO_2\cdot) + KM11a(HCHO) + 2(KM11b)(CH_3OH) + KM11d(H_2O_2)] + KM12b(MF)$

$D = KM4(\cdot OH) + K5(CH_4) + K6(O_2) + K7(HCHO) + KM9(H_2O) + KM9a(H_2O_2) + (HCO\cdot)(K11a + K12b) + 2(K11b)(CH_3O\cdot) + K11d(HO_2\cdot)$

$$\frac{\partial (CH_3OO\cdot)}{\partial t} = E - (CH_3OO\cdot)F \qquad (8\text{-}15)$$

where $E = (CH_3\cdot)[K1(O_2) + KM3(CH_3OOH)] + KM2(\cdot OH)(HCHO) + KM3a(CH_3OOH)(HCO\cdot)$

$F = KM1 + K2 + K3(CH_4) + K3a(HCHO)$

$$\frac{\partial (\cdot COOH)}{\partial t} = G - (\cdot COOH)H \qquad (8\text{-}16)$$

where $G = (HCOOH)[KM5d(CH_3\cdot) + KM7c(HCO\cdot)] + K8a(CO)(\cdot OH)$

$H = K5d(CH_4) + K7c(HCHO) + KM8a$

$$\frac{\partial (HCO\cdot)}{\partial t} = I - (HCO\cdot)J \qquad (8\text{-}17)$$

where $I = (HCHO)[K3a(CH_3OO\cdot) + K4a(O_2) + KM5c(CH_3\cdot) + K7(CH_3O\cdot) + K7c(\cdot COOH) + KM11a(HCHO)] + (HO_2\cdot)[KM6a(CO) + K7b(HCHO)] + (\cdot OH)[KM6b(CO_2) + K7a(HCHO)] + KM11(H_2O_2)(CO) + KM12a(HCOOH) + KM12b(MF)$

$$J = KM3a(CH_3OOH) + (HO_2\cdot)(KM4a + K11) + K5c(CH_4) + (O_2)(K6a + K6b) + KM7(CH_3OH) + KM7a(H_2O) + KM7b(H_2O_2) + KM7c(HCOOH) + (CH_3O\cdot)(K11a+K12b) + K12a(\cdot OH)$$

$$\frac{\partial(\cdot OH)}{\partial t} = L - (\cdot OH)M \qquad (8\text{-}18)$$

where $L = K2(CH_3OO\cdot) + K4(CH_3OOH) + 2(K4b)(H_2O_2) + (CH_3\cdot)[KM5a(H_2O) + K10a(H_2O_2)] + (HCO\cdot)[K6b(O_2) + KM7a(H_2O)] + (HO_2\cdot)[K8(CO) + KM10(H_2O)] + KM8a(\cdot COOH) + KM9(CH_3O\cdot)(H_2O) + KM12(CH_3OH) + KM12a(HCOOH)$

$$M = (HCHO)(KM2 + K7a) + KM4(CH_3O\cdot) + 2(KM4b)(\cdot OH) + K5a(CH_4) + (CO_2)(KM6b + KM8) + K8a(CO) + (CH_3OH)(K9 + KM10a) + K10(H_2O_2) + K12(CH_3\cdot) + K12a(HCO\cdot)$$

$$\frac{\partial(HO_2\cdot)}{\partial t} = N - (HO_2\cdot)P \qquad (8\text{-}19)$$

where $N = (O_2)[K0(CH_4) + K4a(HCHO) + K6(CH_3O\cdot) + K6a(HCO\cdot)] + (H_2O_2)[KM5b(CH_3\cdot) + KM7b(HCO\cdot) + KM9a(CH_3O\cdot) + K10(\cdot OH) + KM11(CO) + 2(KM11c)(O_2) + KM11d(HCHO)] + KM8(CO_2)(\cdot OH)$

$$P = KM0(CH_3\cdot) + (HCO\cdot)(KM4a + K11) + K5b(CH_4) + (HCHO)(KM6 + K7b) + (CO)(KM6a + K8) + K9a(CH_3OH) + KM10(H_2O) + 2(K11c)(HO_2\cdot) + K11d(CH_3O\cdot)$$

Using the same technique as Semenov (83), steady-state was assumed for the radical concentration equations, so that these derivatives from Equations 8-13 to 8-19 for the radical concentrations were set equal to zero. The radical specie differential equations then degenerated into algebraic equations. Using the nomenclature from above, the radical concentrations were found to be

$$(CH_3\cdot) = A / B \qquad (8\text{-}20)$$

$$(CH_3O\cdot) = C / D \qquad (8\text{-}21)$$

$$(CH_3OO\cdot) = E / F \qquad (8\text{-}22)$$

$$(\cdot COOH) = G / H \qquad (8\text{-}23)$$

$$(HCO\cdot) = I / J \qquad (8\text{-}24)$$

$$(\cdot OH) = L / M \qquad (8\text{-}25)$$

$$(HO_2\cdot) = N / P \qquad (8\text{-}26)$$

It was found during the course of this study that the steady-state approximation was also necessary for the methyl hydroperoxide molecule concentration. By setting the derivative of the methyl hydroperoxide concentration equal to zero, the concentration of the hydroperoxide was found from Equation 8-3 to be

$$(CH_3OOH) = \frac{(CH_3OO\cdot)\,[K3\,(CH_4) + K3a\,(HCHO)] + KM4\,(CH_3O\cdot)\,(\cdot OH)}{KM3\,(CH_3\cdot) + KM3a\,(HCO\cdot) + K4} \qquad (8\text{-}27)$$

For the purpose of developing the equations listed above, the overall reaction was considered to be isothermal and isochoric with negligible transport. Therefore, wall terminations reactions were ignored. Reactions that might require a collision with any other molecule to add or remove excess energy were considered to proceed without the collision. This assumption was justified in that at the pressures being considered, extraneous collisions should be occurring almost continuously. The two reactions that were assumed to be series reactions, Reactions G-2 and G-6b, were considered to be simple reactions with no intermediate equilibrium. This assumption was necessary as no information was available to determine either rate constants for the individual reactions or concentrations for the intermediate radicals.

It is recognized that the neglect of wall terminations is a serious limitation to the analysis. This simplification was necessary, however, since no information is, as yet, available on what actually occurs at the wall.

Since rate constants were not available for most of the reactions, they had to be estimated using the Arrhenius equation

$$k = Ae^{-E/RT} \tag{8-28}$$

where k is the rate constant, E is the activation energy, and A is the pre-exponential factor. These factors were estimated

by one of several methods. Activation energies for exothermic, molecular reactions were estimated using the Hirschfelder Rule (47), which states that the activation energy is approximately equal to 28 percent of the sum of the bond energies of the ruptured bonds. Activation energies for radical-molecule reactions were estimated using Semenov's results (83) based on the Polanyi relation. Semenov found that for exothermic reactions

$$E = 11.5 - 0.25\,|q| \tag{8-29}$$

while for endothermic reactions

$$E = 11.5 + 0.75\,|q| \tag{8-30}$$

where q is the heat of reaction. The activation energies of exothermic radical-radical combinations were assumed to be equal to zero; conversely, the activation energy of an endothermic molecular decomposition into radicals was set equal to the heat of decomposition. Values of pre-exponential factors for several different types of reactions were found in the literature and are tabulated in Table 1.

This approach for estimating the rate constants assumes that the high density gas phase reactions are similar to the low density reactions. This model should be correct to the point where the high density gas starts acting more like a liquid than a gas.

Values of the rate constants were calculated from Equation 8-28 for each of the forward and reverse reactions

For the purpose of developing the equations listed above, the overall reaction was considered to be isothermal and isochoric with negligible transport. Therefore, wall terminations reactions were ignored. Reactions that might require a collision with any other molecule to add or remove excess energy were considered to proceed without the collision. This assumption was justified in that at the pressures being considered, extraneous collisions should be occurring almost continuously. The two reactions that were assumed to be series reactions, Reactions G-2 and G-6b, were considered to be simple reactions with no intermediate equilibrium. This assumption was necessary as no information was available to determine either rate constants for the individual reactions or concentrations for the intermediate radicals.

It is recognized that the neglect of wall terminations is a serious limitation to the analysis. This simplification was necessary, however, since no information is, as yet, available on what actually occurs at the wall.

Since rate constants were not available for most of the reactions, they had to be estimated using the Arrhenius equation

$$k = Ae^{-E/RT} \qquad (8\text{-}28)$$

where k is the rate constant, E is the activation energy, and A is the pre-exponential factor. These factors were estimated

by one of several methods. Activation energies for exothermic, molecular reactions were estimated using the Hirschfelder Rule (47), which states that the activation energy is approximately equal to 28 percent of the sum of the bond energies of the ruptured bonds. Activation energies for radical-molecule reactions were estimated using Semenov's results (83) based on the Polanyi relation. Semenov found that for exothermic reactions

$$E = 11.5 - 0.25\,|q| \qquad (8\text{-}29)$$

while for endothermic reactions

$$E = 11 \qquad (8\text{-}30)$$

where q is the heat of re energies of exothermic radical-radic ned to be equal to zero; conversel of an endothermic molecular decompos s set equal to the heat of decomposition. exponential factors for several different types of reactions were found in the literature and are tabulated in Table 1.

This approach for estimating the rate constants assumes that the high density gas phase reactions are similar to the low density reactions. This model should be correct to the point where the high density gas starts acting more like a liquid than a gas.

Values of the rate constants were calculated from Equation 8-28 for each of the forward and reverse reactions

TABLE 1

REACTION PRE-EXPONENTIAL FACTORS

Reaction	log A $(\ell/mole)^{-1}$ sec^{-1}	n	Reference
Molecular Reactions			
Unimolecular Decomposition	11.5 - 15	1	90
Bimolecular Reaction	7 - 10	2	95
Trimolecular Reaction	7 - 10	3	95
Radical Reactions			
Radical Transfer Reactions	8 - 10	2	10
Radical Disproportionation	10	2	77
Radical Decomposition	13 - 16	1	13
Radical Isomerization	13 - 16	1	13
Radical Terminations*	8 - 11	2	13

*Small radicals tend to have high values for pre-exponential terms; larger radicals tend to have lower values due to steric hinderance (13).

listed in the proposed mechanism. The activation energies and pre-exponential factors used in this study are tabulated in Table 2. The Arrhenius parameters were, for the most part, calculated as stated previously. However, literature values were used for the rate constants of several reactions. A tabulation of Arrhenius parameters taken from the literature is given in Tables 3A and 3B.

The only preliminary steps remaining before the analysis was completed was specifying the initial concentrations of the reactants, selecting the time parameters for the integration, and choosing which integration scheme to use.

The initial reactant concentrations were fixed in the following manner: The reaction pressure was selected. The reaction temperature was chosen to be in the reaction range, as shown in Figure 10. The compressibility factor was determined iteratively, using the Benedict-Webb-Rubin (BWR) equation of state, as described by Bauerle (9). The reaction mixture was considered to be entirely methane for this computation, rather than using mixing rules to estimate the BWR constants at the reaction composition. Since most of the work in this study was at pressures below 1000 atm, low pressure BWR constants were used rather than Bauerle's high pressure constants. The initial concentrations of methane and oxygen were then set at fixed compositions, normally at 8 percent oxygen and 92 percent methane. The concentrations of all other molecules and all radicals were initialized at zero.

TABLE 2

TERMS USED IN ESTIMATING RATE CONSTANTS

No.	Reaction	ΔH* kcal/mole	Forward Reaction E kcal/mole	Forward Reaction log (A)	Reverse Reaction E kcal/mole	Reverse Reaction log (A)
0	$CH_4 + O_2 \rightarrow CH_3\cdot + HO_2\cdot$	+56.9	55.0	10.0	0	10.0
1	$CH_3\cdot + O_2 \rightarrow CH_3OO\cdot$	-27.3	0	7.48	27.0	15.0**
2	$CH_3OO\cdot \rightarrow HCHO + \cdot OH$	-25.0	20.0	10.3**	39.0	10.0
3	$CH_3OO\cdot + CH_4 \rightarrow CH_3OOH + CH_3\cdot$	+14.3	22.0	8.0	8.0	10.0
3a	$CH_3OO\cdot + HCHO \rightarrow CH_3OOH + HCO\cdot$	- 2.7	8.2	8.0	21.3	10.0
4	$CH_3OOH \rightarrow CH_3O\cdot + \cdot OH$	+35.7	32.0	10.6**	0	8.0
4a	$HCHO + O_2 \rightarrow HCO\cdot + HO_2\cdot$	+39.9	44.0	10.0	0	10.0
4b	$H_2O_2 \rightarrow 2\ \cdot OH$	+51.4	50.0	15.0**	0	10.0
5	$CH_4 + CH_3O\cdot \rightarrow CH_3\cdot + CH_3OH$	+ 0.4	11.8	9.78	11.4	10.0
5a	$CH_4 + \cdot OH \rightarrow CH_3\cdot + H_2O$	-15.3	5.9	11.0	23.0	8.0
5b	$CH_4 + HO_2\cdot \rightarrow CH_3\cdot + H_2O_2$	+14.3	22.3	9.7	8.0	10.0
5c	$CH_4 + HCO\cdot \rightarrow CH_3\cdot + HCHO$	+17.0	24.2	10.0	7.0	10.0
5d	$CH_4 + \cdot COOH \rightarrow CH_3\cdot + HCOOH$	+12.4	20.8	10.0	8.4	9.0

*Heat of formation data taken from Reference (12).

**Marked reactions are considered to be unimolecular [units of A = sec^{-1}]. All others are considered to be bimolecular [units of A = ℓ/(mole-sec)].

TABLE 2--Continued.

No.	Reaction	ΔH* kcal/mole	Forward Reaction E kcal/mole	Forward Reaction log (A)	Reverse Reaction E kcal/mole	Reverse Reaction log (A)
6	$O_2 + CH_3O\cdot \rightarrow HO_2\cdot + HCHO$	-26.2	4.9	9.3	31.0	8.7
6a	$O_2 + HCO\cdot \rightarrow HO_2\cdot + CO$	-28.6	4.3	11.6	33.0	6.0
6b	$O_2 + HCO\cdot \rightarrow \cdot OH + CO_2$	-91.9	0	7.3	90.0	8.0
7	$HCHO + CH_3O\cdot \rightarrow HCO\cdot + CH_3OH$	-16.6	7.4	10.0	23.0	10.0
7a	$HCHO + \cdot OH \rightarrow HCO\cdot + H_2O$	-32.3	3.4	10.0	35.7	8.0
7b	$HCHO + HO_2\cdot \rightarrow HCO\cdot + H_2O_2$	- 2.7	10.7	8.0	13.4	8.0
7c	$HCHO + \cdot COOH \rightarrow HCO\cdot + HCOOH$	- 4.6	10.4	8.0	15.0	10.0
8	$CO + HO_2\cdot \rightarrow CO_2 + \cdot OH$	-63.2	8.0	6.3	65.0	8.0
8a	$CO + \cdot OH \rightarrow \cdot COOH$	-34.0	0	9.3	34.0	14.0**
9	$CH_3OH + \cdot OH \rightarrow CH_3O\cdot + H_2O$	-15.7	7.6	10.0	23.3	10.0
9a	$CH_3OH + HO_2\cdot \rightarrow CH_3O\cdot + H_2O_2$	+13.9	22.0	10.0	8.1	10.0
10	$H_2O_2 + \cdot OH \rightarrow HO_2\cdot + H_2O$	-29.6	4.1	8.0	33.7	8.0
10a	$H_2O_2 + CH_3\cdot \rightarrow \cdot OH + CH_3OH$	-40.0	1.5	9.0	41.5	10.0
11	$HCO\cdot + HO_2\cdot \rightarrow CO + H_2O_2$	-71.2	0	10.0	71.0	8.0
11a	$CH_3O\cdot + HCO\cdot \rightarrow 2\ HCHO$	-66.1	0	9.0	66.0	8.0

*Heat of formation data taken from Reference (12).

**Marked reactions are considered to be unimolecular [units of A = sec^{-1}]. All others are considered to be bimolecular [units of A = ℓ/(mole-sec)].

TABLE 2--Continued.

No.	Reaction	ΔH* kcal/mole	Forward Reaction E kcal/mole	Forward Reaction log (A)	Reverse Reaction E kcal/mole	Reverse Reaction log (A)
11b	$2\ CH_3O\cdot \rightarrow CH_3OH + HCHO$	-82.7	0	7.0	82.7	8.0
11c	$2\ HO_2\cdot \rightarrow H_2O_2 + O_2$	-42.6	0	6.0	42.0	8.0
11d	$CH_3O\cdot + HO_2\cdot \rightarrow HCHO + H_2O_2$	-68.8	0	10.0	68.8	10.0
12	$CH_3\cdot + \cdot OH \rightarrow CH_3OH$	-91.4	0	9.9	91.4	15.0**
12a	$HCO\cdot + \cdot OH \rightarrow HCOOH$	-107.1	0	10.0	***	***
12b	$HCO\cdot + CH_3O\cdot \rightarrow CH_3OOCH$	-91.7	0	9.18	91.7	15.0**
12c	$2\ CH_3\cdot \rightarrow C_2H_6$	-88.2	0	9.95	88.2	15.0**
13	Radical $\xrightarrow{wall}$ Termination	--	--	--	--	--

*Heat of formation data taken from Reference (12).

**Marked reactions are considered to be unimolecular [units of A = sec^{-1}]. All others are considered to be bimolecular [units of A = ℓ/(mole-sec)].

***Activation energy is so large, rate constant was set equal to zero.

TABLE 3A

LITERATURE VALUES OF RATE CONSTANT FACTORS

No.	Reaction	E (kcal/mole)	log (A) $^{n-1}$ (ℓ/mole) sec^{-1}	Reference
0	$CH_4 + O_2 \rightarrow CH_3\cdot + HO_2\cdot$	55	10.8	83
1	$CH_3\cdot + O_2 \rightarrow CH_3OO\cdot$	2-3		85
			10.6 (3rd order)	8
		0	9.5 (3rd order)	12
		±0.5	10.9 (2nd order)	91
M1	$CH_3OO\cdot \rightarrow CH_3\cdot + O_2$	26	15.8 (2nd order)	46
2	$CH_3OO\cdot \rightarrow HCHO + \cdot OH$	36.5		12
	$ROO\cdot \rightarrow R'CHO + R''O\cdot$	20	13	85
3	$ROO\cdot + RH \rightarrow ROOH + R\cdot$	10	9	85
	$ROO\cdot + CH_4 \rightarrow ROOH + CH_3\cdot$		8	46
3a	$ROO\cdot + HCHO \rightarrow ROOH + HCO\cdot$		8	46
4	$ROOH \rightarrow RO\cdot + \cdot OH$	43	15	12
	$CH_3OOH \rightarrow CH_3O\cdot + \cdot OH$	32±5	11±2	13
4a	$HCHO + O_2 \rightarrow HCO\cdot + HO_2\cdot$	32	10.8	83
5	$CH_3O\cdot + CH_4 \rightarrow CH_3OH + CH_3\cdot$	11	8.6	39
			8.6	24
M5	$CH_3\cdot + CH_3OH \rightarrow CH_4 + CH_3O\cdot$	8.2	6.4	10
		8.2	7.6	77

TABLE 3A--Continued.

No.	Reaction	E (kcal/mole)	log (A) $(\ell/\text{mole})^{n-1}$ sec^{-1}	Reference
5a	$CH_4 + \cdot OH \rightarrow CH_3\cdot + H_2O$	2.6	10.9	39
		8.5		83
		8.5		88
			10.9	24
7	$HCHO + CH_3O\cdot \rightarrow HCO\cdot + CH_3OH$	3.0	7.1	46
7a	$HCHO + \cdot OH \rightarrow HCO\cdot + H_2O$	0.5		83
11b	$2\ CH_3O\cdot \rightarrow CH_3OH + HCHO$	0	10.5	12
11c	$2\ HO_2\cdot \rightarrow H_2O_2 + O_2$	0	9.3	6
12	$CH_3\cdot + \cdot OH \rightarrow CH_3OH$	0	9.6	13
12c	$2\ CH_3\cdot \rightarrow C_2H_6$	0	9.9	13

TABLE 3B

LITERATURE VALUES OF RELATIONSHIPS BETWEEN RATE CONSTANT TERMS

Relationships	Value	Reference
$E_{5b} - E_{7b}$	11	14, 83
$E_{5a} - E_{7a}$	6	83
k_{5a}/k_{5b}	30-40	49
k_{7b}/k_{8}	280	49

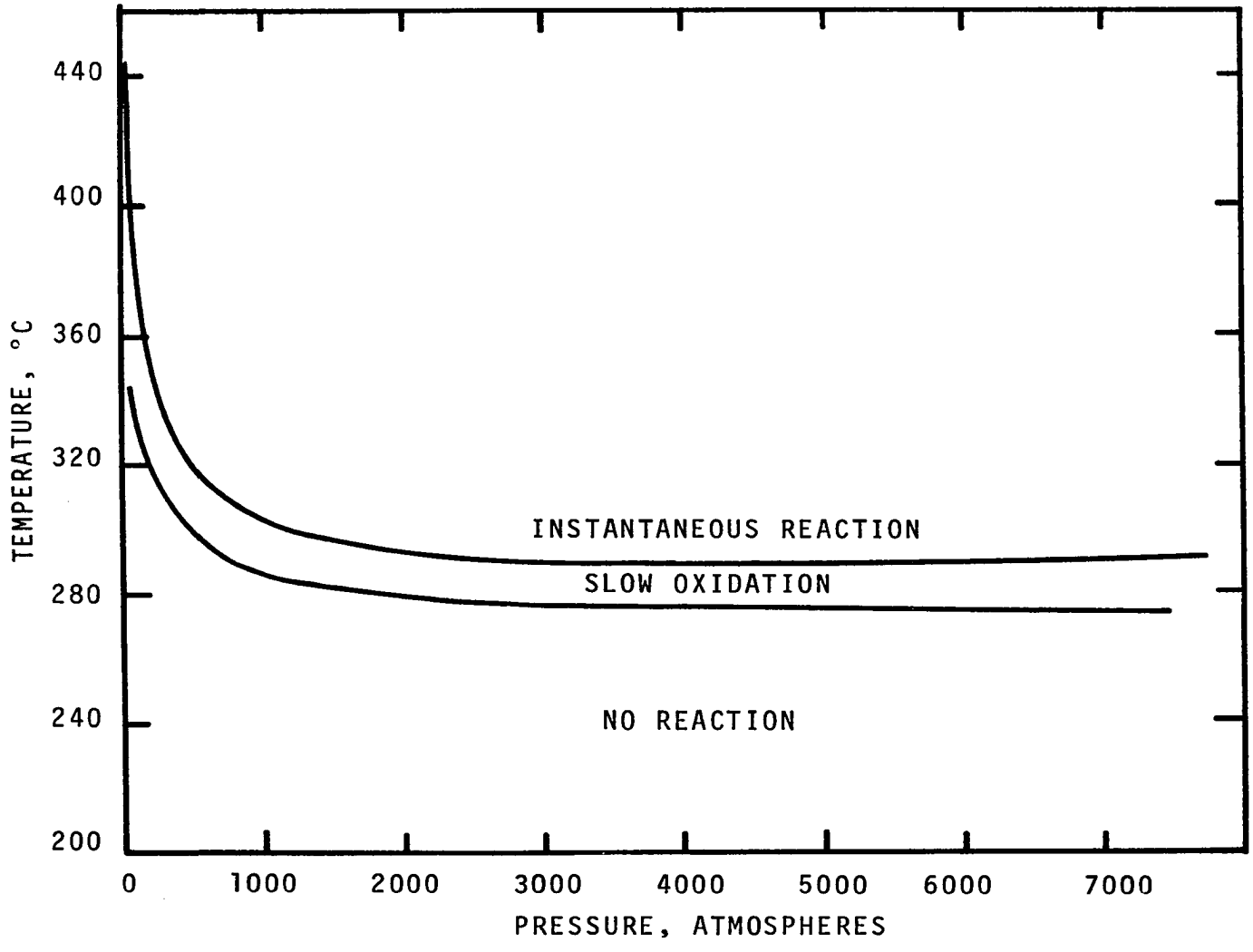

Figure 10. The Effect of Pressure and Temperature on the Region of Slow Oxidation for a Nominal 10:1 Methane-Oxygen Mixture. Data Compiled From Previous Investigators (9, 42, 60, 67).

The reaction time parameters to be selected were the simulated time of reaction and the number of integrations to be used in this time period. The simulated reaction time was normally set at thirty minutes. This time period was then divided into 18,000 equal parts, so that the simulated reaction was considered during intervals of 0.1 seconds. This 0.1 second interval was the step size for the integration.

Once these parameters had been chosen, the analysis could be made. The partial differential equations describing the molecule concentrations were integrated simultaneously on an IBM 360/50 digital computer. Several different integration methods were tried.

Problems with the integration technique plagued the early portion of this study. The first integration technique used was a double precision, fourth-order Runge-Kutta method. The integration was slow and unstable, often requiring several minutes of computer time for only a few iterations through the program cycle. Similar difficulties were later reported by Edelson (27) in similar studies. Since the time parameters selected required about 18,000 cycles through the program, this technique was abandoned in favor of a faster one. Several predictor-corrector methods were analyzed next, but they were passed over for initial studies because of computer time requirements.

A rectangular integration technique (51) was finally selected. This technique assumed that the derivative remains

constant during the step so that the equations can be integrated by multiplying the derivative at the start of the step by the integration step size. It was realized that this type of integration could lead to erroneous results, so a smaller step size was tried. These runs yielded approximately the same results as previous runs. This lack of variation in the results was attributed to a very slow change in concentration of all species. However, since 18,000 cycles through the program used approximately five minutes of computer time, reducing the step size a significant amount--while maintaining the total reaction time constant--required a very large amount of computer time. The previously specified step size was then considered to be reasonable for initial studies.

It was decided to investigate other integration techniques to determine if the rectangular integration was a large source of error. Both a trapezoidal rule and a Simpson's rule integration schemes were used in the analysis. Only very minor differences were observed between the computed results from the three integration methods. It was therefore concluded that little error was introduced using the crude rectangular integration technique.

The relatively large step size used, 0.1 seconds, did cause one problem. The integration of the methyl hydroperoxide CH_3OOH molecule concentration was not stable when a step size this large was used, especially early in the simulated

reaction. The basic problem was that while the methyl hydroperoxide was formed and destroyed very rapidly, its concentration was small. It was possible that during a long step, more molecules were calculated to be destroyed than were present at the start of the step, resulting in oscillating positive and negative concentrations. This problem can be solved by using smaller step sizes, but the difficulties with this solution have already been discussed.

The methyl hydroperoxide problem was finally eliminated in the following manner: It was realized that the methyl hydroperoxide behaved in the same way as the radicals in that it was formed and destroyed very rapidly, while its concentration remained extremely low and practically constant. Therefore, the steady state approximation was also applied to methyl hydroperoxide, so that its concentration and the radical concentrations were assumed to be constant during each integration step. The concentrations were allowed to vary from step to step according to the concentration changes of the molecules that formed them.

CHAPTER IX

RESULTS AND DISCUSSION

Results of Experimental Work

The slow oxidation of methane was studied experimentally in the pressure range of 1700 to 7000 atmospheres and temperatures of 230° to 310°C. As in previous studies (9, 42, 60), a methane-rich reaction mixture was used. The feed gas contained approximately 8.2 mole percent oxygen to keep the reaction mixture outside the explosive region. All of the experimental runs were essentially isothermal with the exception of two runs with instantaneous reactions. Equipment problems, however, permitted only a limited amount of data to be taken. Leakage from the reactor sideport, apparently caused by slippage of the inner liner in relation to the outer shell,* finally became so severe that the experimental program had to be terminated prematurely. A discussion of the vessel design and recommended repair is given in Appendix D.

The tabulated results of the experimental study are given in Appendix E. However, the percent conversion of the

---

*This shifting of the inner liner possibly occurred during Lott's final run (60), which was the only time the vessel had ever reached the design pressure of 13,600 atmospheres.

methane was far below that found by previous investigators (9, 42, 60). It is thought that the low conversion was due to an aromatic heating oil that had contaminated the reactor system prior to the first reported experimental run. The reactor electrode had fractured and had been blown out of the system twice during heated pressure tests, thereby leaving a direct opening into the reactor for oil bath vapor. Although the reactor was subsequently cleaned several times, the inability to remove the jammed bottom closure prevented an effective cleaning. The aromatic oil is thought to have acted as a radical scavenger, thus greatly slowing the reaction. Due to the questionable accuracy of this low conversion data and due to the limited amount of data that were obtained, only qualitative analysis of the data is possible.

Water and carbon dioxide were the two main products formed in the experimental runs, although methanol, formaldehyde, and carbon monoxide were formed in relatively large proportions. Relatively minor concentrations of ethanol and acetone were found on occasions, while formic acid was found during only one run at 3400 atm and 270°C. Other products that have been reported in previous studies (9, 60), such as methyl formate and acetic acid, were not found.

Analysis of the slow oxidation process was possible using data available from previous investigators (9, 42, 60, 67). Newitt and Haffner (67) studied the oxidation of an

8.1:1 molar methane to oxygen mixture at pressures from 50 to 150 atm. Lott (60), Hardwicke (42), and Bauerle (9) studied the oxidation of nominal 10:1 methane to oxygen mixtures, with Lott in the pressure range of 150 to 1000 atm, Hardwicke at 1000 to 6800 atm, and Bauerle from 100 to 750 atm. Newitt and Haffner, Lott, and Bauerle used external heating for their reactors, while Hardwicke used an internal heater wound on an alumina heater support. Hardwicke's experiments were made under essentially isothermal conditions, while the temperature in the runs conducted by Newitt and Haffner, Lott, and Bauerle normally increased to a maximum.

Additional high pressure oxidation data were not used, those of Lott (60) at pressures of 3,400 to 13,600 atm and Hardwicke (42) at pressures of 1000 to 6800 atm, both using an internal heater wound on a Pyrex heater support. Hardwicke observed that runs made using a Pyrex heater support were not reproducible, probably due to devitrification of the Pyrex. Hardwicke did not observe a similar change in reaction parameters when using an alumina heater core. One unusual aspect of Lott's Pyrex heater data was that his reaction temperatures were much lower than were possible in the other studies, possibly due to a catalytic effect of the Pyrex. Similar results of low reaction temperatures were found by Townsend (89) for ignition experiments carried out in a silica vessel.

When studying the slow oxidation of methane, it is of first importance to know the pressure-temperature domain of the slow oxidation reaction. Lott (60) showed the boundary of the instantaneous reaction domain for reactions with external heating. However, for many applications, it is necessary to know both the upper and lower limits to the region of slow oxidation. These limits were shown previously in Figure 10, using data from Newitt and Haffner (67), Bauerle (9), Hardwicke (42), and Lott (60) (data below 1000 atm only). The upper temperature limit at a given pressure is fairly obvious to the experimenter since the characteristic pressure and temperature pulses of an explosion are easy to identify. The lower limit of the reaction is much more subjective due to the slow transition out of the region. Thus, some arbitrary definition must be made to establish the lower limit. In this study the lower limit was defined to be the temperature at which less than twenty percent of the inlet oxygen had reacted after a thirty minute residence time. Fortunately, conversion dropped off rapidly with decreasing temperature so that little error was introduced by the choice of a specific conversion for the limit.

The experimental data from Newitt and Haffner (67), Lott (60), Hardwicke (42), and Bauerle (9) were compiled to obtain experimental curves describing the concentration histories of the major products. These product distribution curves are shown in Figure 11 through 15. It was found that

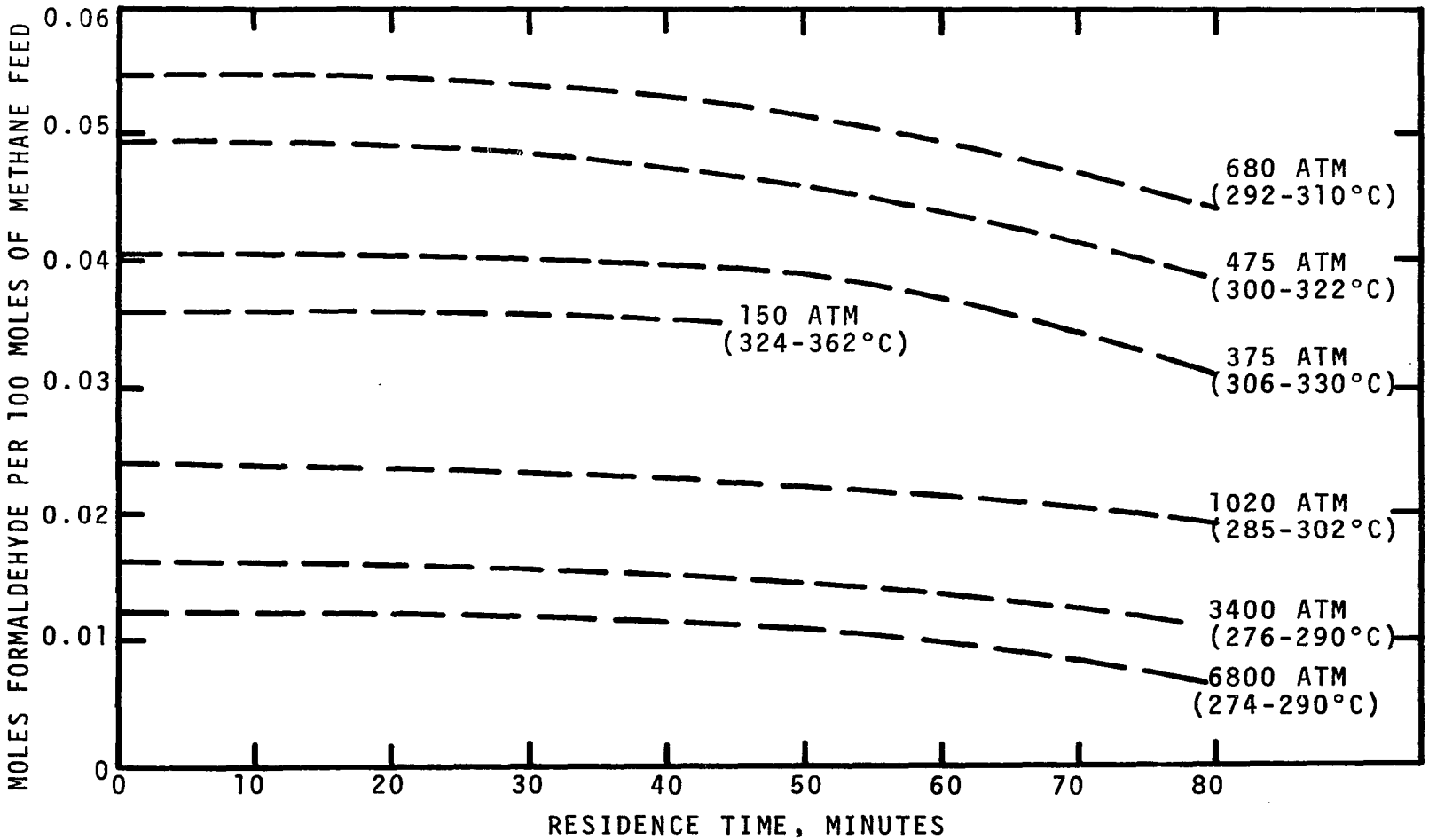

Figure 11. The Effect of Pressure on the Observed Formaldehyde Concentration. Data Compiled from Previous Investigators (9, 42, 60, 67) for a Nominal 10:1 Methane-Oxygen Feed Ratio; 80 Percent of Data is within 10 Percent of Curves.

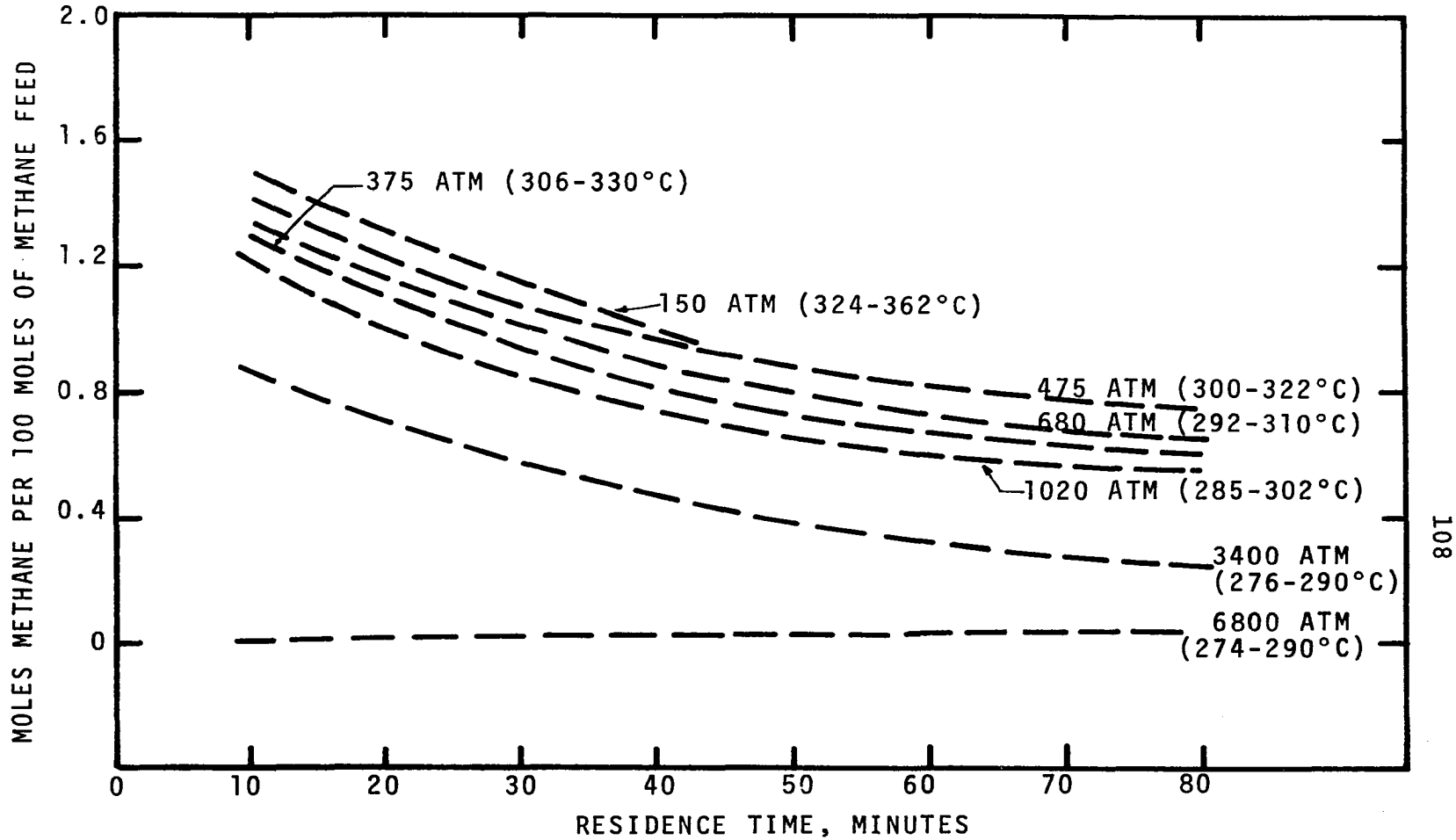

Figure 12. The Effect of Pressure on the Observed Methanol Concentration. Data Compiled from Previous Investigators (9, 42, 60, 67) for a Nominal 10:1 Methane-Oxygen Feed Ratio; 80 Percent of Data is within 10 Percent of Curves.

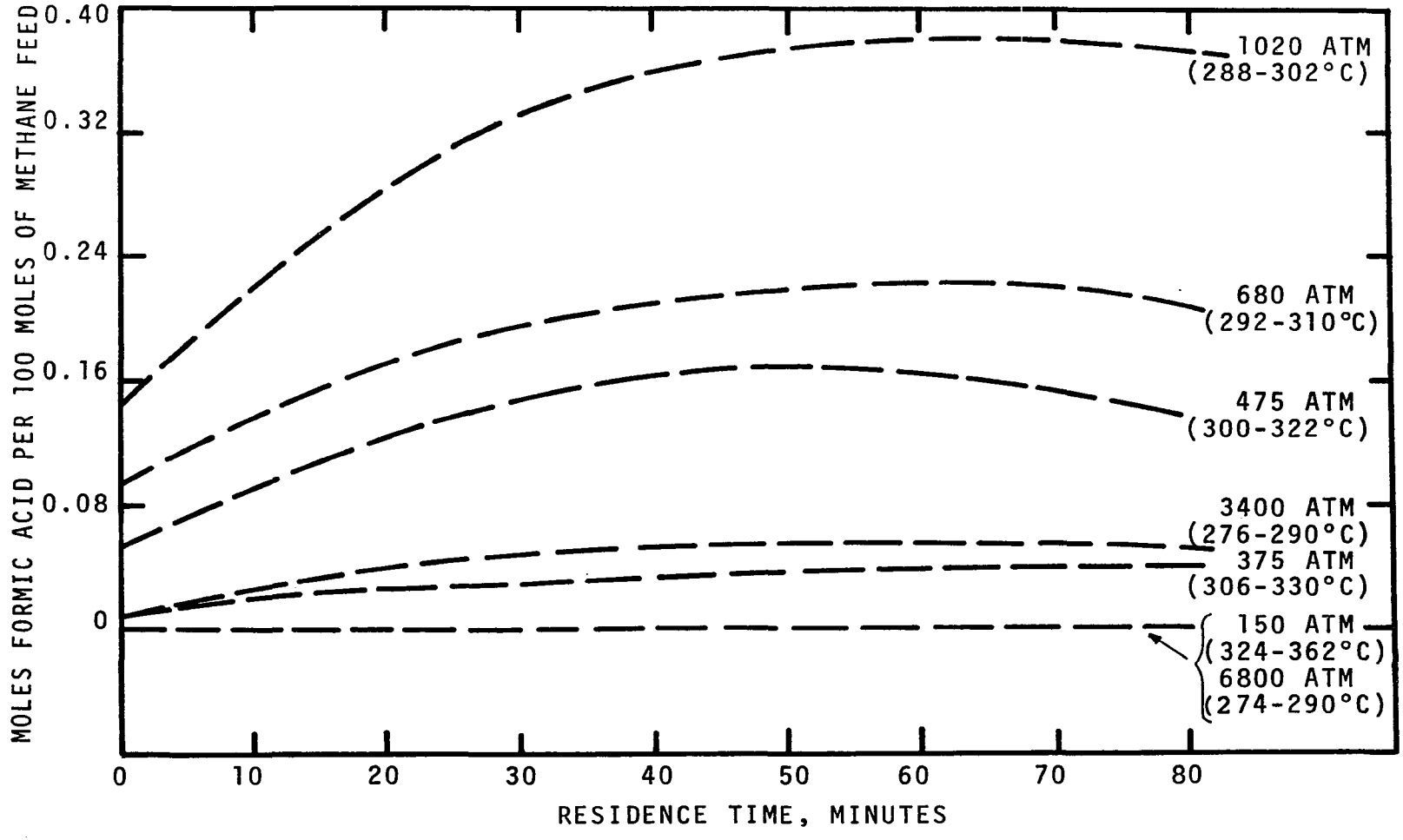

Figure 13. The Effect of Pressure on the Observed Formic Acid Concentration. Data Compiled from Previous Investigators (9, 42, 60, 67) for a Nominal 10:1 Methane-Oxygen Feed Ratio; 80 Percent of Data is within 10 Percent of Curves.

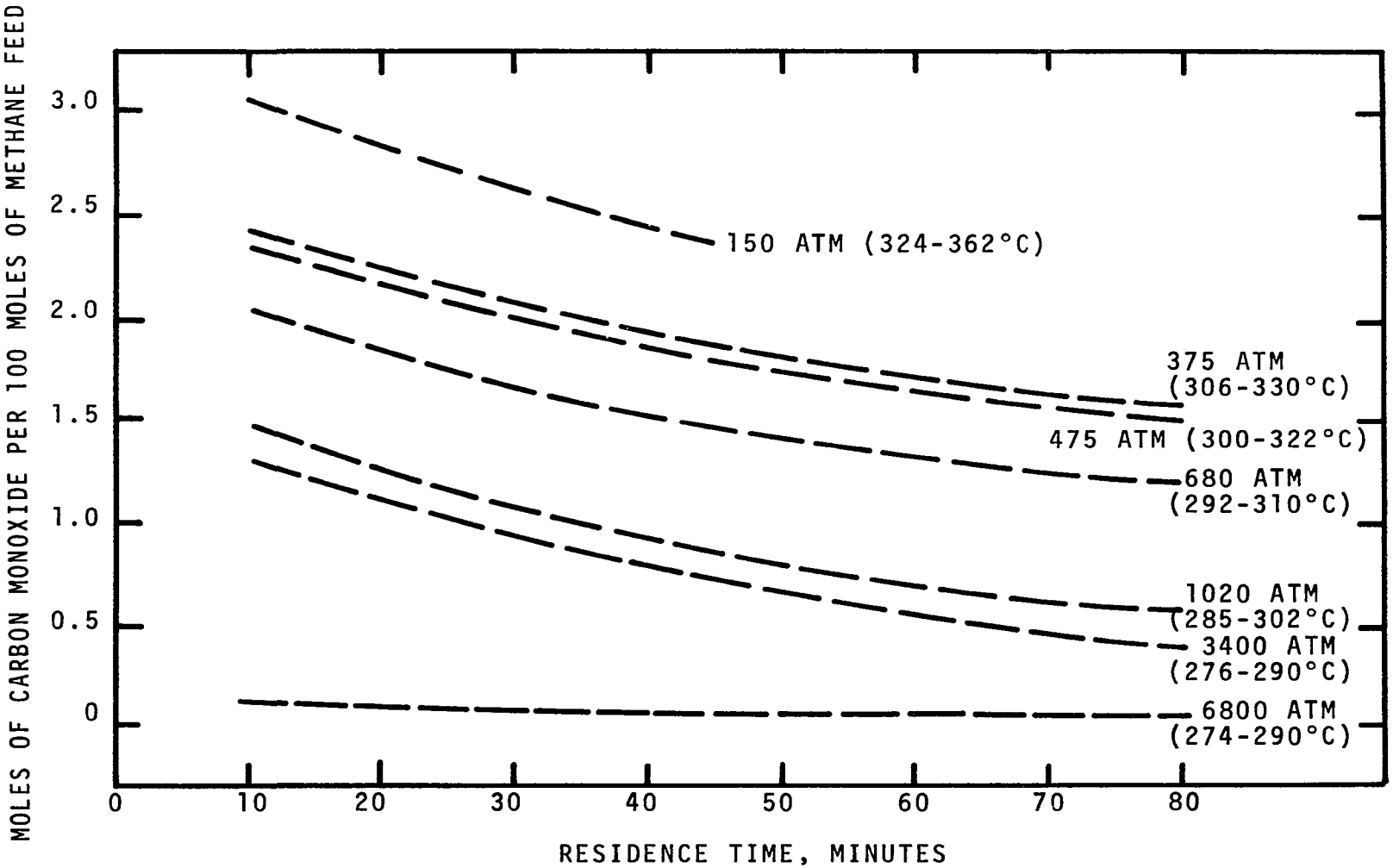

Figure 14. The Effect of Pressure on the Observed Carbon Monoxide Concentration. Data Compiled from Previous Investigators (9, 42, 60, 67) for a Nominal 10:1 Methane-Oxygen Feed Ratio; 80 Percent of Data is within 10 Percent of Curves.

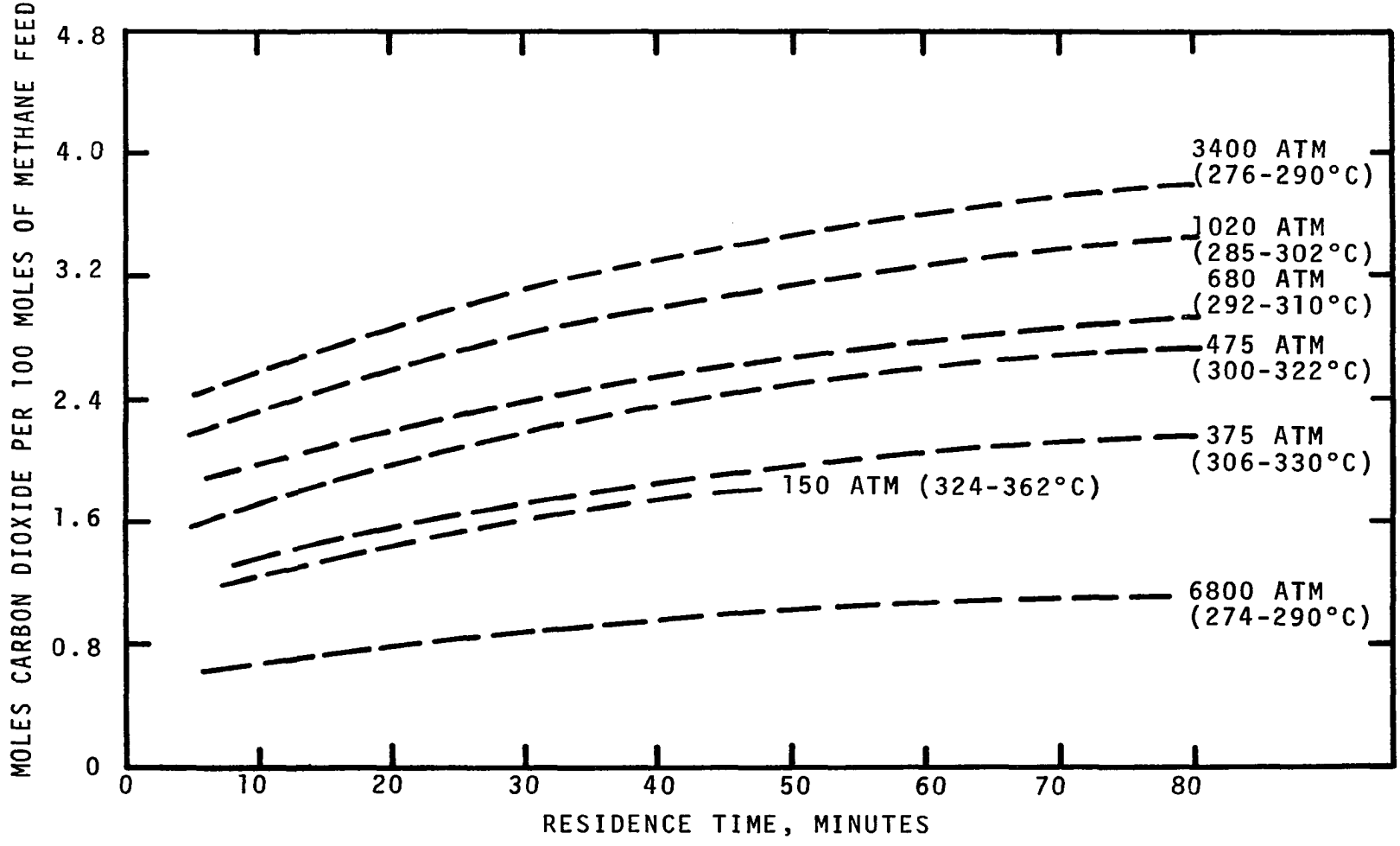

Figure 15. The Effect of Pressure on the Observed Carbon Dioxide Concentration. Data Compiled from Previous Investigators (9, 42, 60, 67) for a Nominal 10:1 Methane-Oxygen Feed Ratio; 80 Percent of Data is within 10 Percent of Curves.

approximately eighty percent of the data points fell within ten percent of the curves, even though the data at each pressure level varied over the entire temperature range, as shown previously in Figure 10.

It must be noted that the data used in Figures 11 through 15 were taken using two different experimental methods depending on the pressure, and thus two different definitions of reaction residence time are used in these figures. At pressures of 1000 atm and below, the investigators rapidly added the reaction gas mixture to the hot reactor. Zero residence time was then defined to be the time at which the filling procedure was completed. Several data points were then taken along different isotherms up to the point of the temperature maximum. At pressures above 1000 atm, the reaction mixture was added to a warm reactor, at which time the reactor was internally heated to the reaction temperature. In this case zero residence time was defined to be the time when the gas reached the desired reaction temperature. Since there was seldom a temperature maximum in this pressure range, residence time was measured from the zero point to some predetermined time.

Several different types of behavior are visible from the trend curves in Figures 11 to 15. The concentration of all the major components, except carbon dioxide, reaches a maximum and then decreases with time. The exact maxima for

methanol and carbon monoxide are not certain due to scattered data at low residence times, so portions of those curves have been deleted.

The concentrations of the products also have varying dependencies on pressure. Carbon monoxide and methanol concentrations decrease with increasing pressure, while carbon dioxide concentration increases with pressure. On the other hand, formaldehyde and formic acid trend curves reach a maximum and then decrease with increasing pressure. The decrease in the methanol production curve with increasing pressure is at variance with the results of Lott's work (60) above 1000 atm. However, it is thought that Lott's high methanol conversions were caused either by the catalytic effect of the Pyrex surface used or by the very low reaction temperatures obtained.

Two of the product distribution curves appear to be out of sequence, the 375 atm curve for methanol in Figure 12 and the 6800 atm curve for carbon dioxide in Figure 15. It is thought that the carbon dioxide curve is displaced due to a much lower methane conversion at extreme pressures than is found at lower pressures. The experimental curves for the other components have probably also been lowered due to this low conversion at extreme pressures, but the effect is not obvious since they were already decreasing with increasing pressure. No reason is obvious for the displaced methanol curve in Figure 12.

Several additional products that have been reported previously, namely ethanol, acetone, acetic acid, and methyl formate, have not been included in these results. All of these compounds have been found occasionally and in relatively minute quantities. Little generalization can be made about these products, other than to say that acetone and ethanol normally appear at low pressures, below 1000 atmospheres, while methyl formate has been found mainly at pressures above 1000 atmospheres (9, 60). Lott (60), however, reported finding some methyl formate at pressure levels from 475 to 1000 atmospheres. This author found ethanol and acetone in small quantities during experiments at pressures of 1700 atmospheres, but none in the 7000 atm studies. It is possible, though doubtful, that acetone is not formed at all in the reaction, but is picked up as a contaminant from the dry ice-acetone product recovery bath. The possibility also exists that methyl formate is produced by an esterification reaction between formic acid and methanol, either in the reactor or in the sample collection bottle, rather than by direct reaction. This possibility must be minimized since both formic acid and methanol are formed in major proportions at pressure levels where methyl formate has not been reported.

Little has been done previously to show theoretically the effect of temperature and pressure on the equilibrium of the overall oxidation reaction. Pressure would seem to increase the reaction rate and should therefore increase the

yield of reaction product. However, Wiezevich (99) found that increasing pressure caused a decrease in maximum overall conversion. The connection between these two observations is found in Figure 15, in that higher pressure increases carbon dioxide formation. Each molecule of methane that forms carbon dioxide ultimately consumes two molecules of oxygen. Other reactions as shown in Table 4 require less oxygen, thus causing the overall methane conversion to decrease due to a deficiency of oxygen.

Methane conversion data from previous studies were plotted at different pressures, temperatures, and residence times, with a representative plot shown in Figure 16 for a ten minute residence time. This figure shows that at constant temperature methane conversion increases with pressure, probably due to the increasing number of collisions per unit time. However, the figure also shows that at constant temperature the maximum possible conversion, without crossing into the explosive region, decreases with increasing pressure. This finding is supported by Wiezevich's results (99).

Even though dividing the absolute concentration of each component by the initial concentration of methane in Figure 11 through 15 put each reaction mixture on the same molar bases, obvious changes in the product distribution curves with pressure are found due to the reaction mechanism's complicated dependence on pressure. Such changes are seen as

TABLE 4

STOICHIOMETRIC OXYGEN CONSUMPTION TO FORM REACTION PRODUCTS

1	CH_4	+	$2\ O_2$	⟶	CO_2	+	$2\ H_2O$
2	CH_4	+	$3/2\ O_2$	⟶	CO	+	$2\ H_2O$
3	CH_4	+	$3/2\ O_2$	⟶	HCOOH	+	H_2O
4	CH_4	+	O_2	⟶	HCHO	+	H_2O
5	CH_4	+	$1/2\ O_2$	⟶	CH_3OH		
6	$2\ CH_4$	+	$2\ O_2$	⟶	$HCOOCH_3$	+	$2\ H_2O$
7	$2\ CH_4$	+	O_2	⟶	C_2H_5OH	+	H_2O
8	$2\ CH_4$	+	$1/2\ O_2$	⟶	C_2H_6	+	H_2O
9	$3\ CH_4$	+	$2\ O_2$	⟶	CH_3COCH_3	+	$3\ H_2O$

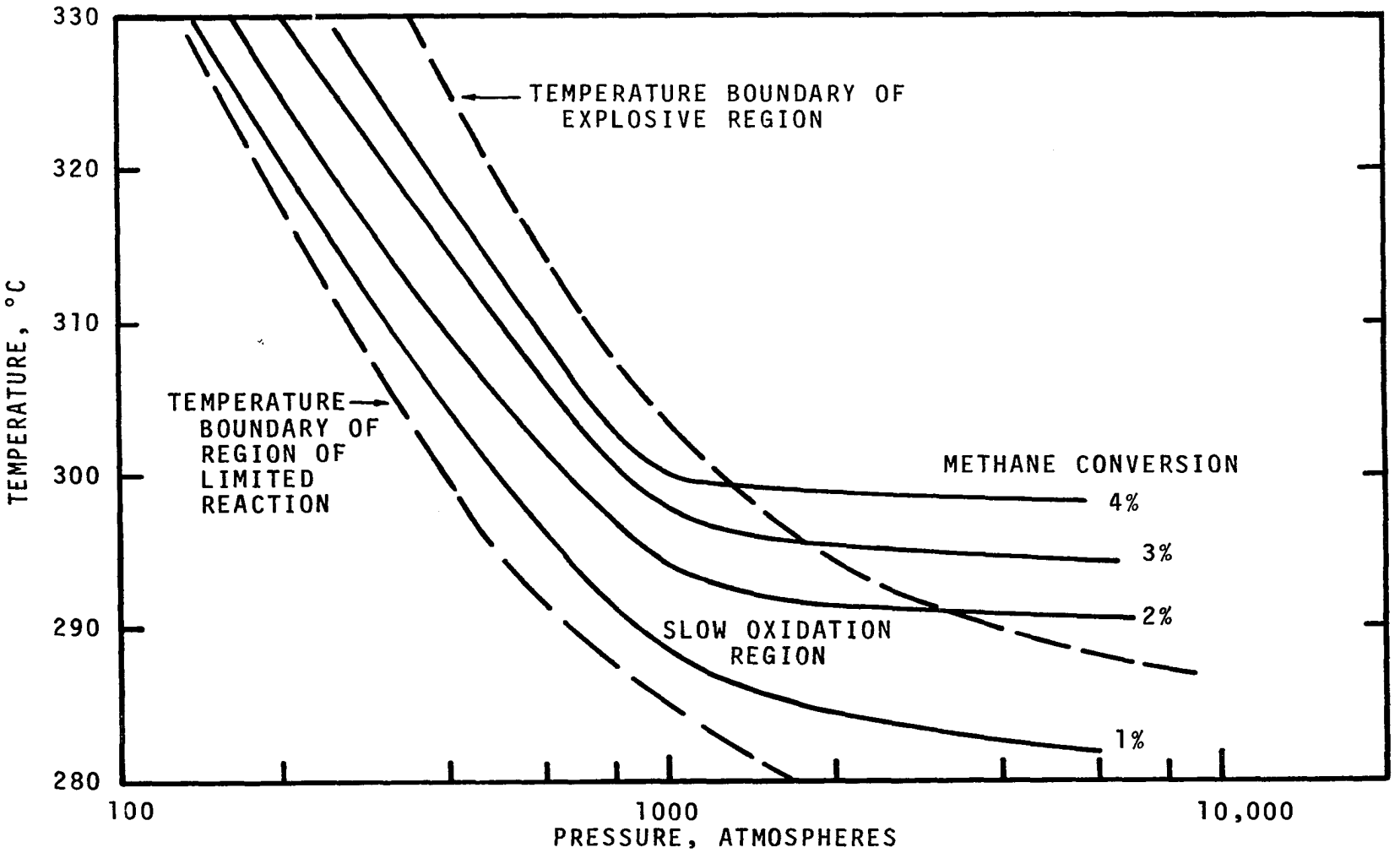

Figure 16. The Effect of Pressure and Temperature on the Methane Percent Conversion at Ten Minute Residence Time for a Nominal 10:1 Methane-Oxygen Feed Mixture. Data Compiled from Results of Lott (60) Bauerle (9) and Hardwicke (42).

the concentrations of the different product molecules increase, decrease, or reach a maximum with increasing pressure.

There are several possible explanations for the effect of pressure on the product composition. The first is a concentration effect, in which increasing the pressure increases the number of collisions per unit time between reacting species. Since the time between collisions is decreased, any reaction that requires time for isomerization or for other transformations may not compete with other reactions.

The second possibility is a temperature effect. Figure 10 shows that reactions at higher pressures do not need as high a reaction temperature. However, as will be discussed further, changing the temperature can greatly affect the equilibrium of different reactions. Therefore, although one reaction may be controlling at one temperature level, it may have little effect at another.

A third major effect, which becomes very important at extreme pressures, can be attributed to density brought about by the increasing proximity of the molecules and/or the solvent cage effect, which will be amplified in the following.

Table 5 shows the relative densities of methane at different pressure levels. The table shows that, at extreme pressures, the gas density approaches the density of liquids, even though the gas may be well above the critical temperature. The close proximity of molecules can greatly affect a chemical reaction as can be shown by the Transition State Theory (TST).

TABLE 5

DENSITY OF METHANE AT EXTREME PRESSURES

Pressure (atm)	Compressibility Factor*	Density (gm/cc)
1	1.0	0.0003
1,020	1.57	0.22
3,400	3.4**	0.34
6,800	5.5**	0.41

Temperature = 300°C

Liquid References

Water (4°C)	1.0
Hexane (20°C)	0.659
Methane (-164°C)	0.415

*Compressibility factor taken from generalized charts in Reference 61.

**Compressibility factor is extrapolated. Therefore, density may be in error, with density probably being too high rather than too low.

The TST assumes that in going from reactants to products, an equilibrium is established between the reactants and an activated transition state, as in the reaction

$$aA + bB \longleftrightarrow X^{\neq} \rightarrow cC + dD \qquad (9\text{-}1)$$

where A and B are reactants, C and D are products, $X^{\neq}$ is the activated transition state, and the small letters denote the stoichiometric coefficients. The rate constant k of the overall reaction can be calculated to be

$$k = \kappa \frac{\bar{k}T}{h} (K^{\neq}) \qquad (9\text{-}2)$$

where $\bar{k}$ is Boltzmann's constant, h is Planck's constant, T is the absolute temperautre, and $K^{\neq}$ is the equilibrium constant for the formation of the activated specie, $X^{\neq}$. The term κ, the transmission coefficient, or the probability that the transition state will proceed to products, was normally assumed to be close to unity and independent of temperature and pressure (40). Equation 9-2 can be applied to the usual equations relating thermodynamic properties. Of particular importance is the equation

$$-RT \frac{\partial}{\partial P} (\ln k)_T = -RT \frac{\partial}{\partial P} (\ln K^{\neq})_T = \frac{\partial (\Delta G^{\neq})_T}{\partial P} = \Delta V^{\neq} \qquad (9\text{-}3)$$

This equation relates the change of the rate constant with pressure to the volume change in the transition state, $\Delta V^{\neq}$. The value of $\Delta V^{\neq}$ changes rapidly with pressure so the

integrated form of Equation 9-3 must be used cautiously if large changes in pressure are considered.

Equation 9-3 shows that reactions that require a large amount of bond stretching could be practically stopped in extreme density situations due to the fact that molecules must be forced out of the way for the bond stretching to take place. Two extremely important examples of this situation can be seen in the decomposition reactions of Reactions G-2 and G-4. Other examples are found in Reactions G-4b and G-M8a and in the reverse reactions of Group G-12. In each of these cases, a bond must be stretched far enough to cause breakage, or the reaction stops. Since the entire reaction mechanism relies on Reactions G-2 and G-4 to generate radicals and intermediates, it can be seen that the rate of the entire reaction depends strongly on the rate of these two reactions. Thus the significance of the methane densities found in Table 5 can be seen.

Comparing Figures 11 and 12, it appears that extreme pressure reduces the methanol concentration to a greater extent than it reduces the formaldehyde concentration. This observation may be explained by the bond stretching phenomena. The bond breaking in Reaction G-2 is helped by the formation of the double bond to the oxygen in formaldehyde. However, the decomposition of the methyl hydroperoxide molecule in Reaction G-4 does not have bond formation accompanying the bond

breakage. High molecular density should then slow Reaction G-4, and thus the methanol production, more than it does Reaction G-2.

Another density related phenomena would be a cage effect, similar to a solvent cage effect for liquid phase reactions between dilute reactants. In such a situation, reactants would be trapped in a small cage by other molecules so that, instead of escaping from each other, the reactants could collide many times. Thus a high probability exists that consecutive reactions will occur until products with minimum free energy are formed. Reaction sequences that may be likely to occur in a reaction cage could be any of the following:

(R-15) $CH_4 + O_2 \rightarrow CH_3\cdot + HO_2\cdot \rightarrow CH_3O\cdot + \cdot OH \rightarrow HCHO + H_2O$

(R-16) $CH_3OO\cdot \rightarrow HCHO + \cdot OH \rightarrow HCO\cdot + H_2O$

(R-17) $CH_3O\cdot + O_2 \rightarrow HCHO + HO_2\cdot \rightarrow HCO\cdot + H_2O_2$

(R-18) $HCHO + O_2 \rightarrow HCO\cdot + HO_2\cdot \rightarrow CO + H_2O_2$

(R-19) $HCO\cdot + O_2 \rightarrow CO + HO_2\cdot \rightarrow CO_2 + \cdot OH$

Since the majority of the molecules that radicals would collide with would be methane molecules, hydrogen atoms would also be easily abstracted. Reaction sequences, such as R-15 or R-18 in which the intermediate radicals are destroyed, might help explain the slow reaction at extreme pressures.

One might wonder at what transition pressure a cage effect might influence a reaction. An answer which seems

logical is that pressure at which the gas starts acting like a liquid. Babb (4) thought that the pressure at which the viscosity of a gas changes from increasing with temperature to decreasing with temperature like a liquid might be representative of the transition pressure. Such a transition often occurs at about 500-1000 atmospheres (4, 40). A transition to a liquid-like reaction mixture might explain the abrupt change in the methane conversion curves at about 1000 atm in Figure 16, and the sudden increase in carbon dioxide formation with increasing pressure, as shown in Figure 15.

Figure 16 also suggests that temperature may well play an important role in the cage effect. Molecules with enough thermal energy may break out of a cage before they have reacted completely, thus reducing the number of methane molecules that react to completion in a cage and increasing the total amount of reacted methane.

Discussion of the Mechanism Development

It was hoped that a relatively short and simple mechanism could be used to describe the experimental behavior. However, numerical analysis indicated that previous mechanisms and proposed mechanisms initially considered in this study did not include some important equations. At this point the previous mechanisms were closely examined to determine if obvious omissions had been made. Several reactions were visualized that appeared to be chemically feasible and probably very

important. These reactions were added to modify the mechanism. These modifications are discussed below.

Hardwicke, Lott, and Sliepcevich (43) discussed the necessity of writing at least one step to show the formation of carbon dioxide from a source other than carbon monoxide. They suggested the step

(HLS-10) $HCHO + O_2 \rightarrow CO_2 + H_2O$

a non-elementary reaction, possibly occurring at the wall. At high pressures, a wall reaction might be minimized in favor of a gas phase reaction. At least two other steps are possible to form carbon dioxide.

The first possible alternate route to carbon dioxide is by way of Reactions R-20 and R-21, with peroxyformic acid as an intermediate.

(R-20) $HCHO + O_2 \rightarrow HCOOOH$

(R-21) $HCOOOH \rightarrow CO_2 + H_2O$

These two reactions are similar to Reaction HLS-10, but without the requirement of a wall. Both reactions R-20 and R-21 require a four-center reaction with a strained four member ring transition state. However, since the formation of peroxyformic acid has not been proven at high pressures, another reaction might be considered.

A second alternative to carbon dioxide formation is Reaction G-6b. This reaction is actually a series of

reactions containing an isomerization reaction. Reaction G-6b should satisfy the requirements of the carbon dioxide paradox in the following manner. At low pressures, high reaction temperatures are necessary. Therefore, the radical formed in the step

(R-22) $HCO\cdot + O_2 \longleftrightarrow H\overset{O}{\overset{\|}{C}}OO\cdot$

could decompose back into the initial reactants before it has time to isomerize. As the reaction temperature is lowered, such as is done when the reaction pressure is raised, the intermediate radical could survive longer and have time to isomerize, as in the step

(R-23) $H\overset{O}{\overset{\|}{C}}OO\cdot \longleftrightarrow \cdot\overset{O}{\overset{\|}{C}}OOH$

Once the radical has isomerized, it can decompose to carbon dioxide and a hydroxyl radical.

Numerically, the relationship between Reactions G-6a and G-6b should be the following to give the observed behavior:

$$E_{6a} > E_{6b} \qquad (9\text{-}4)$$

$$A_{6a} > A_{6b} \qquad (9\text{-}5)$$

where the E's and A's are the activation energies and pre-exponential factors respectively for Reactions G-6a and G-6b. Therefore, at high temperatures, Reaction G-6a would control the consumption of the HCO radical. At low temperatures the exponential term in the rate equation for Reaction G-6a could

make the rate slow enough that Reaction G-6b could either be dominant or at least observable. In this way carbon dioxide formation can be possible at high pressure, with correspondingly low temperature, without depending on carbon monoxide formation.

Hardwicke (43) and Bauerle (9) discussed the necessity of at least one additional equation to show the formation of methanol, other than Equation HLS-5. For this purpose, they proposed Equation HLS-14. Early in this study, another reaction for methanol formation was added to the proposed mechanism, Reaction G-7. However, when the numerical analysis of this study was started, it became evident that these three equations combined could only account for a small part of the methanol found by previous investigators. This observation substantiated Shtern's conclusions (85) that an aklyl hydroperoxide probably is not the chief source of alcohols since the highly endothermic decomposition of the hydroperoxide could limit the concentration of the CH_3O radical, especially at lower temperatures. The radical termination reaction, HLS-14, contributed an amount eight orders of magnitude smaller than the observed product.

Several equations to form methanol were considered, primarily Reaction G-10a. Equations G-M9, G-M9a, and G-11b were also used, but for different purposes. The reactions of G-9 and G-9a were added as a theoretical basis for the observed destruction of methanol with time, as shown in Figure

12. Equation G-11b was considered to be a gas phase radical termination reaction similar to Reaction HLS-14. When used in the numerical analysis of the mechanism, these new equations showed formation of quantities of methanol equal to that found experimentally.

Several alternative methods have been considered for the formation of formic acid. Hardwicke (43) suggested Reaction HLS-15 as the reaction responsible for formic acid. However, in the computer simulation of the oxidation reaction done in this study, it was found that due to very low radical concentrations the concentration of formic acid formed by Reaction HLS-15 was many orders of magnitude too small.

Another possible route to formic acid would be through the peroxyformic acid intermediate formed in Reaction R-20. The peroxyformic acid could then react in several ways. One would be the direct decomposition to formic acid and atomic oxygen

(R-24) $HCOOOH \rightarrow HCOOH + O:$

as suggested by Harding (41). Two other routes would be by way of four-center reactions with methane or formaldehyde

(R-25) $HCOOOH + CH_4 \rightarrow HCOOH + CH_3OH$

(R-26) $HCOOOH + HCHO \rightarrow HCOOH + HCOOH$

as shown in Reactions R-25 and R-26. Another route consists of peroxyformic acid decomposing into two radicals with one of

these, the HCOO radical, abstracting a hydrogen atom to generate formic acid. All of these routes are suspect because of the lack of evidence for the existence of the peroxyformic acid.

Two methods using carbon monoxide as a reactant were considered. The first was a direct molecular reaction

(R-27) $CO + H_2O \rightarrow HCOOH$

According to the Hirschfelder Rule (47), the activation energy for such a reaction should be about 35 kcal/mole. Even though this reaction shows a decrease in the number of moles of reactants, increasing the reaction pressure would decrease the reaction rate since the higher reaction pressure is accompanied by a temperature drop. The computer study precluded appreciable reaction by this route.

An alternate method of formic acid formation was suggested and included in this report. The basic reaction

(G-8a) $CO + \cdot OH \leftrightarrow \cdot COOH$

is an equilibrium radical reaction similar to a commercial, liquid phase, ionic reaction to make formic acid from carbon monoxide and sodium hydroxide. The forward reaction of G-8a should have a zero activation energy while the unimolecular, reverse reaction is estimated to have an activation energy of about 34 kcal/mole. Coupled with this reaction are two steps, Reactions G-5d and G-7c, to make formic acid.

An interesting development was found when the equations describing the formation of formic acid and the COOH radical were written. Although at low pressures, the concentration of carbon monoxide was high, the accompanying high temperatures caused the equilibrium of Reaction G-8a to shift to the left. However, since lowering the reaction temperature reduced the rate constant of the reverse reaction faster than the carbon monoxide concentration decreased, the COOH radical concentration increased with increasing pressure. This trend was reversed at pressures around 1000 atmospheres as the temperature stopped dropping while the carbon monoxide concentration did not. Since the formic acid concentration calculated from Reactions G-5d and G-7c was proportional to the concentration of the COOH radical, the formic acid should follow the same trend, by increasing with pressure and then decreasing after a maximum at about 1000 atmospheres. The postulated series of reactions, G-8a, G-5d, and G-7c, describe the observed experimental behavior shown in Figure 13.

The formation of methyl formate was considered next. Hardwicke (43) again suggested a radical termination step, Reaction HLS-16. This reaction was analyzed in the simulated reaction with the same results as were found for Reaction HLS-15 for formic acid; i.e., a concentration of six to eight orders of magnitude too small with normal values for the gas phase rate constants. Other reactions were then considered.

The first reaction considered was a molecular reaction

(R-28) $HCHO + HCHO \longrightarrow CH_3O\overset{O}{\overset{\|}{C}}H$

Analysis was done as stated previously with estimated values of the rate constants. Use of Reaction R-28 increased the concentration of methyl formate two orders of magnitude above that calculated from Reaction HLS-16, but this result was still several orders of magnitude below that found experimentally.

Several radical reactions can be postulated as part of a sequence to form methyl formate, such as Reactions R-29 and R-30

(R-29) $HCO\cdot + HCHO \longleftrightarrow H\overset{O}{\overset{\|}{C}}OCH_2\cdot$

(R-30) $CH_3O\cdot + CO \longleftrightarrow CH_3O\overset{O}{\overset{\|}{C}}\cdot$

to form two different radicals. Either of these new radicals could abstract a hydrogen atom from a hydrogen donor, such as methane or formaldehyde, to complete the formation of methyl formate. However, no thermodynamic data were found for either of these radicals, so activation energies for the reactions were not estimated. It might be assumed that the pressure effect on methyl formate might be similar to the effect on formic acid since, experimentally, pressure affected formaldehyde concentration in the same way as it did carbon monoxide. No generalization to the formation of methyl formate can be made other than that only a small fraction of it can come from the radical termination step of HLS-16 and that the possibility

of methyl formate production by an esterification reaction between methanol and formic acid cannot be overlooked.

Ethanol formation has been discussed by Bauerle (9). Bauerle noted that ethanol formation appears to be favored at low pressures. He therefore concluded that ethanol was formed either as a product of a reaction with an increasing number of moles or as a wall reaction which is diffusion controlled. Also possible is a reaction series that is temperature controlled, similar to those discussed earlier for formic acid and methyl formate.

An example of a reaction sequence to form ethanol, similar to that postulated for formic acid, was tested with the major reaction being

(R-31) $CH_3^{\cdot} + HCHO \leftrightarrow C_2H_5O^{\cdot}$

This step would then be coupled with one or more hydrogen abstraction equations. Analysis of this step in the previously described manner, however, showed that this set of equations had the wrong temperature dependency.

Bauerle's approach (9) appears to be accurate. He stated that ethanol probably is formed by oxidizing ethane in a manner similar to methane oxidation. Since for many experimental runs, Bauerle found more ethane in the product than was added initially as a methane contaminant, he postulated that ethane was produced in the reaction, probably by the radical

termination step of Reaction G-12c. He postulated that at elevated pressures the cross termination step with a hydroxyl radical in Reaction G-12 would deplete the methyl radical supply, therefore decreasing both ethane and ethanol production while increasing methanol production slightly. This conclusion was substantiated in the reaction simulation done in this study. First it was found that appreciable quantities of ethane can be produced by way of Reaction G-12c. Also, it was found that by increasing the reaction pressure ethane production decreased and hydroxyl radical concentration increased.

Other reaction products were anticipated but were not found. Dimethyl ether was expected to be formed by another radical termination step

$$\text{(R-32)} \qquad CH_3\cdot + CH_3O\cdot \rightarrow CH_3OCH_3$$

although it had not been reported previously. It is thought that this and similar termination reactions probably occur, but in such small quantities as to be undetectable due to extremely low concentrations for some radical species. This conclusion was supported by the computer simulation study.

Fisher and Tipper (31) concluded that methyl hydroperoxide CH_3OOH is formed chiefly by Reaction G-3a. They based their conclusion on the finding that the hydroperoxide is formed only after formaldehyde is in the system. Contrary to their conclusion, it was found in the computer simulation

that the major reaction should be Reaction G-3

$$(G\text{-}3) \qquad CH_3OO\cdot + CH_4 \longleftrightarrow CH_3OOH + CH_3\cdot$$

rather than Reaction G-3a. Even though the activation energy for Reaction G-3a was estimated to be lower than for G-3, the overall rate of G-3 was higher due to the much higher concentration of methane than formaldehyde. Fisher and Tipper's observation that the reaction did not proceed until after formaldehyde was present in the system can be explained by the fact that the CH_3OO radical reaches its maximum concentration at about the same time as the formaldehyde maximum.

Discussion of the Mechanism Analysis

The direct oxidation of methane by molecular oxygen was simulated, as discussed previously, by simultaneously integrating the differential equations, Equations 8-1 through 8-12, describing the formation and consumption of each molecular specie. The concentration of each radical specie was calculated using Equations 8-20 through 8-26. The tabulated Arrhenius parameters from Table 2 were used to calculate the rate constants for each forward and reverse reaction in the proposed high pressure oxidation mechanism. The results of this simulation study are compared to experimentally observed molecular concentrations in Figures 17 through 26 for pressures of 375, 475, 680, 1020, and 3400 atm. Both sets of curves have been shifted to the left to eliminate the

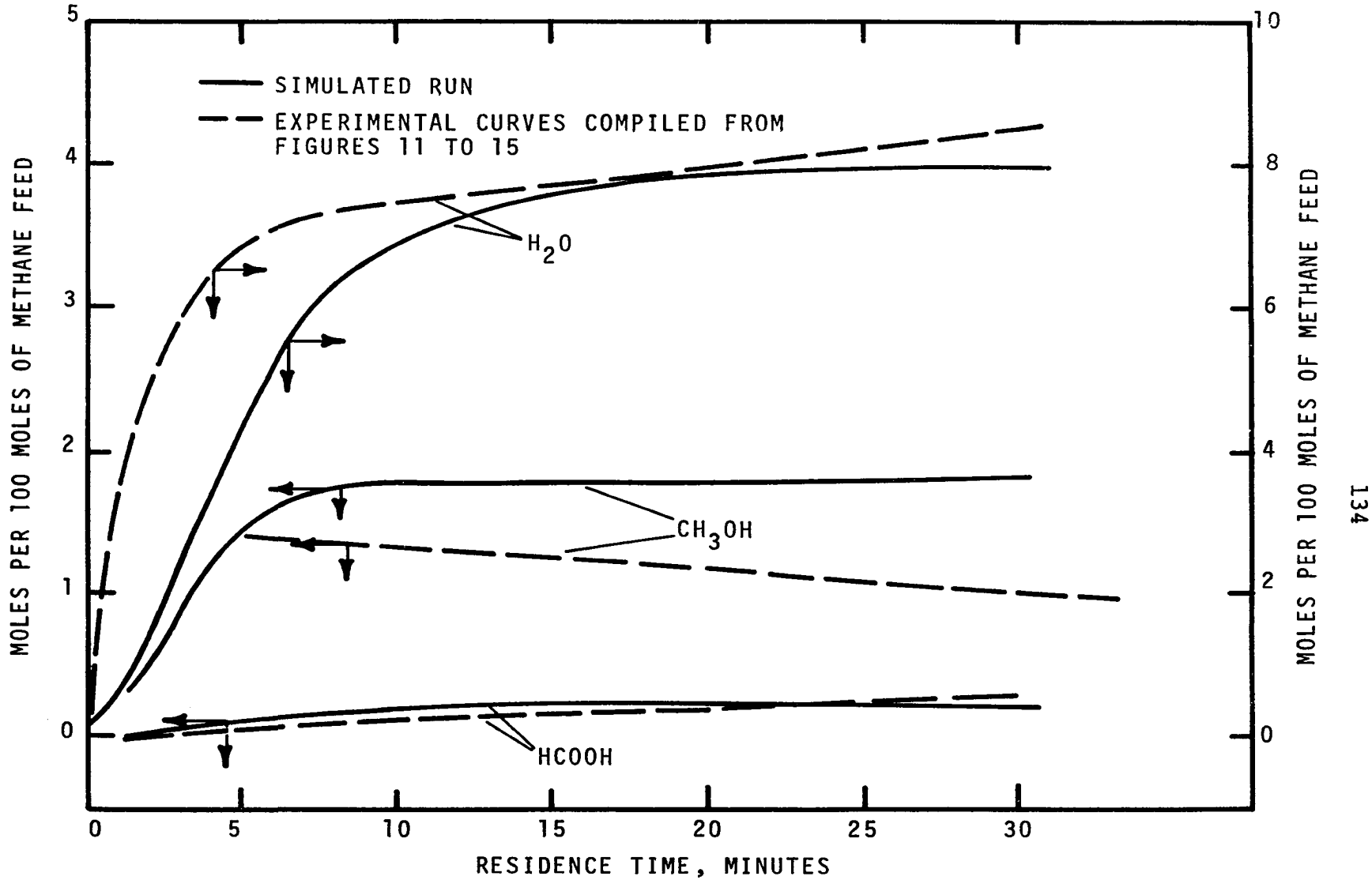

Figure 17. The Comparison Between Observed and Simulated Liquid Concentrations at 375 atm and 326°C.

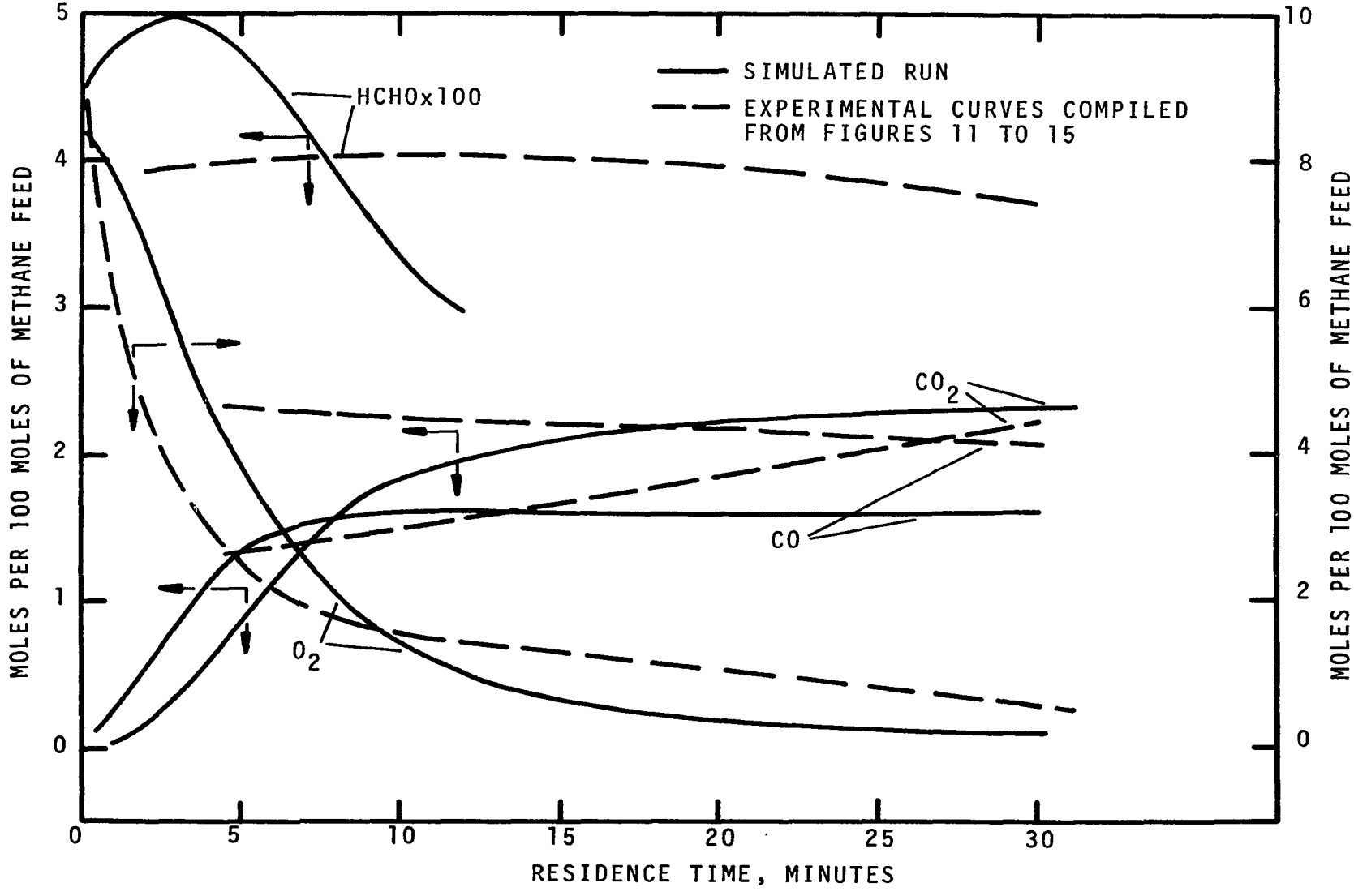

Figure 18. The Comparison Between Observed and Simulated Gaseous Concentrations at 375 atm and 326°C.

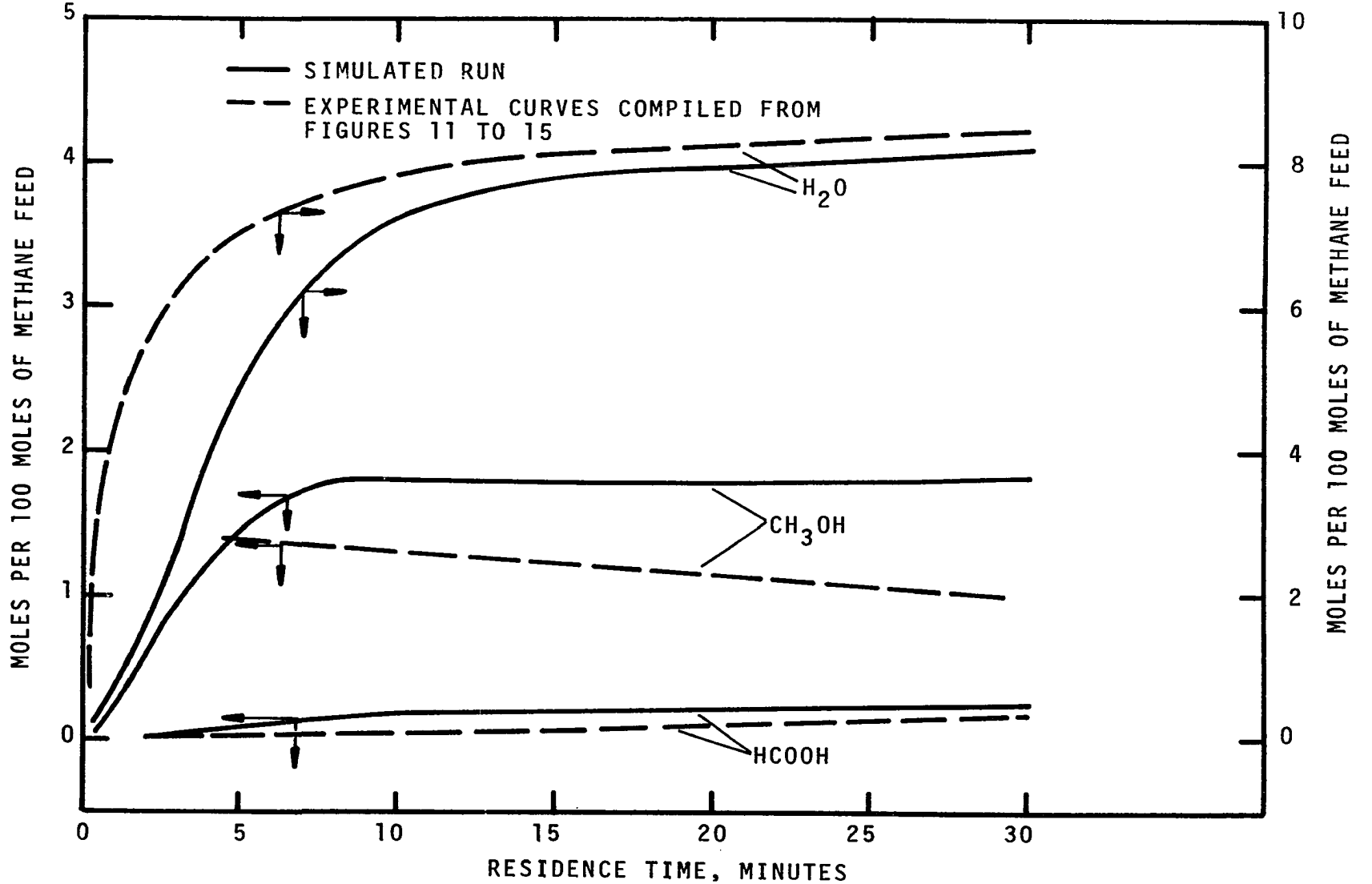

Figure 19. The Comparison Between Observed and Simulated Liquid Concentrations at 475 atm and 420°C.

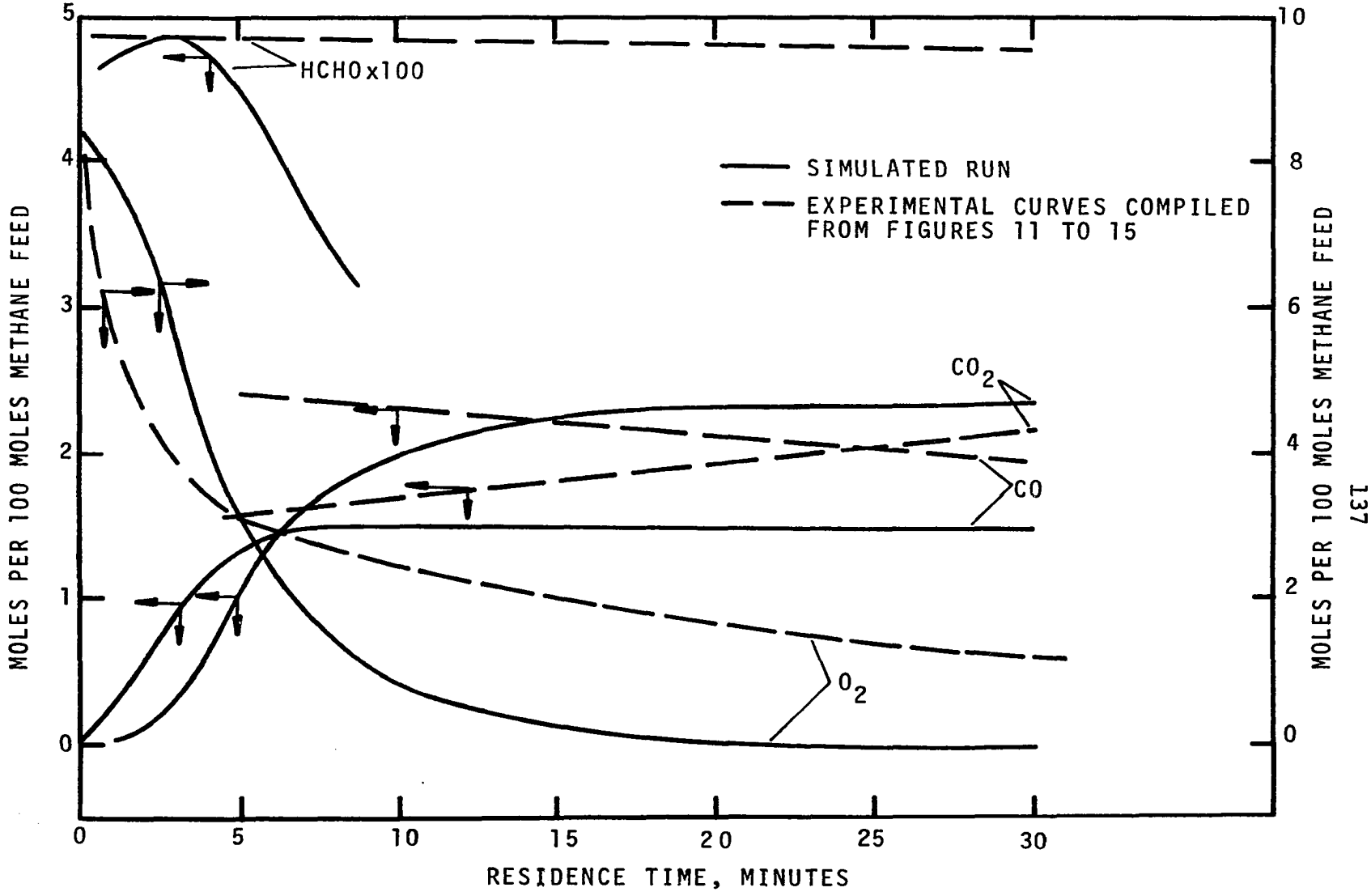

Figure 20. The Comparison Between Observed and Simulated Gaseous Concentrations at 475 atm and 320°C.

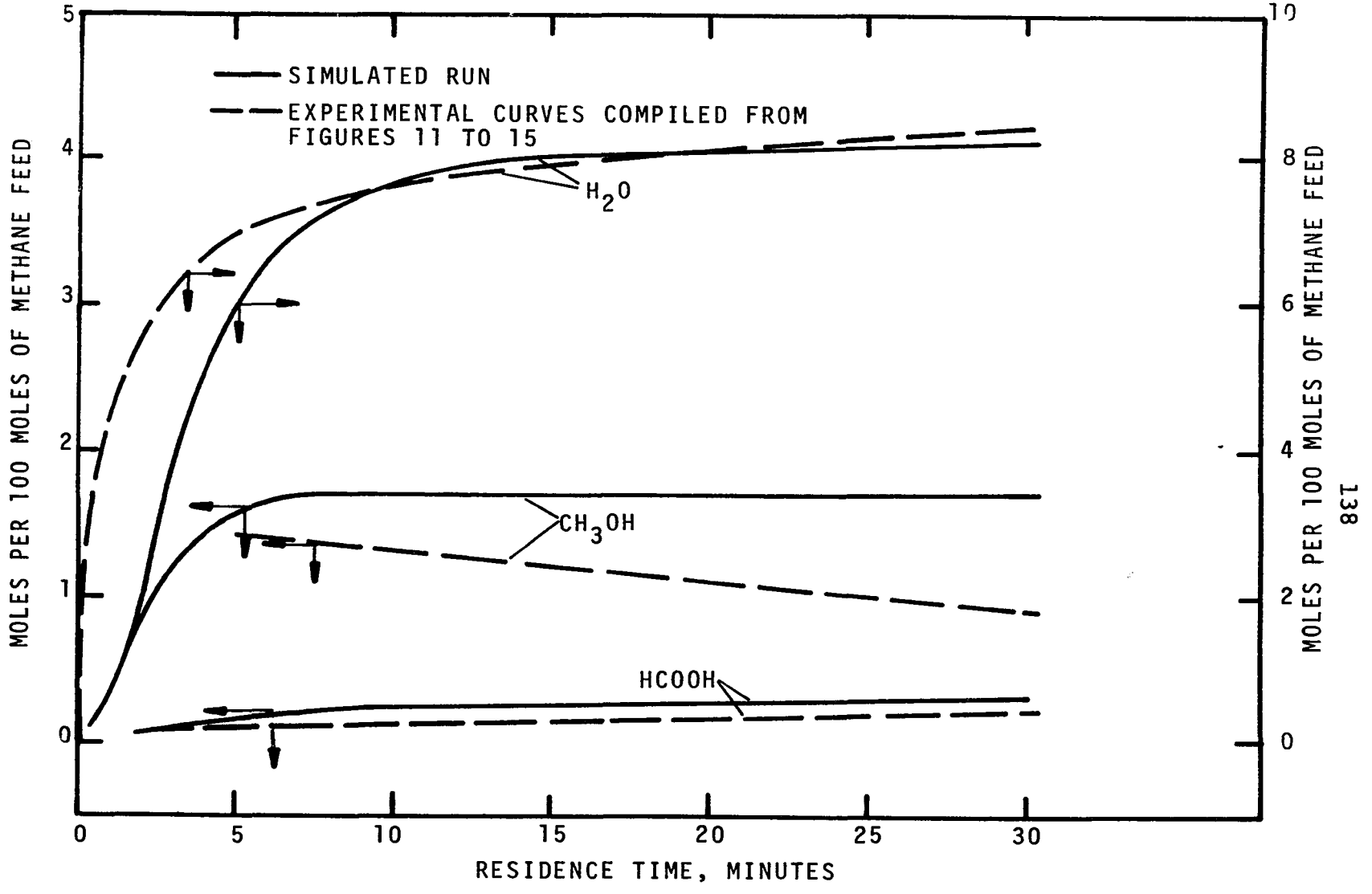

Figure 21. The Comparison Between Observed and Simulated Liquid Concentrations at 680 atm and 306°C.

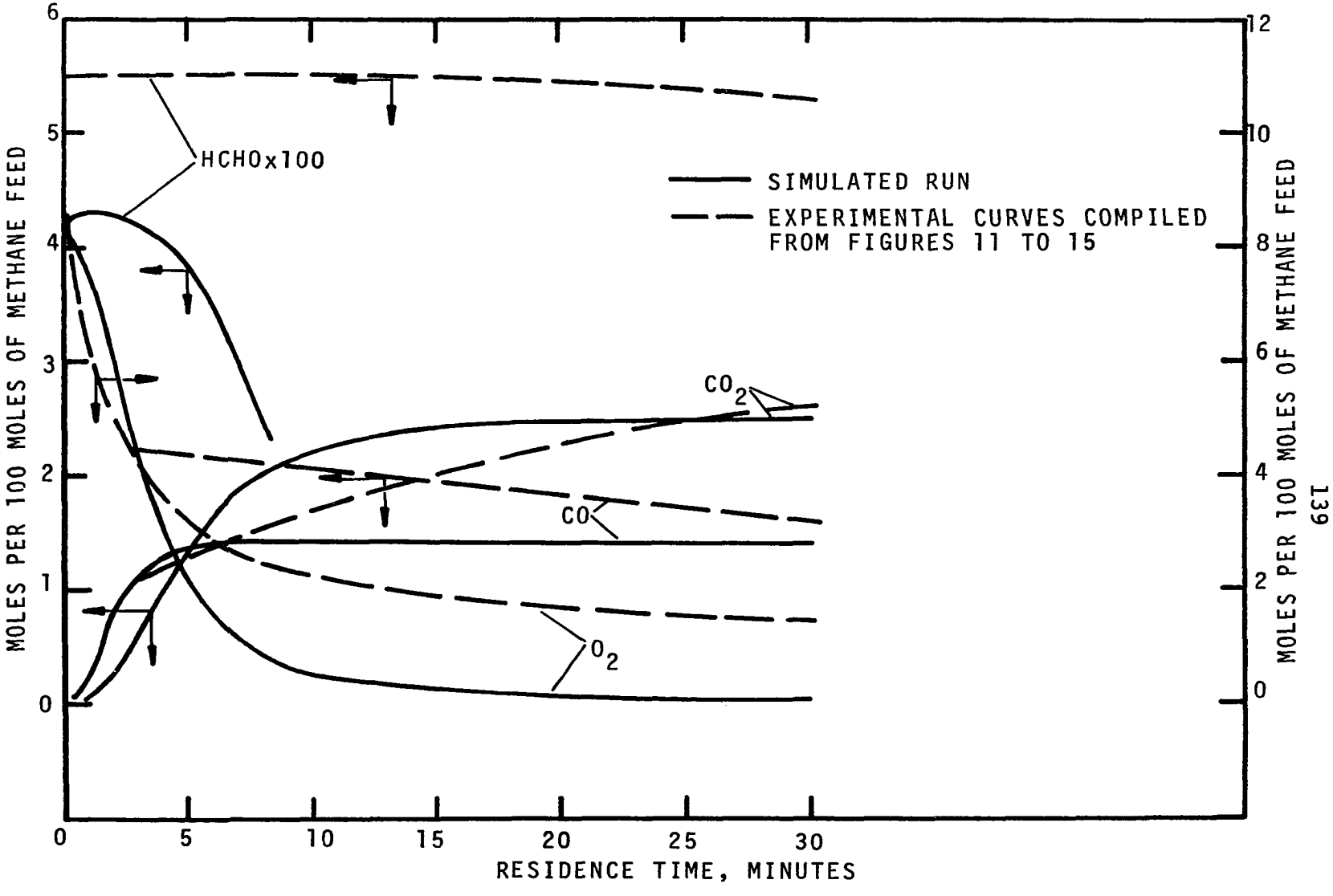

Figure 22. The Comparison Between Observed and Simulated Gaseous Concentrations at at 680 atm and 306°C.

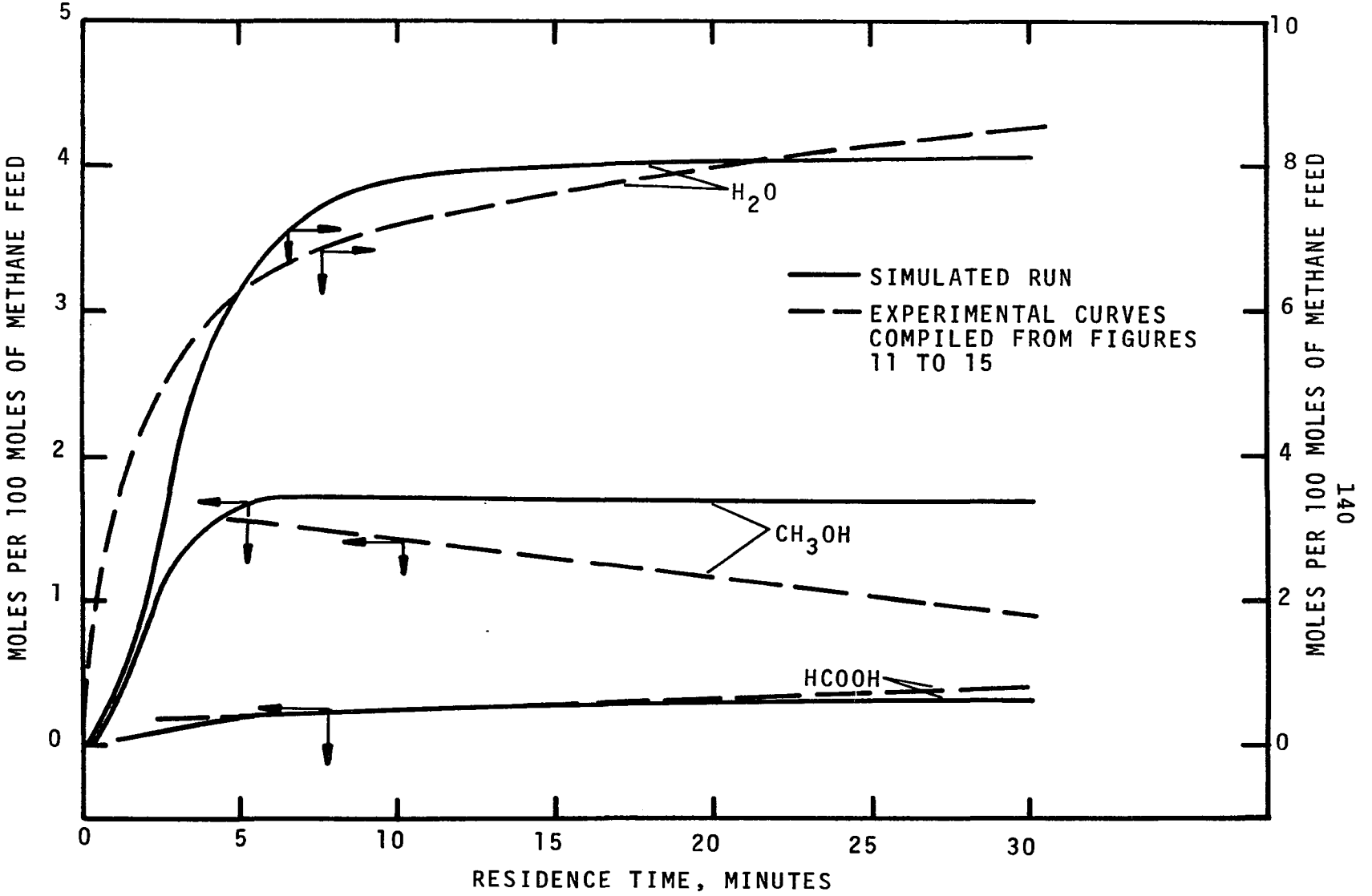

Figure 23. The Comparison Between Simulated and Observed Liquid Concentrations at 1020 atm and 304°C.

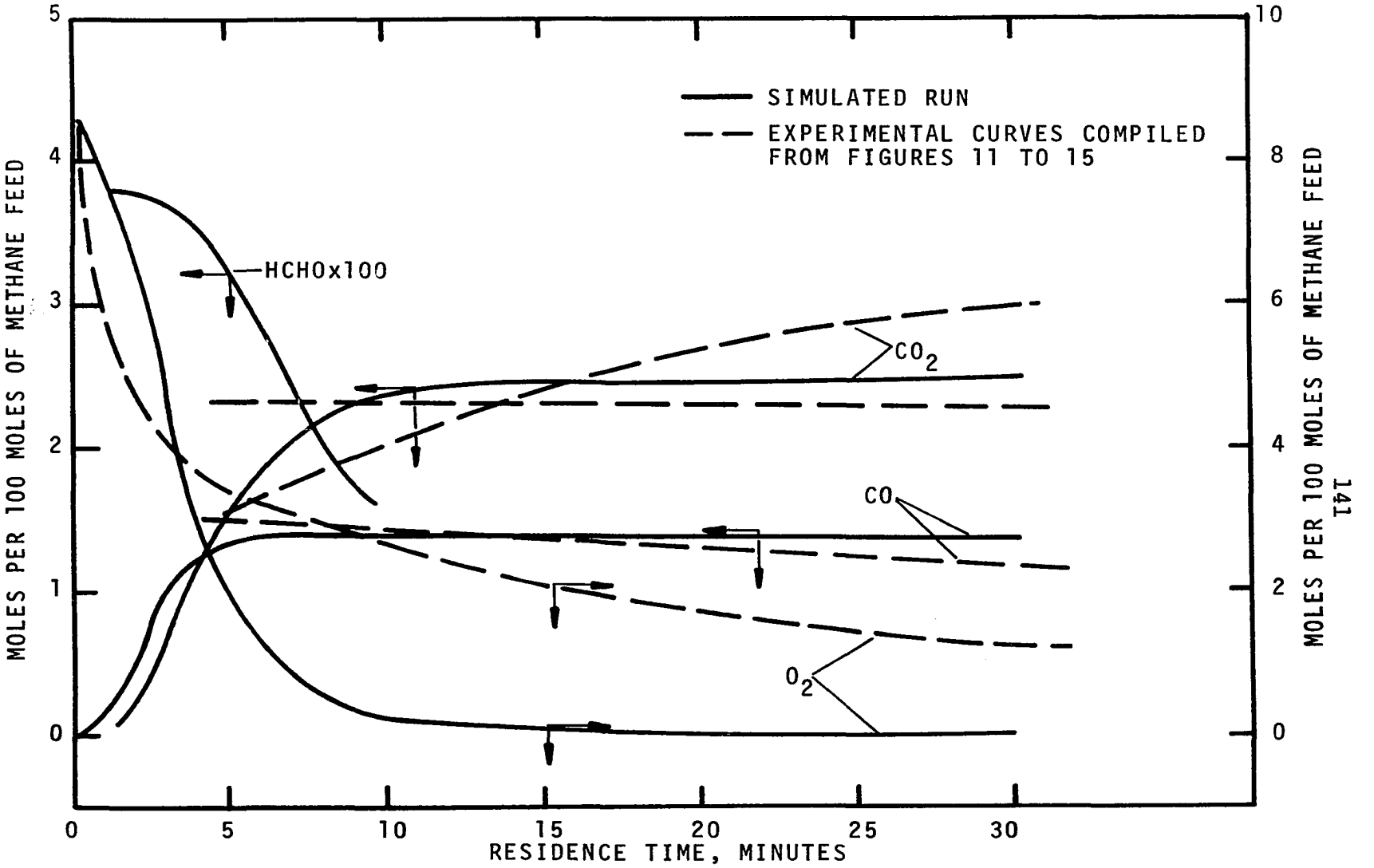

Figure 24. The Comparison Between Observed and Simulated Gaseous Concentrations at 1020 atm and 304°C.

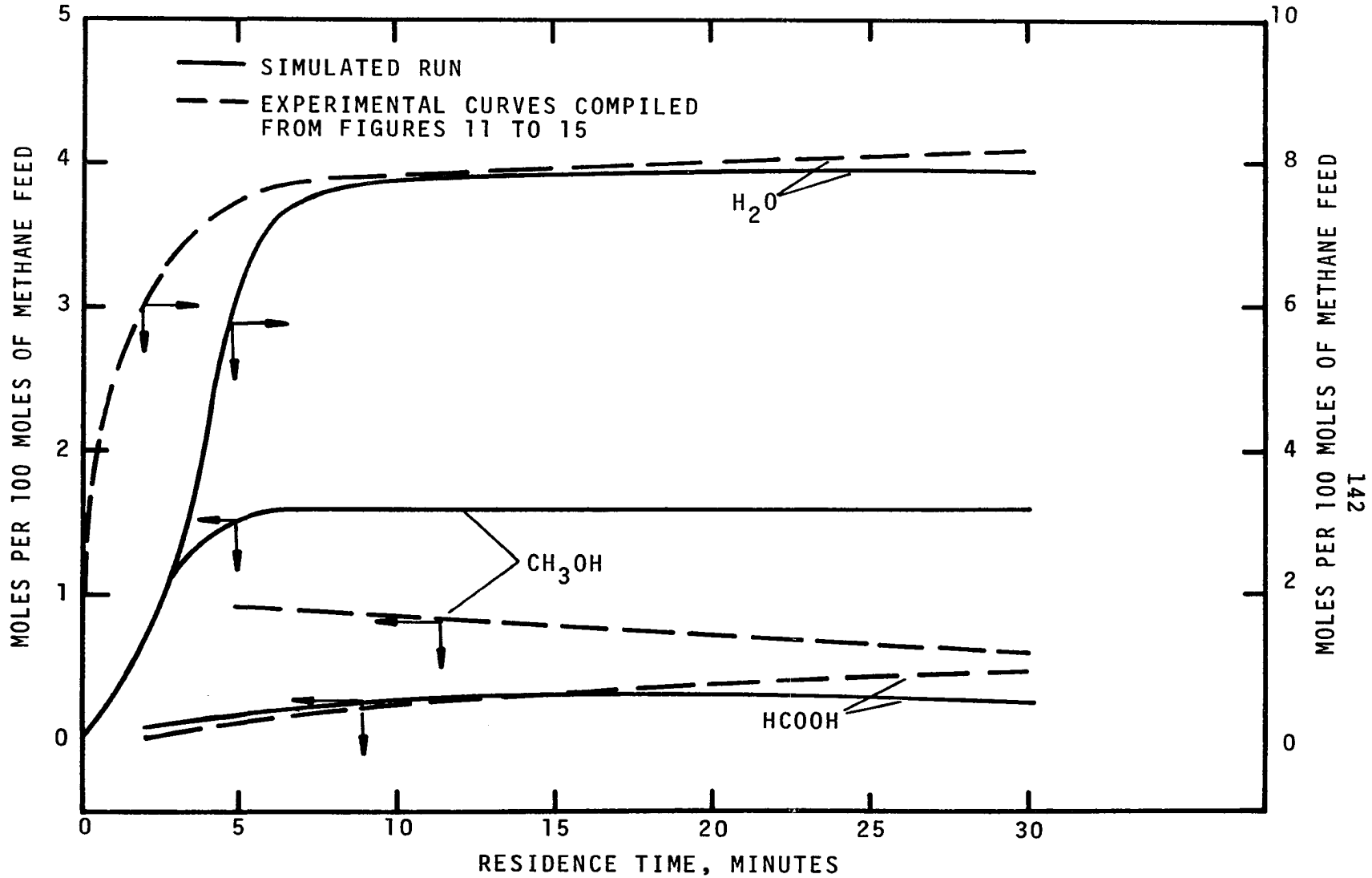

Figure 25. The Comparison Between Observed and Simulated Liquid Concentrations at 3400 atm and 290°C.

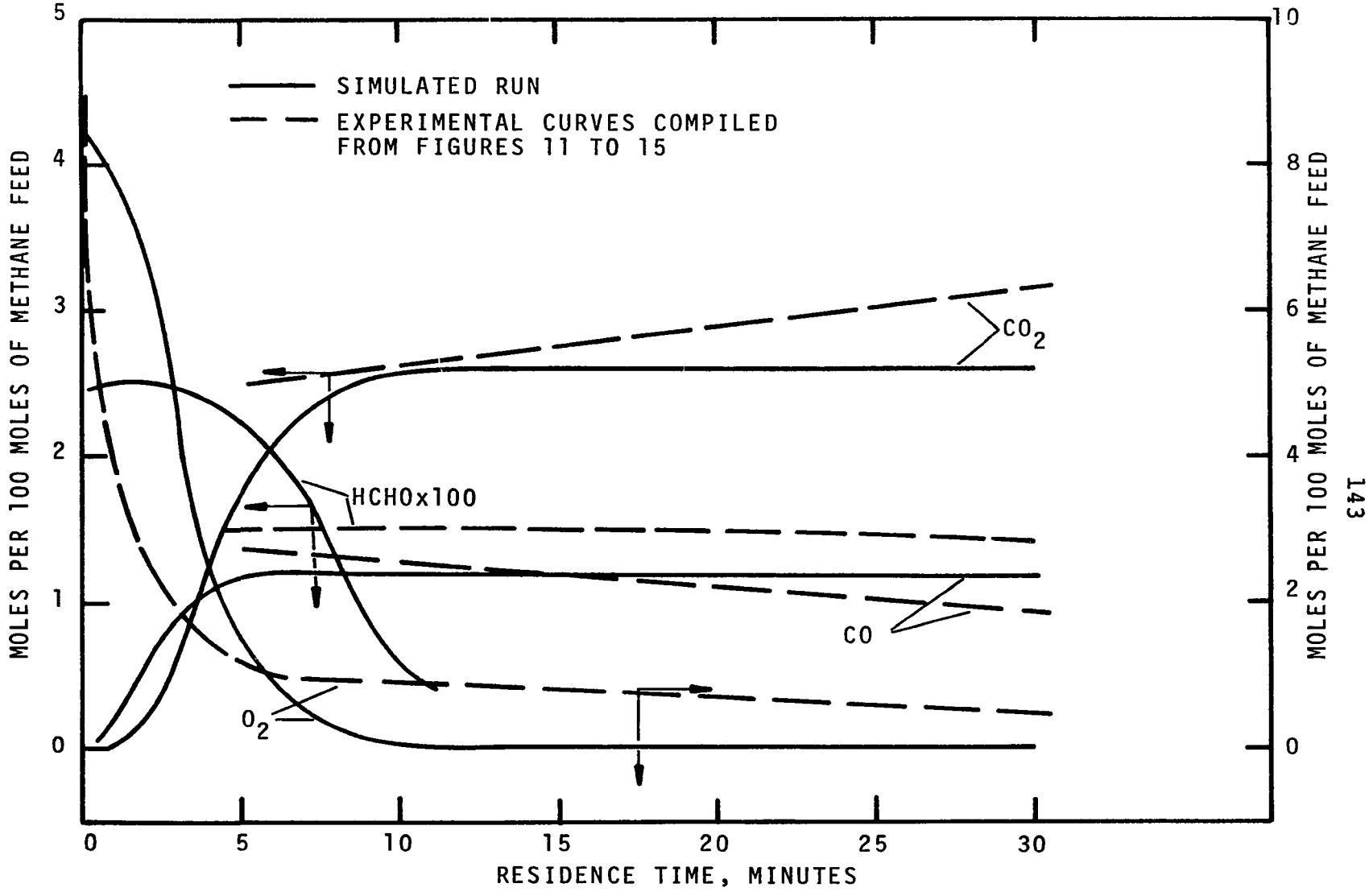

Figure 26. The Comparison Between Observed and Simulated Gaseous Concentrations at 3400 atm and 290°C.

induction period, during which no appreciable reaction occurred.

The first basic result obtained from this study was the selection of the best set of Arrhenius parameters to use with each elementary reaction in the proposed mechanism. As shown previously in Table 1, a predicted pre-exponential factor can be in error by several orders of magnitude. Several trial simulation runs were made using Arrhenius parameters estimated early in this study. These initial computations showed that the estimated pre-exponential factors for a few reactions, most notably Reaction G-4, could not be correct. While it was thought that the molecular decomposition in Reaction G-4 might have a pre-exponential factor as high as 10^{15} sec^{-1}, simulations using values near this yielded results grossly different from the observed experimental results. It was found that when the pre-exponential factor for Reaction G-4 was lowered to the value shown in Table 2, $10^{10.6}$ sec^{-1}, the predicted results approximated the experimental results. It was then discovered that this trial and error approach had given a value for the pre-exponential factor that was in agreement with that reported by Benson (13), as shown in Table 3a.

It can be seen from Figures 17 through 26 that the simulated results approximate the experimental curves. Probably the most serious deviation of the calculated from the observed values is in the oxygen results. The observed and

simulated results are different on two accounts, the simulated rate of consumption starts too slowly and then shows more consumption than was observed experimentally. The following additional generalizations can be made from the results of the other components at all pressure levels:

1. The methanol predictions remain slightly high and do not decrease with time as do the experimental curves.
2. The carbon monoxide predictions stay below the experimental curves and reach a constant level, rather than decrease with time.
3. The carbon dioxide predictions are very close to the experimental values.
4. The predicted formaldehyde concentrations start off in approximately the same area as the experimental, but rapidly decrease with time.
5. The formic acid predictions remained reasonably close to the experimental values at all times.

There are several possible explanations for the disagreement between the calculated and the experimental results:

1. The reaction pressure is so high that the ideal gas treatment used in developing the numerical analysis is not accurate. This explanation is plausible at the higher pressure levels, but it is not applicable at the lower levels.
2. The method of analysis is correct, but not all of the elementary reactions have been considered. The reactions

listed in the proposed mechanism can show the formation of individual components in amounts greater than were found experimentally with the exception of methyl formate. However, additional reactions to show the destruction of molecules, particularly methanol and carbon monoxide, might be needed.

3. The method for estimating the rate constants of one or more reactions is probably inadequate. It was found in the computer simulation that small changes in some rate constant terms could cause large variations in the results. (This topic will be further developed later in this section.)
4. It is possible that the experimental curves may be in error. The experimental plots were determined by drawing the best curves through scattered data taken at varying conditions. Although it was attempted to use data that were consistent, it was realized that some of the experimental runs had different reaction histories than others.
5. The simulation conditions did not match the reaction conditions. The most obvious example of this possibility is reaction temperature. In the experimental runs the reaction temperature normally increased, often as much as 30°C (42) or more, due to limited heat conduction out of the reactor. On the other hand, the simulated reaction had a constant temperature. The experimental temperature rise

may have caused a change in which reactions controlled the mechanism during the run.

All of the above situations might have had an appreciable effect on the correlation between the simulated and the observed reaction. However, it is felt that the largest source of deviation between the two situations was caused by neglecting the effect of surfaces on the reaction. Several aspects of this complication will be discussed.

The most evident aspect of this problem was the neglect of radical destruction at surfaces, as in Reaction G-13 of the proposed mechanism, although the destruction of reactive intermediate molecules is also important. It was originally felt that since the possibility for a gas phase reaction was much greater than a wall reaction at high pressure, surface reactions could be ignored. However, radical terminations and intermediate molecule destruction take place continually at surfaces in experimental studies. If a significant fraction of the radicals and intermediate molecules are destroyed before they can react, the overall rate may decrease and finally stop without all of the oxygen being consumed. This destruction could be extremely important late in the reaction when the rate of formation of the reactive species has slowed. This feature may explain the fact that oxygen was consumed to a greater degree in the simulated reactions, where there was no wall termination, than was observed in the experimental studies.

Figure 27 shows an additional effect of neglecting wall destruction reactions. The figure shows a plot of the radical concentrations in a simulation run at 375 atm and 326°C. It can be seen that most of the radical concentrations reached a maximum about the same time as the broad formaldehyde maximum, and then decreased very slowly. It would be expected that towards the end of a reaction the radical concentrations should decrease more rapidly due to the decreasing concentrations of the intermediate molecules and of oxygen, both of which are important in the generation of new radicals.

An attempt was made in the computer simulation to destroy more radicals by increasing the gas phase radical termination reactions, mainly Reactions G-11a, G-11b, G-11c, G-12, G-12b, and G-12c, up to the point that the rate constant for each reaction was 10^{10} (l/mole) sec^{-1}. This increase in the rate constants did little to the molecule concentrations other than to reduce the oxygen concentration at an even faster rate and reduce somewhat the HCHO, H_2O_2, and CH_3OOH molecule concentrations towards the end of the reaction. The final radical concentrations were all decreased, with most decreasing slightly, although both the CH_3OO and HO_2 radicals were greatly reduced due to the rapid consumption of oxygen.

The failure of the increased gas phase terminations to slow the reaction implies that wall reactions are needed to destroy reactive molecules, as suggested by Semenov (83)

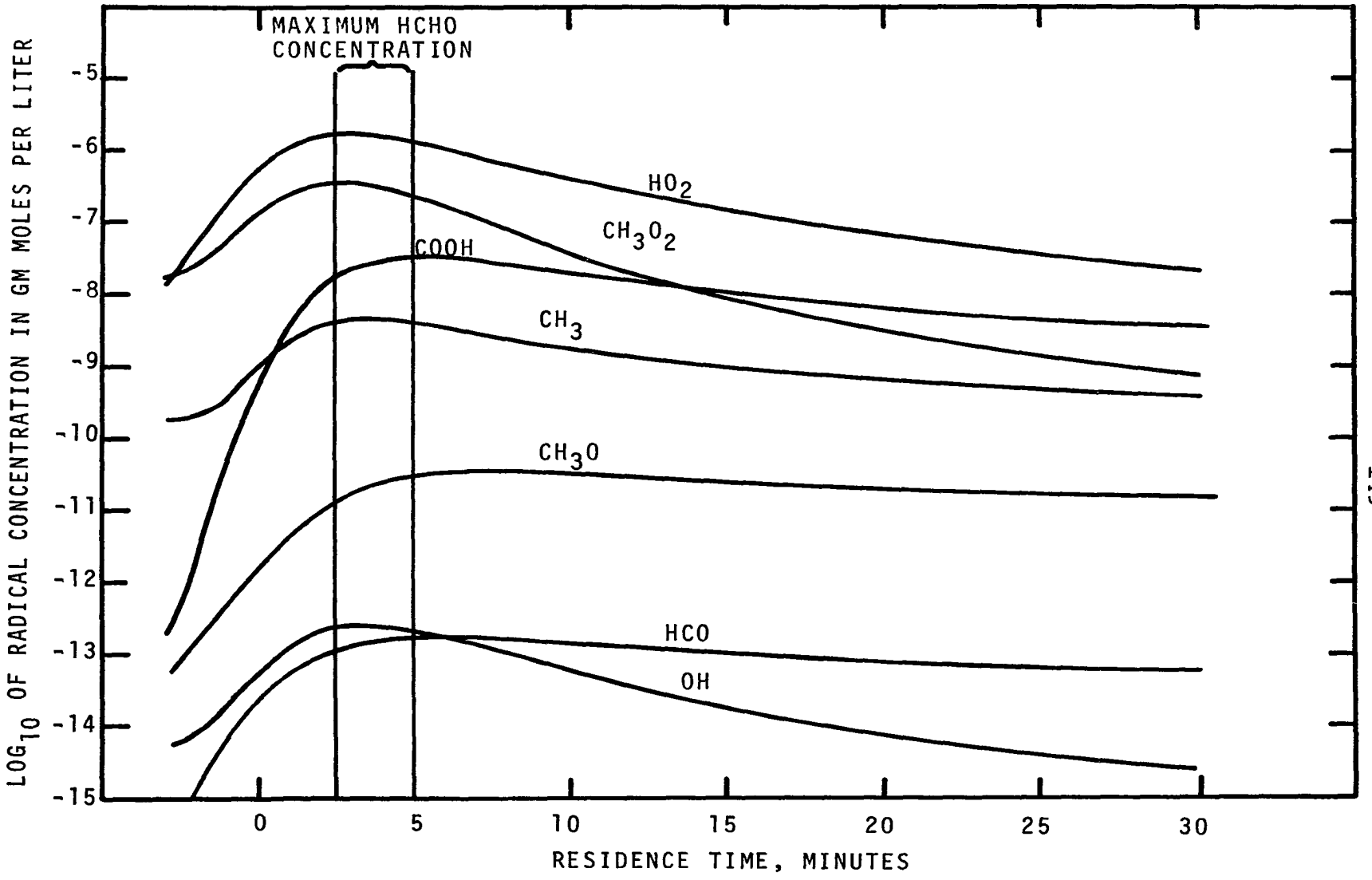

Figure 27. The Effect of Residence Time on the Simulated Radical Concentrations at 375 atm and 326°C.

and others. The first four of the gas phase termination reactions that were increased produced reactive intermediate molecules, HCHO, CH_3OH, and H_2O_2, so that the overall reaction was not effectively hindered by the increased termination. If even small quantities of these molecules were removed from the reaction by adsorption on a surface and converted to inert or relatively unreactive products, a significant decrease in the radical concentrations would occur. The combination of lower radical concentrations and lower intermediate molecule concentrations would then slow the reaction rate further. The removal of reactive molecules at the surface might well explain the observed decrease with time of carbon monoxide and methanol.

A further example of the effect of the wall destruction reactions can be found by comparing the simulated to the observed ignition delay. Bauerle's definition (9) of ignition delay was the time from the end of filling the reactor to the time of maximum temperature. Since in the simulation run the temperature remained constant, some other definition must be used. Bauerle noted that two other definitions had frequently been used to define the ignition delay, that of the time to maximum rate of temperature rise and that of the time to the start of auto-acceleration. This last definition is the only one of the three that could be applied to the simulated study. It was graphically observed that the inflection point in the

oxygen consumption curve approximated the time of maximum formaldehyde concentration. Since the formaldehyde maximum was much easier to determine than the point of auto-acceleration, the time to the formaldehyde maximum was used as a rough estimate of the ignition delay. Bauerle's graphical results show that this assumption is reasonable.

The comparison of the simulated to the observed ignition delay is found in Table 6 for several different temperature and pressure levels. The observed ignition delay was obtained from graphs prepared by Bauerle (9). It will be observed that the higher temperature values give reasonably good correlation while the lower temperature values are considerably in error. It will also be seen that at pressures of 680 atm and above, the high temperature values start diverging from the observed results.

It is thought that the diverging results at elevated pressures generally show the expected result of the high density problem. The pressure of 680 atm is in the region discussed earlier in which the reaction was expected to cease acting like a gas phase reaction.

The low temperature divergence at each of the pressure levels is thought to be due to the lack of surface decompositions in the simulated reaction. In the low temperature experimental runs, wall destruction of reactive intermediate molecules can cause very lengthy ignition delays. However,

TABLE 6

SIMULATED VERSUS CALCULATED IGNITION DELAY

Pressure (atm)	Temperature (°C)	Calculated (min)	Simulated (min)
150	324	122	20.1
	342	14.6	16.7
	355	2.7	16
375	306	83	7.4
	318	19.8	4.7
	330	3.8	5.0
475	300	45	6.0
	311	10.9	3.7
	320	2.3	4.4
680	292	60.5	3.3
	300	33.2	2.7
	306	11.0	2.7
1020	285	167	3.3
	295	30.7	3.3
	304	12.4	1.7
3400	276	∿100	2.0
	283	39	1.3
	290	17	1.3

at higher temperatures the wall destruction is offset by much faster initiation reactions. Since the simulated reaction did not contain wall destruction reactions, the simulated ignition delay was dependent only on the speed of initiation reactions. Thus, it would be expected that the simulated and the observed ignition delays should approach each other at the higher temperatures for each pressure level, as is found in Table 6.

It was mentioned earlier that the possibility exists that incorrect values for some of the rate constants might have been used. The following discussion may shed some light on which equations most influence the formation and destruction of the major molecules when the tabulated values for the rate constants are used.

The largest usage of oxygen was through Reaction G-1, with the reverse reaction, Reaction G-M1, being the largest source of oxygen. Both Reactions G-6 and G-6a used minor quantities of oxygen, approximately one tenth of that used in G-1. The largest calculated source of formaldehyde was through Reaction G-6 with G-2 forming an additional 10 percent of the total. The largest source of methanol was Reaction G-10a with Reaction G-5 forming about one fiftieth of that amount.

The lack of correlation between the observed and the simulated concentration of formaldehyde was initially disturbing. It was graphically noted, though, that most of the formation of the individual products occurred while the formaldehyde concentration was still in the general region of the

observed concentration. It is possible that some of the rate constants for the formation or usage of formaldehyde are incorrect, but the extra products from these reactions are minor due to the small concentration of the formaldehyde. The possibility still remains that the lack of wall termination reactions again has a large effect. The accuracy of the experimental curves for formaldehyde are also questionable due to the small quantities produced and its volatility in the liquid state.

It was mildly surprising to find how interrelated the different reactions in the mechanism are. In trying to determine the optimum set of rate constants, it was attempted to find some method to force the methanol to fit the experimental data better. The obvious route consisted of reducing the rate constant of the major reaction forming methanol, namely Reaction G-10a. However, since Reaction G-10a was also the major route of hydrogen peroxide destruction, reducing the rate constant of the reaction increased the concentration of the peroxide, so that there was no overall effect. The next alternative was to reduce the formation of hydrogen peroxide. Reaction G-7b was the largest source of the peroxide and reducing the rate constant of Reaction G-7b gave the desired results for the methanol concentration. However, it also had other less desirous effects. Besides being a major source of hydrogen peroxide, Reaction G-7b was also one of the chief sources

for the HCO radical. Reducing the rate of G-7b decreased the concentration of HCO and therefore reduced the formation of carbon monoxide, which was formed chiefly through Reaction G-6a. It was therefore learned that using only the reactions in the proposed mechanism, it would be difficult to manipulate the results for one component in the simulated run without affecting the other products. These results again illustrated the need for an additional source of destruction of reactive intermediate products.

Several of the results from the computer simulation have all pointed to a common problem, the possible need for surface destruction of some intermediate molecules. For this reason, a preliminary study was made with the present mechanism using the following wall destruction reaction:

(R-33) $H_2O_2 \rightarrow H_2O + 1/2\ O_2$

In the preliminary study it was assumed that ten percent of the hydrogen peroxide present underwent decomposition according to Reaction R-33.

The results of this simulation study are shown as the half-dashed lines in Figure 28 for methanol and water at a pressure of 375 atm and a temperature of 326°C. The solid lines show the results of the simulation without the surface reaction, while the dashed lines show the experimentally observed results. The methanol plot shows definite improvement

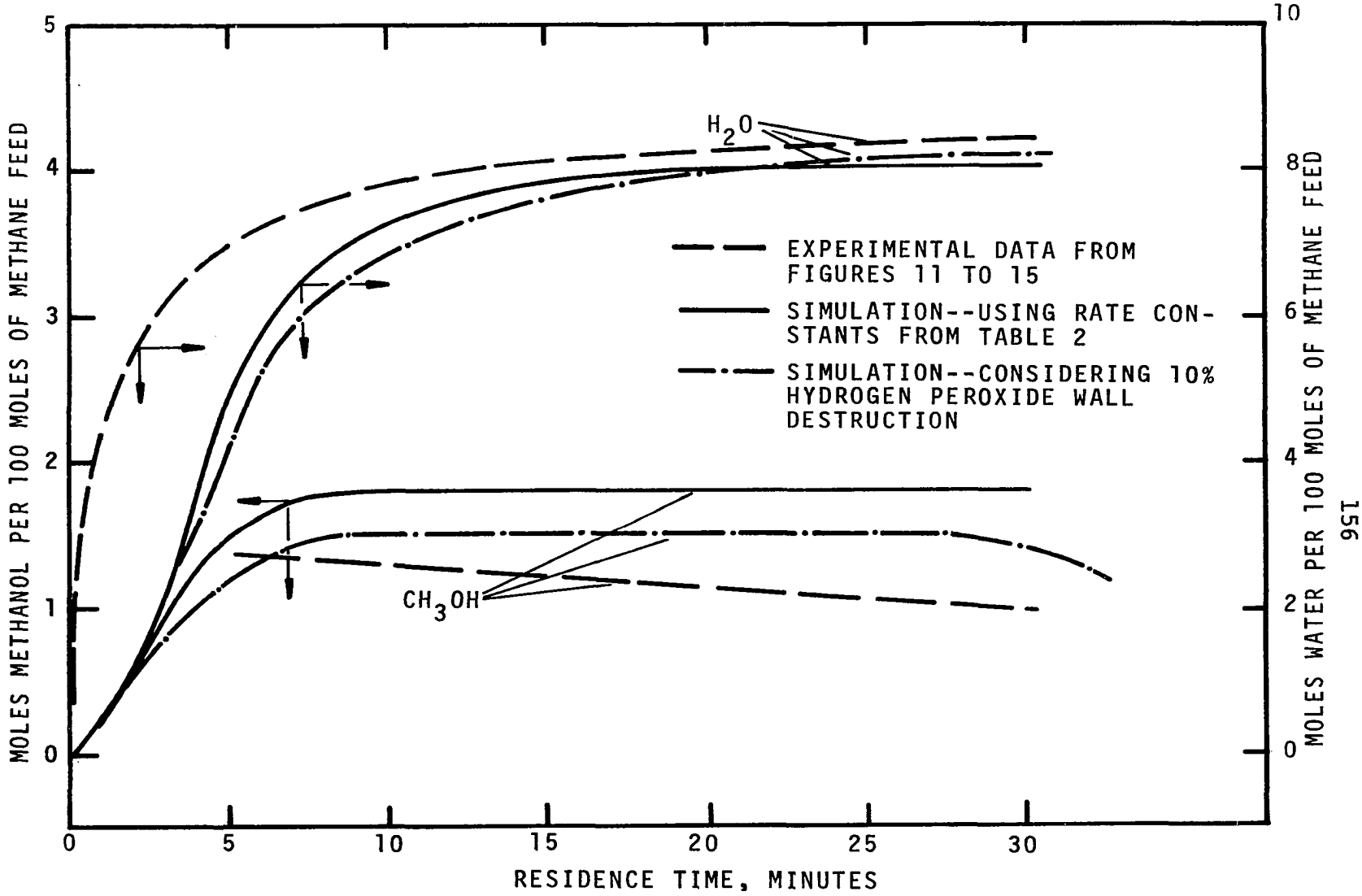

Figure 28. The Comparison of the Concentration of Methanol and Water as Observed Experimentally with the Predictions of Two Simulation Runs at 375 atm and 325°C.

over the previous results. In fact the methanol concentration even started to decrease at the end of the thirty minute study similar to the experimental decrease in concentration. The slight discrepancy between the two plots for the water curve was probably caused by the induction period lasting slightly longer due to the destruction of the intermediate H_2O_2 molecule. Similar plots for the other components were not included as the hydrogen peroxide destruction had little effect on them.

The value of ten percent for the hydrogen peroxide destruction was strictly an assumed number. Further theoretical work is needed to calculate the frequency of wall reactions and the various products obtained from them. Also other reactions involving other reactive intermediate molecules need to be considered.

It was found that by altering the rate constants of several reactions, and by increasing the amount of hydrogen peroxide that is destroyed heterogeneously to about twenty percent, it was possible to make the simulated concentrations of carbon monoxide, carbon dioxide, and methanol closely approximate experimental behavior. However, one would be reluctant to state that these changes would bring the mechanism any closer to true behavior without doing further studies on the wall reactions.

Even though it was realized that the mechanism did not fit observed behavior exactly, the mechanism was tested to

determine if it would qualitatively describe some experimentally observed characteristics. Fok and Nalbandyan (32) studied a photo-initiated oxidation of methane at 1 atm and 100°C. They found methyl hydroperoxide to be the exclusive product of the reaction. This reaction was simulated in the computer by generating a constant CH_3 radical concentration of 10^{-9} moles per liter as would be caused by acetone decomposition. The chief product of the simulated reaction was methyl hydroperoxide, with its concentration almost two orders of magnitude greater than the next closest product.

Norrish (69) found that adding an amount of formaldehyde much greater than the normal maximum amount present in a reaction caused the reaction to start immediately and at a rapid rate. However, the excess formaldehyde was rapidly consumed and the formaldehyde concentration and the rate of reaction quickly returned to normal. This experiment was simulated at a pressure of 375 atm and 326°C, with an initial formaldehyde concentration six times the normal maximum concentration. The results of this simulation are shown graphically in Figures 29 and 30. The solid curves show the results of a previous simulation under the same conditions but without the initial formaldehyde concentration. The curves have been shifted three minutes as was done earlier to eliminate the induction period. The half dashed curves, on the other hand, have not been shifted at all. It is most interesting to note

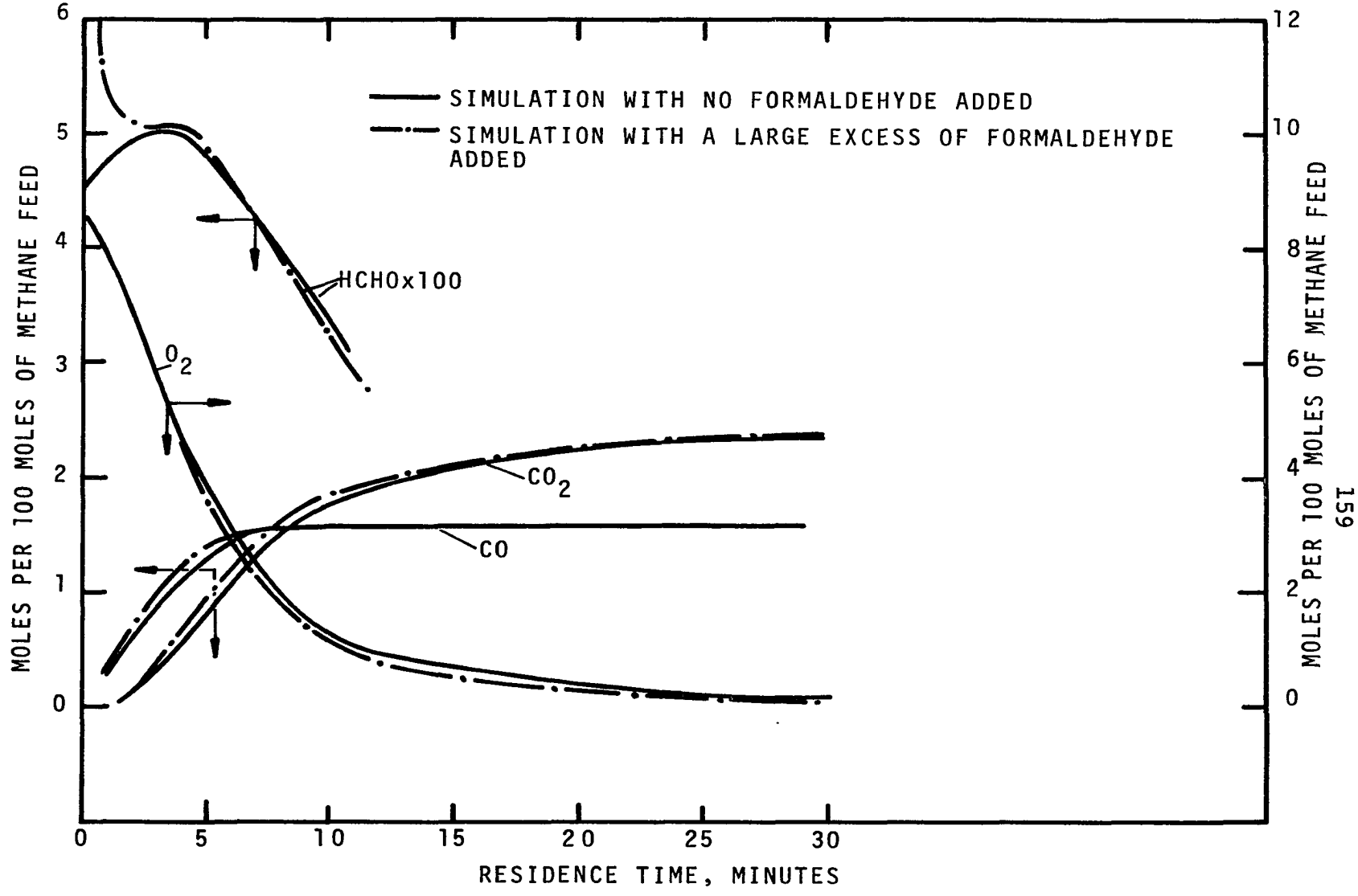

Figure 29. A Comparison of Gaseous Products from Two Simulated Runs at 375 atm and 326°C.

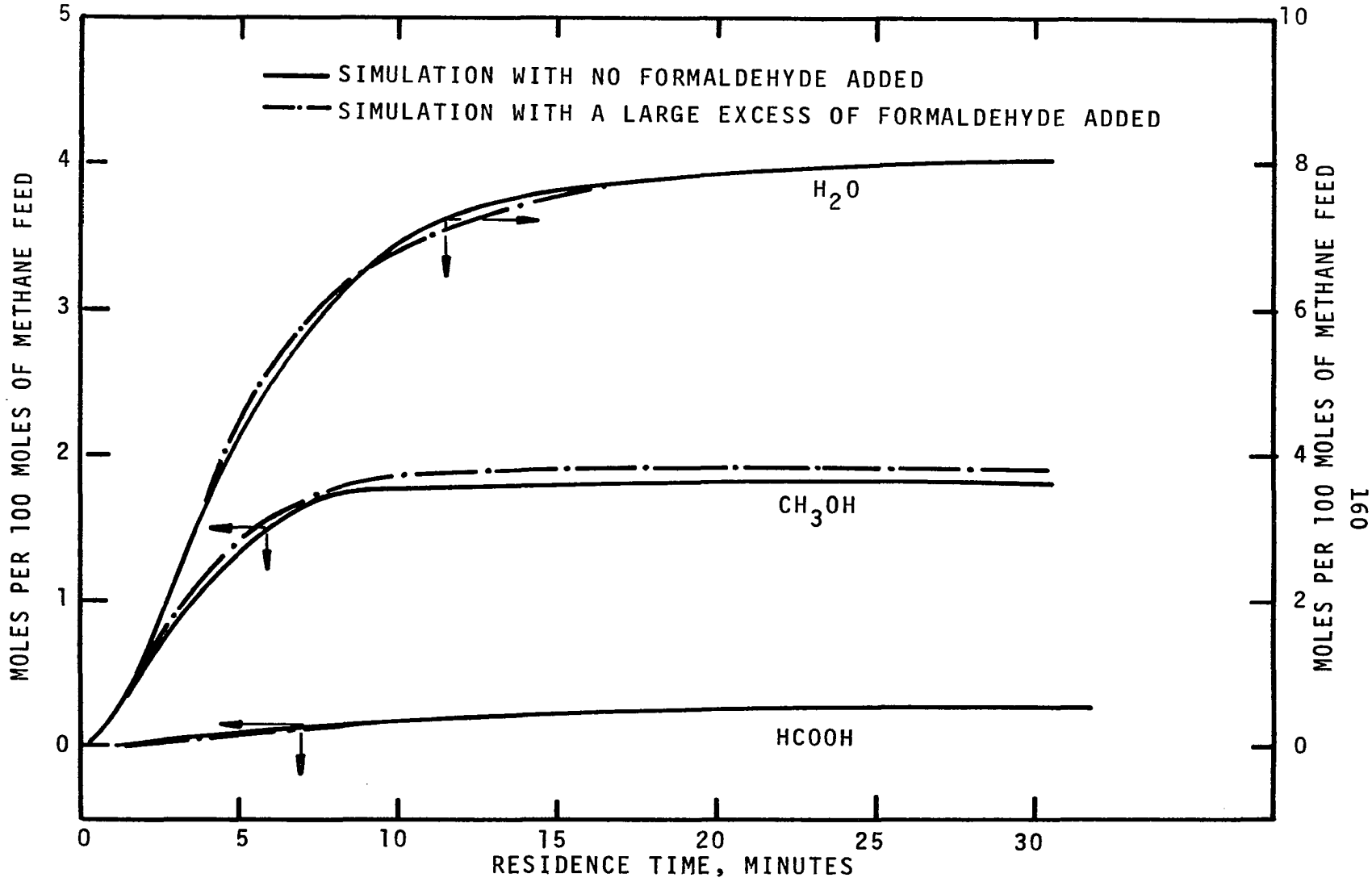

Figure 31. A Comparison of Liquid Products from Two Simulated Runs at 375 atm and 326°C.

that the simulated reaction started immediately but then slowed to the original rate as the formaldehyde concentration reached the normal value. Only minor changes were observed in the concentration curves for the various reaction products.

CHAPTER X

CONCLUSIONS

A mechanism for the high pressure oxidation of methane has been proposed. The mechanism is basically a radical chain reaction with degenerate branching.

Computer simulation of previous mechanisms showed that several additional reactions must be included to describe experimental behavior adequately, particularly for methanol and formic acid. The numerical results from a reaction simulation using the proposed mechanism approximated the experimental behavior reasonably well.

It was shown that even though gas phase reactions predominate at high pressures, surface destruction reactions must be considered in order to describe accurately experimental results. A preliminary study using one surface destruction reaction showed definite improvement in predicting both the magnitude and general shape of the methanol curve.

From the mechanism it was concluded that the reduced rate of non-explosive reactions at extreme pressures is due to a combination of the low reaction temperatures and the high densities preventing the bond stretching and breaking of at least two important reactions.

The numerical analysis only showed that the proposed mechanism was plausible. Proof of the mechanism can only come after additional data are obtained on the concentration of reactants, products, and intermediate species, on the rate constants of individual elementary reactions, and on the extent of heterogeneous reactions.

It is recommended that future work be continued in both the theoretical and experimental areas. More theoretical work is needed to develop a basis for wall destruction reactions which would probably lead to modifications in the proposed high pressure mechanism. In addition a temperature rise during reaction, similar to that observed experimentally, should be included in the reaction simulation.

In addition to these suggested mechanistic studies, more experimental data are needed on the effect of time on product concentrations at constant temperatures. Photo-initiated studies should also be used to check the mechanism at low temperatures, as suggested previously by Bauerle.

The following experimental work would be important to both mechanistic studies and studies for possible commercial uses. The variation of oxygen concentration and the addition of inerts, as might be found from oxidation with air, need to be studied. A study of what occurs in the early phase of a reaction will be necessary if the reaction is ever to be considered for commercial applications. The possible use of

of additives, such as formaldehyde, to reduce the induction period of the reaction might be studied in conjunction with the low residence time experiments.

NOMENCLATURE

a,b,c,d	Stoichiometric coefficients in Equation 9-1
A	Arrhenius pre-exponential factor
A,A'	Area in Appendix D
A,B	Reactants in Equation 9-1
b	Outer radius of a vessel shell
C,D	Products in Equation 9-1
d	Diameter
E	Arrhenius activation energy
E	In Appendix D, modulus of elasticity
F	Force
$\Delta G^{\neq}$	Free energy change going to the transition state
h	Planck's constant
k	Reaction rate constant
k	In Appendix D, diameter ratio of a shell
$\bar{k}$	Boltzmann's constant
K	Diameter ratio of a cylinder ($2 r_o/2 r_i$)
$K^{\neq}$	Equilibrium constant for the formation of the activated specie, $X^{\neq}$
m	Total number of shells in a compound vessel
n	Shell being considered in a compound vessel
P	Pressure

P_n Contact pressure

P_n' Residual contact pressure

P_{os} Overstrain pressure

ΔP Pressure change across a shell or across a complete vessel

q Heat of reaction

r Radius

r_e Radius of inelastic strain

R Gas constant

S Surface area

T Temperature

ΔT Temperature change, $T_i - T_o$

$\Delta V^{\neq}$ Volume change going to the transition state

x Shell thickness

$X^{\neq}$ Activated specie in transition state

Greek Letters

α Coefficient of thermal expansion

β Thermal stress terms, $\alpha E \Delta T/(1 - \nu)$

γ Fraction of the yield strength available in shear

κ Transmission coefficient

ν Poisson's ratio

σ_y Yield strength

σ_r Radial stress

σ_{rn} Radial stress at radius b_n in a monoblock cylinder

σ_t Tangential stress

σ_z Axial stress

τ Shear stress

τ_y Maximum shear stress

Subscripts

i Internal

o External

n Shell n

BIBLIOGRAPHY

1. Allara, D. L.; Edelson, D.; and Irwin, K. C. "Computational Modeling of the Mechanisms of the Free-Radical-Chain Reaction of Alkanes with Oxygen. The Oxidation of Isobutane, n-Butane, and Isopentane." Preprint of paper given at National ACS Meeting, Washington, D.C., September 13, 1971. To be published, International Journal of Chemical Kinetics.

2. Antonova, I. N., et al. Izvest. Akad. Nauk USSR Otdel Khim Nauk (1955), 789. Cited by N. N. Semenov, Some Problems in Chemical Kinetics and Reactivity, Vol. I. Translated by M. Boudart. Princeton, New Jersey: Princeton University press, 1958.

3. Ault, R. T., Republic Steel Research Center, Cleveland, Ohio. Private communication, June, 1971.

4. Babb, S. E., Jr., University of Oklahoma Physics Department, Norman, Oklahoma. Private communication, June, 1971.

5. Bach, A. N. Zh. Russk. Fiz-Khim. Obshch, 29 (1897), 373. Cited by V. Ya. Shtern, The Gas Phase Oxidation of Hydrocarbons. Translated by M. F. Mullins. A Pergamon Press Book. New York: Macmillan Company, 1964.

6. Baldwin, R. R., et al. "The High Temperature Oxidation of Aldehydes." Thirteenth Symposium (International) on Combustion. Pittsburgh: The Combustion Institute, 1971, pp. 251-258.

7. Bardwell, J., and Hinshelwood, C. "The Cool Flame of Methyl Ethyl Ketone." Proc. Royal Soc. London, A205 (1951), 375-390.

8. Barnard, J. A., and Cohen, A. "Reaction of Methyl Radicals with Oxygen." Trans. Faraday Soc., 64, 2 (1968), 396-404.

9. Bauerle, G. L. "Surface and Catalytic Effects in High Pressure Oxidation of Methane." Unpublished Ph.D. dissertation. University of Oklahoma, Norman, Oklahoma, 1969.

10. Benson, S. W. The Foundation of Chemical Kinetics. New York: McGraw-Hill Book Company, Inc., 1960.

11. _____. "Some Current Views of the Mechanism of Free Radical Oxidations." Oxidation of Organic Compounds-II. Advances in Chemistry Series, Vol. 76. Washington, D.C.: American Chemical Society, 1968, pp. 143-153.

12. _____. Thermochemical Kinetics. New York: John Wiley & Sons, Inc., 1968.

13. _____, and O'Neal, H. E. Kinetic Data on Gas Phase Unimolecular Reactions. U.S. Dept. of Commerce, NSRDS-NBS21. U.S. Government Printing Office, 1970.

14. Blundell, R. V., et al. "Rates of Radical Reactions in Methane Oxidation." Tenth Symposium (International) on Combustion. Pittsburgh: The Combustion Institute, 1965, pp. 445-451.

15. Bone, W. A., and Allum, R. E. "The Slow Combustion of Methane." Proc. Royal Soc. London, A134 (1932), 578-591.

16. _____, and Cain, J. C. "The Explosion of Acetylene with Less Than Its Own Volume of Oxygen." Journal of the Chemical Society, 71 (1897), 26-41.

17. _____, and Gardner, J. B. "Comparative Studies of the Slow Combustion of Methane, Methyl Alcohol, Formaldehyde, and Formic Acid." Proc. Royal Soc. London, A154 (1936), 297-328.

18. _____, and Wheeler, R. V. "The Slow Oxidation of Methane at Low Temperatures." Journal of the Chemical Society. Part 1: 81 (1902), 535-549. Part 2: 83 (1903), 1074-1087.

19. Boomer, E. H., and Broughton, J. W. "The Oxidation of Methane at High Pressures. Part I. Preliminary Experiments." Canadian Journal of Research, 15B (1937), 375-382.

20. Boomer, E. H., and Naldrett, S. N. "The Oxidation of Methane at High Pressures. Part IV. Experiments Using Pure Methane and Copper, Silver, Zinc, Nickel, or Monel Metal as Catalysts." Canadian Journal of Research, 25B (1947), 494-501.

21. _____, and Thomas V. "The Oxidation of Methane at High Pressures. Part II. Experiments with Various Mixtures of Viking Natural Gas and Air. Part III. Experiments Using Pure Methane and Principally Copper as Catalyst." Canadian Journal of Research, 15B (1937), 401-413, 414-433.

22. Boudart, M. Kinetics of Chemical Processes. Englewood Cliffs, New Jersey: Prentice-Hall, Inc., 1968.

23. Comings, E. High Pressure Technology. New York: McGraw-Hill Book Company, Inc., 1956.

24. Cullis, C. F. "Recent Developments in the Controlled Oxidation of Hydrocarbons." Chemistry and Industry (London), 29 (1968), 961-965.

25. Cvetanovic, R. J. "Reaction of Oxygen Atoms with Ethylene." Journal of Chemical Physics, 23 (1955), 1375-1380.

26. Dalton, J. New Systems of Chemical Philosophy, Part II (1807), 442. Cited by V. Ya. Shtern, The Gas Phase Oxidation of Hydrocarbons. Translated by M. F. Mullins. A Pergamon Press Book. New York: Macmillan Company, 1964.

27. Edelson, D., Bell Telephone Laboratories, Murray Hill, New Jersey. Private communication, September 24, 1971.

28. Enikolopyan, N. S. Dok. Akad. Nauk SSSR, 1958. Cited by N. N. Semenov, Some Problems in Chemical Kinetics and Reactivity, Vol. II. Translated by M. Boudart. Princeton, New Jersey: Princeton University Press, 1959.

29. _____. "Kinetics and Mechanism of Methane Oxidation." Seventh Symposium (International) on Combustion. The Combustion Institute. London: Butterworths Scientific Publications, 1959.

30. _____. Zh. Fiz. Khim., 30 (1956), 769. Cited by V. Ya. Shtern, The Gas Phase Oxidation of Hydrocarbons. Translated by M. F. Mullins. A Pergamon Press Book. New York: Macmillan Company, 1964.

31. Fisher, I. P., and Tipper, C. F. H. "Oxidation of Methane at about 400°C. Part 1. Reaction Catalyzed by the Photo-Decomposition of Acetone." "Part 2. Role of Peroxides and the Reaction of Methyl Radicals and Oxygen." Trans. Faraday Soc., 59, 5 (1963), 1163-1173, 1174-1180.

32. Fok, N. V., and Nalbandyan, A. B. Dokl. Akad. Nauk USSR, 89 (1953), 125, and 86 (1952), 589. Cited by N. N. Semenov, Some Problems in Chemical Kinetics and Reactivity, Vol. I. Translated by M. Boudart. Princeton, New Jersey: Princeton University Press, 1958.

33. Fort, R., and Hinshelwood, C. N. "Further Investigations on the Kinetics of Gaseous Oxidation Reactions." Proc. Royal Soc. London, A129 (1930), 284-299.

34. Frank-Kamenetskii, A. A. J. Phys. Chem. (USSR), 14 (1940), 30. Cited by S. W. Benson, The Foundation of Chemical Kinetics. New York: McGraw-Hill Book Company, Inc., 1960.

35. Furman, M. S. Khimicheskaya Promyshlennost, 1-2 (1946), 24. Cited by M. G. Gonikberg, Chemical Equilibria and Reaction Rates at High Pressures. 2nd ed. Jerusalem: Israel Program for Scientific Translations, for the National Science Foundation, Washington, D.C., 1963.

36. _____, and Tsiklis, D. S. Doklady Akademii Nauk SSSR, 91 (1953), 597. Cited by M. G. Gonikberg, Chemical Equilibria and Reaction Rates at High Pressures. 2nd ed. Jerusalem: Israel Program for Scientific Translations, for the National Science Foundation, Washington, D.C., 1963.

37. Gear, C. W. "The Numerical Integration of Ordinary Differential Equations." Mathematics of Computation, 21, 98 (1967), 146-156.

38. Gonikberg, M. G. Chemical Equilibria and Reaction Rates At High Pressures. 2nd ed. Jerusalem: Israel Program for Scientific Translations, for the National Science Foundation, Washington, D.C., 1963.

39. Gray, P., and Jones, A. "Attack of Related Free Radicals on Methane: Arrhenius Parameters and Thermochemistry." Canadian Journal of Chemistry, 45, 4 (1967), 333-337.

40. Hamann, S. D. Physico-Chemical Effects of Pressure. New York: Academic Press, Inc., 1957.

41. Harding, A. J., and Norrish, R. G. W. "Role of Formaldehyde in the Oxidation of Ethylene." Nature, 163 (1949), 797.

42. Hardwicke, N. L. "The Mechanism of Partial Oxidation of Methane at High Pressures." Unpublished Ph.D. dissertation. University of Oklahoma, Norman, Oklahoma, 1966.

43. _____; Lott, J. L.; and Sliepcevich, C. M. "Mechanism for the High Pressure Oxidation of Methane." University of Oklahoma, Norman, Oklahoma, 1969 (Typewritten).

44. _____; Lott, J. L.; and Sliepcevich, C. M. "Oxidation of Methane at High Pressures." I&EC Product Research and Development, 8, 2 (1969), 133-140.

45. Harris, G. M. Chemical Kinetics. Topics in Modern Chemistry Series. Boston: D. C. Heath and Company, 1966.

46. Heicklen, J. "Gas-Phase Reactions of Alkylperoxy and Alkoxy Radicals." Oxidation of Organic Compounds-II. Advances in Chemistry Series, Vol. 76. Washington, D. C.: American Chemical Society, 1968.

47. Hirschfelder, J. O. "Semi-Empirical Calculations of Activation Energies." Journal of Chemical Physics, 9 (1941), 645-653.

48. Hoare, D. E. "Reproducibility in the Slow Combustion of Methane." Trans. Faraday Soc., 49 (1953), 628-629.

49. _____, and Milne, G. S. "Role of Hydroxyl and Hydroperoxyl Radicals in Slow Combustion of Methane." Trans. Faraday Soc., 63, 1 (1967), 101-110.

50. _____: Protheroe, J. B.; and Walsh, A. D. "The Thermal Decomposition of Hydrogen Peroxide Vapour." Trans. Faraday Soc., 55 (1959), 548-557.

51. IBM Corporation. System/360 Continuous System Modeling Program User's Manual. Program Number 360A-CX-16X. 4th ed. IBM Corporation, 1969.

52. Ingold, K. U., and Bryce, W. A. "Mass Spectrometric Investigation of the Hydrogen-Oxygen and Methyl-Oxygen Reactions." Journal of Chemical Physics, 24, 2 (1956), 360-364.

53. Johnston, H. S., and Cramarossa, F. "Highly Complex Photochemical Mechanisms." Advances in Photochemistry, Vol. 4. Edited by W. A. Noyes, Jr., G. S. Hammond, and J. N. Pitts, Jr. New York: Interscience Publishers, 1966, pp. 1-24.

54. Karmilova, L. V.; Enikolopyan, N. S.; and Nalbandyan, A. B. Zhur. Fiz. Khim., 34 (1960), 550, 990. Cited by N. L. Hardwicke, "The Mechanism of Partial Oxidation of Methane at High Pressures." Unpublished Ph.D. dissertation. University of Oklahoma, Norman, Oklahoma, 1966.

55. _____; Enikolopyan, N. S.; and Nalbandyan, A. B. Zhur. Fiz. Chim, 35 (1961), 1458. Cited by R. V. Blundell, et al., "Rates of Radical Reactions in Methane Oxidation." Tenth Symposium (International) on Combustion. Pittsburgh: The Combustion Institute, 1965, pp. 445-451.

56. Lamé, G. "Lecns sur la Theorie Mathematique de L'Elasticite des Corps. Solides." Bachelier, Paris (1852), 188-191. Cited by J. L. Skinner, R. D. Daniels, and C. M. Sliepcevich, "Design of Vessels for Commercial Service at Extreme Pressures." British Chemical Engineering, 8, 4 (1963), 245-250.

57. Lean, B., and Bone, W. A. "The Behavior of Ethylene on Explosion with Less Than Its Own Volume of Oxygen." Journal of the Chemical Society, 61 (1892), 873-888.

58. Lewis, B. "Low Temperature Oxidation of Hydrocarbons," Journal of the Chemical Society, 130 (1927), 1555-1572; "Low Temperature Oxidation of Hydrocarbons. Part I. The Pressure-Temperature Curves of Amylene-Oxygen Mixtures." 132 (1929), 759-767; "Low Temperature Oxidation, Part II. The Ignition of Some Hydrocarbons in Oxygen." 133 (1930), 58-74.

59. _____, and von Elbe, G. Combustion, Flames and Explosions of Gases. 2nd ed. New York: Academic Press, Inc., 1961.

60. Lott, J. L. "The Selective Oxidation of Methane at High Pressures." Unpublished Ph.D. dissertation. University of Oklahoma, Norman, Oklahoma, 1965.

61. Ludwig, E. E. Applied Process Design for Chemical and Petrochemical Plants. Vols. 1-3. Houston, Texas: Gulf Publishing Company, 1964.

62. Lukovnikov, S. F., and Neiman, M. B. Zhurn. Fiz. Khim., 29 (1955), 1410. Cited by N. N. Semenov, Some Problems in Chemical Kinetics and Reactivity, Vol. I. Translated by M. Boudart. Princeton, New Jersey: Princeton University Press, 1958.

63. Manning, W. R. D. "The Design of Compound Cylinders for High-Pressure Service." Engineering,(London), May 2, 1947, 349-352.

64. Minkoff, G. J., and Salooja, K. C. "Hydrogen Peroxide and the Slow Oxidation of Methane." Fuel, 32, 4 (1953), 516-517.

65. Mise, V. R. Gottinger Nachr (1913), 582. Cited by H. Ll. D. Pugh, Mechanical Behavior of Materials Under Pressure. Amsterdam: Elsevier Publishing Company, Ltd., 1970.

66. Newitt, D. M., and Gardner, J. B. "The Initial Formation of Alcohols During the Slow Combustion of Methane and Ethane at Atmospheric Pressure." Proc. Royal Soc. London, A154 (1936), 329-335.

67. _____, and Haffner, A. E. "The Formation of Methyl Alcohol and Formaldehyde in the Slow Combustion of Methane at High Pressures." Proc. Royal Soc. London, A134 (1932), 591-603.

68. _____, and Szego, P. "Slow Oxidations at High Pressures. I--Methane and Ethane. II--Methyl Alcohol, Ethyl Alcohol, Acetaldehyde, and Acetic Acid." Proc. Royal Soc. London, A147 (1934), 555-571.

69. Norrish, R. G. W. "Evidence Relating to Combustion of Hydrocarbons." Faraday Society Discussion, 10 (1951), 269-278.

70. _____, and Foord, S. G. "The Kinetics of the Combustion of Methane." Proc. Royal Soc. London, A157 (1936), 503-525.

71. _____, and Reagh, J, D. "The Surface as a Limiting Factor in the Slow Combustion of Hydrocarbons." Proc. Royal Soc. London, A176 (1940), 429-448.

72. _____, and Wallace, J. "The Reaction of Methane and Oxygen Sensitized by Nitrogen Peroxide. Part I. Thermal Ignition." Proc. Royal Soc. London, A145 (1934), 307-321.

73. Paris, A. "Mild Oxidation of Methane Under Pressure." Chimie & Industrie, (1943), 411-420. Cited in Chemical Abstracts, CA 28:5806.

74. Polyak, S. S., and Shtern, V. Ya. Zhurn. Phys. Khim., 27 (1953), 341, 631, 950; Dokl. Akad. Nauk USSR, 95 (1954), 1231. Cited by N. N. Semenov, Some Problems in Chemical Kinetics and Reactivity, Vol, I. Translated by M. Boudart. Princeton, New Jersey: Princeton University Press, 1958.

75. Poole, S. W.; Ault, R. T.; and Stotler, C. D. "The Effect of Elevated Temperature Exposure on the Strength and Toughness of HP 9-4-30 Steel." Technical Memorandum. Cleveland, Ohio: Republic Steel Corporation Research Center, November 19, 1968.

76. Pope, J. C.; Dykstra, E. J.; and Edgar, G. "The Mechanism of the Vapor Phase Oxidation of Isomeric Octanes. I. Normal Octane. II. Octanes with Branched Chains." Journal of the American Chemical Society, 51 (1929), 1875-1889, 2203 - 2213.

77. Pryor, W. A. Free Radicals. New York: McGraw-Hill Book Company, Inc., 1966.

78. Pugh, H. Ll. D. Mechanical Behavior of Materials Under Pressure. Amsterdam: Elsevier Publishing Company, Ltd., 1970.

79. Rice, F. O., and Teller, E. "The Role of Free Radicals in Elementary Organic Reactions." Journal of Chemical Physics, 6 (1938), 489-496.

80. Ridge, M. J. "The Slow Oxidation of Gaseous Hydrocarbons." Reviews of Pure and Applied Chemistry (Austrailian), 6, 3 (1956), 121-152.

81. Rouchaud, J., and Nietera, P. "Competitive Liquid-Phase Oxidation of Butanes." I&EC Process Design and Development, 7, 2 (1968), 295-300.

82. Semenov, N. N. Chemical Kinetics and Chain Reactions. English Edition. London: Oxford University Press, 1935.

83. _____. Some Problems in Chemical Kinetics and Reactivity, Vol. I and II. Translated by M. Boudart. Princeton, New Jersey: Princeton Univeristy Press, 1958, 1959.

84. Shtern, V. Ya. "Chain Reactions of Hydrocarbon Oxidation." Publ. Akad. Nauk SSSR, 37 (1955). Cited by V. Ya. Shtern, The Gas Phase Oxidation of Hydrocarbons. Translated by M. F. Mullins. A Pergamon Press Book. New York: Macmillan Company, 1964.

85. _____. The Gas Phase Oxidation of Hydrocarbons. Translated by M. F. Mullins. A Pergamon Press Book. New York: Macmillan, 1964.

86. _____. Zhurn. Fiz. Khim., 28 (1954), 613. Cited by N. N. Semenov, Some Problems in Chemical Kinetics and Reactivity, Vol. I. Translated by M. Boudart. Princeton, New Jersey: Princeton University Press, 1958.

87. Skinner, J. L.; Daniels, R. D.; and Sliepcevich, C. M. "Design of Vessels for Commercial Service at Extreme Pressures." British Chemical Engineering, 8, 4 (1963), 245-250.

88. Steacie, E. W. R. Atomic and Free Radical Reactions. New York: Reinhold Publishing Company, 1946.

89. Townsend, D. T. A., and Chamberlain, E. A. C. "The Influence of Pressure on the Spontaneous Ignition of Inflammable Gas-Air Mixtures. Part IV. Methane-, Ethane-, and Propane-Air Mixtures." Proc. Royal Soc. London, A154 (1936), 95-112.

90. Trotman-Dickenson, A. F. Free Radicals. London: Methuen and Company, Ltd., 1959.

91. _____. Gas Kinetics. London: Butterworths Scientific Publications, 1955.

92. Vanadium-Alloys Steel Company. "Vascomax 200, 250, 300, 350--18 Percent Nickel Ultra High Strength Maraging Steels." Latrobe, Pennsylvania: Vanadium-Alloys Steel Company (now called Vasco, A Teledyne Company), 1966.

93. Vanpee, M., and Grard, F. "Formaldehyde and the Oxidation of Methane." Fuel, 34, 4 (1955), 433-443.

94. Vartanyan, L. S.; Maizus, Z. K.; and Emanuel, N. M. Zhur. Fiz. Khim., 30 (1956), 856. Cited by N. N. Semenov, Some Problems in Chemical Kinetics and Reactivity, Vol. II. Translated by M. Boudart. Princeton, New Jersey: Princeton University Press, 1959.

95. Walas, S. M. Reaction Kinetics for Chemical Engineers. New York: McGraw-Hill Book Company, Inc., 1959.

96. Walling, C. Free Radicals in Solution. New York: John Wiley & Sons, Inc., 1957.

97. Whalley, E. "The Design of Pressure Vessels Subjected to Thermal Stress: Parts I, II." Canadian Journal of Technology, 34 (1956), 268-303.

98. _____, and Morris, S. "The Design of Pressure Vessels Subjected to Thermal Stress: Part IV." International Journal of Mechanical Science, 1 (1960), 369-378.

99. Wiezevich, P. J., and Frolich, P. K. "Direct Oxidation of Saturated Hydrocarbons at High Pressures." Industrial and Engineering Chemistry, 26, 3 (1934), 267-276.

100. Winnick, J. "Liquid-Liquid Phase Behavior of Binary Solutions at Elevated Pressures." Unpublished Ph.D. dissertation. University of Oklahoma, Norman, Oklahoma, 1963.

APPENDICES

APPENDIX A

CALIBRATION OF MANGANIN CELL AND DYNALOG RECORDER

Early in this study, the manganin cell pressure gauge, with the attached Foxboro Dynalog recorder was calibrated by comparing the readings from the Dynalog to the pressure reading observed on a Bourdon tube pressure gauge. For pressures below 1360 atm, direct pressure gauge readings were used. For pressures above 1360 atm pressure, readings were obtained with the pressure gauge attached to the low pressure side of a 10:1 intensifier. It was found that the manganin cell followed Winnick's calibration chart (60, 100), which is shown in Figure 36. The chart was originally prepared by calibration against a manganin gauge which had been calibrated against the freezing point of mercury.

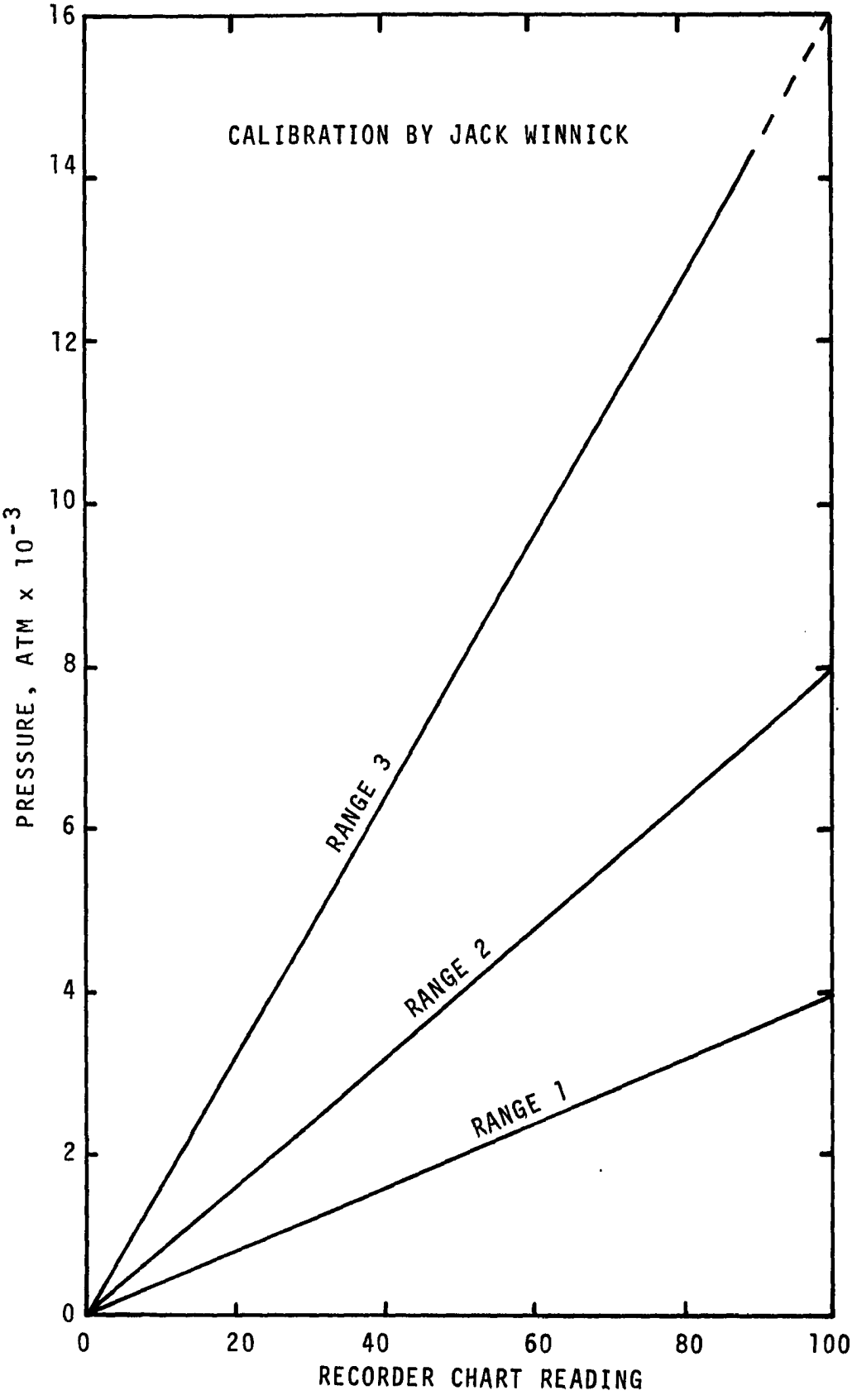

Figure 31. Manganin Cell and Foxboro Recorder Calibration.

APPENDIX B

CALIBRATION OF GAS CHROMATOGRAPH

Analysis of all experimental products was made with a Hewlett-Packard F&M Scientific 700 Laboratory Chromatograph. Gas samples were analyzed using a pair of 0.91 meter columns, filled with 60-80 mesh of 5A molecular sieve. The liquid samples were analyzed using two 2.44 meter columns of 50-80 mesh Porapak T.

The chromatograph was calibrated by analyzing samples of known composition. The liquid samples were prepared gravimetrically with water being the chief constituent. Gas samples were prepared manometrically with methane being the chief constituent.

The area under each peak of the known samples was divided by the area under the main peak. The ratios were plotted versus the mass ratios of the same peaks for the liquid samples and versus the mole ratios of the peaks for the gas samples. These plots are shown in Figures 37 to 45.

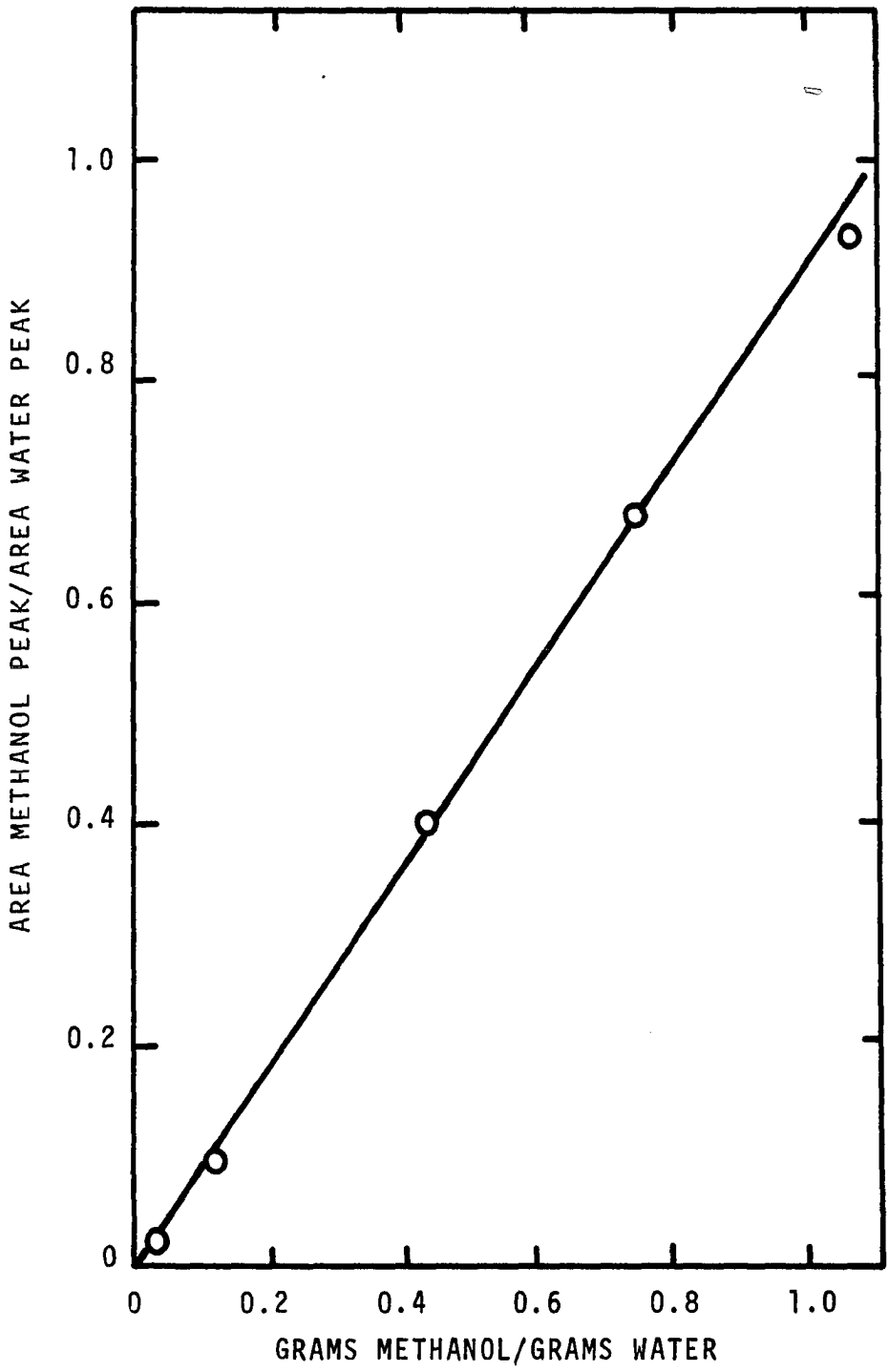

Figure 32. Chromatographic Calibration Curve for Methanol.

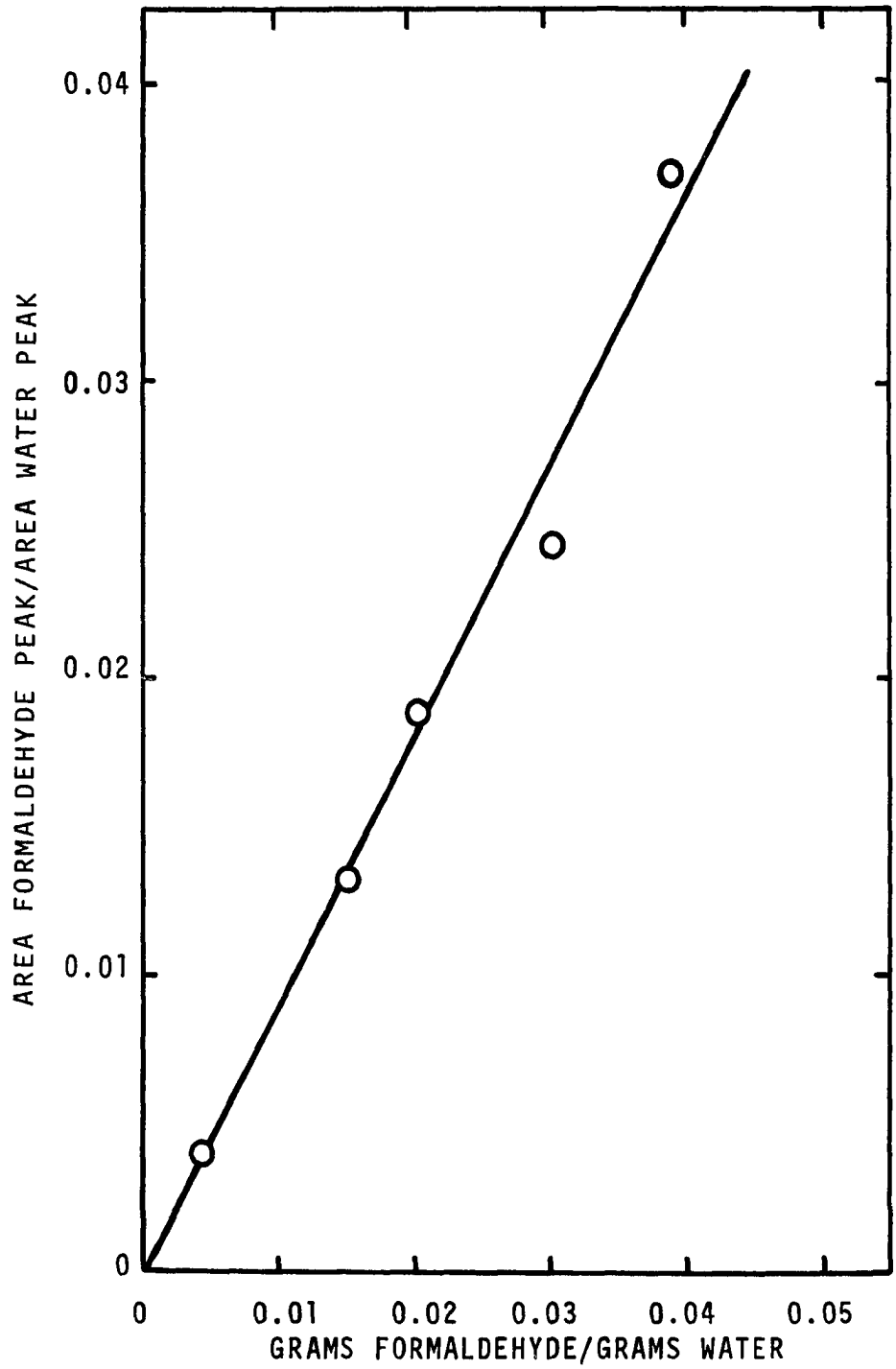

Figure 33. Chromatographic Calibration Curve for Formaldehyde.

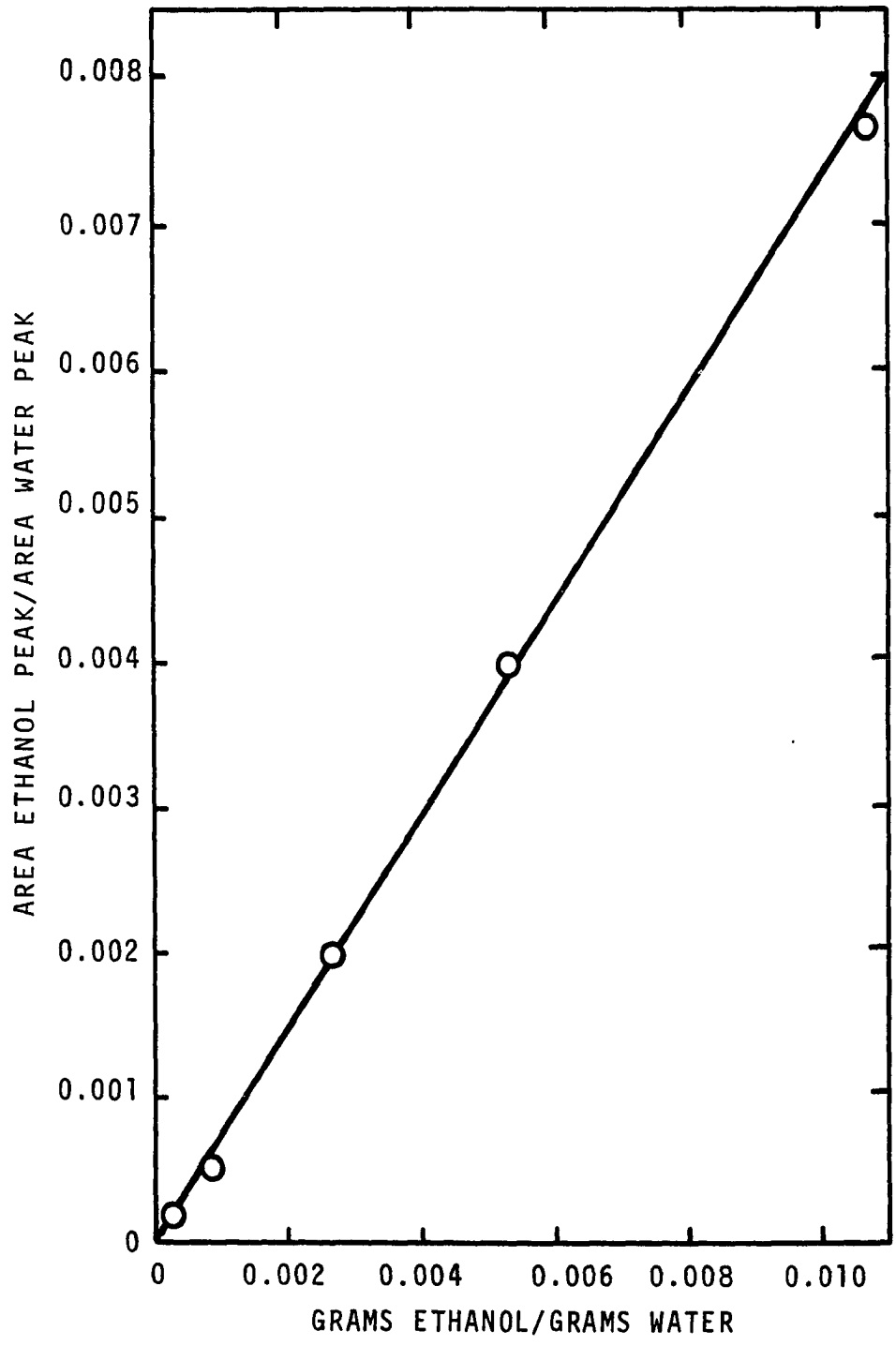

Figure 34. Chromatographic Calibration Curve for Ethanol.

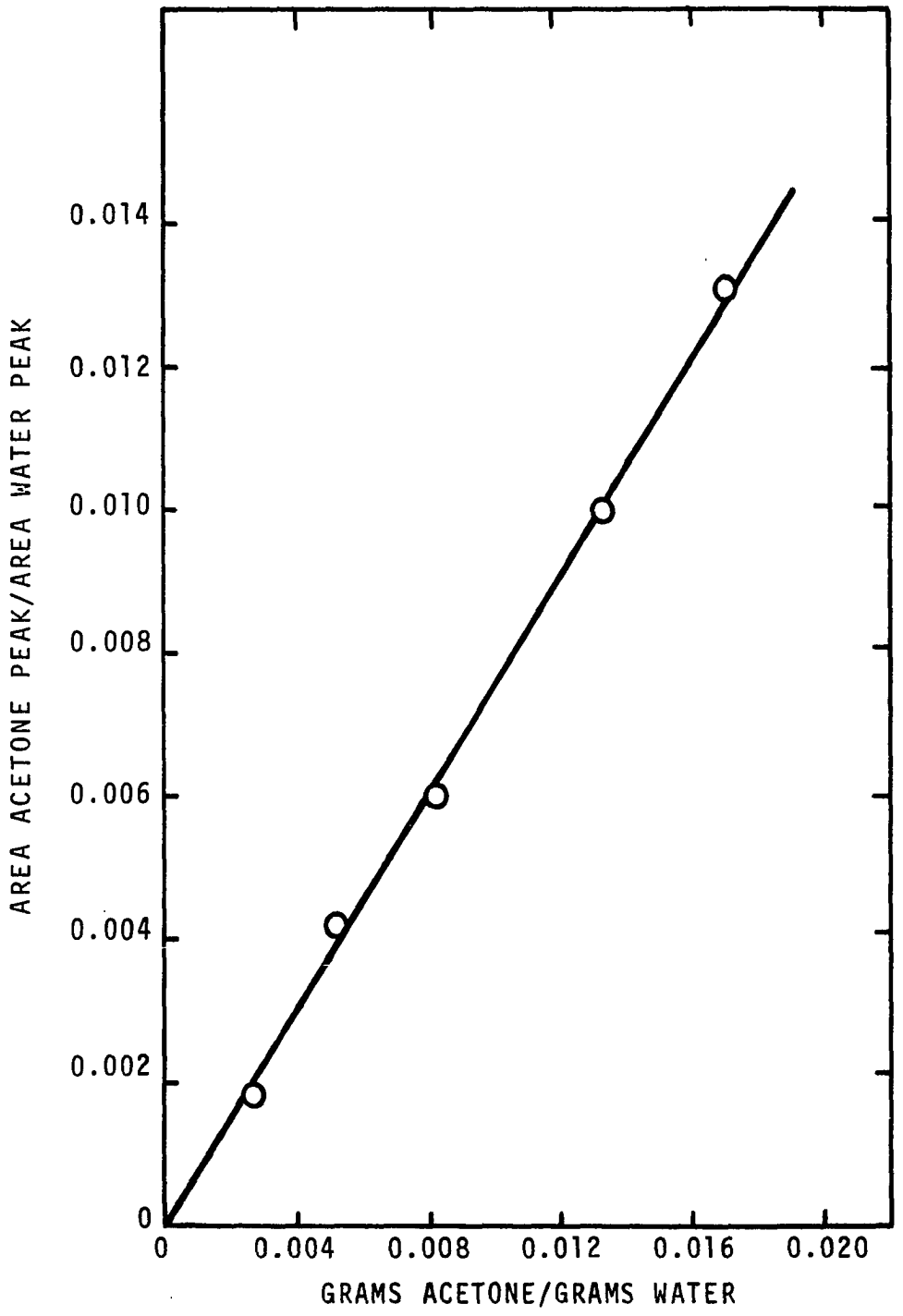

Figure 35. Chromatographic Calibration Curve for Acetone.

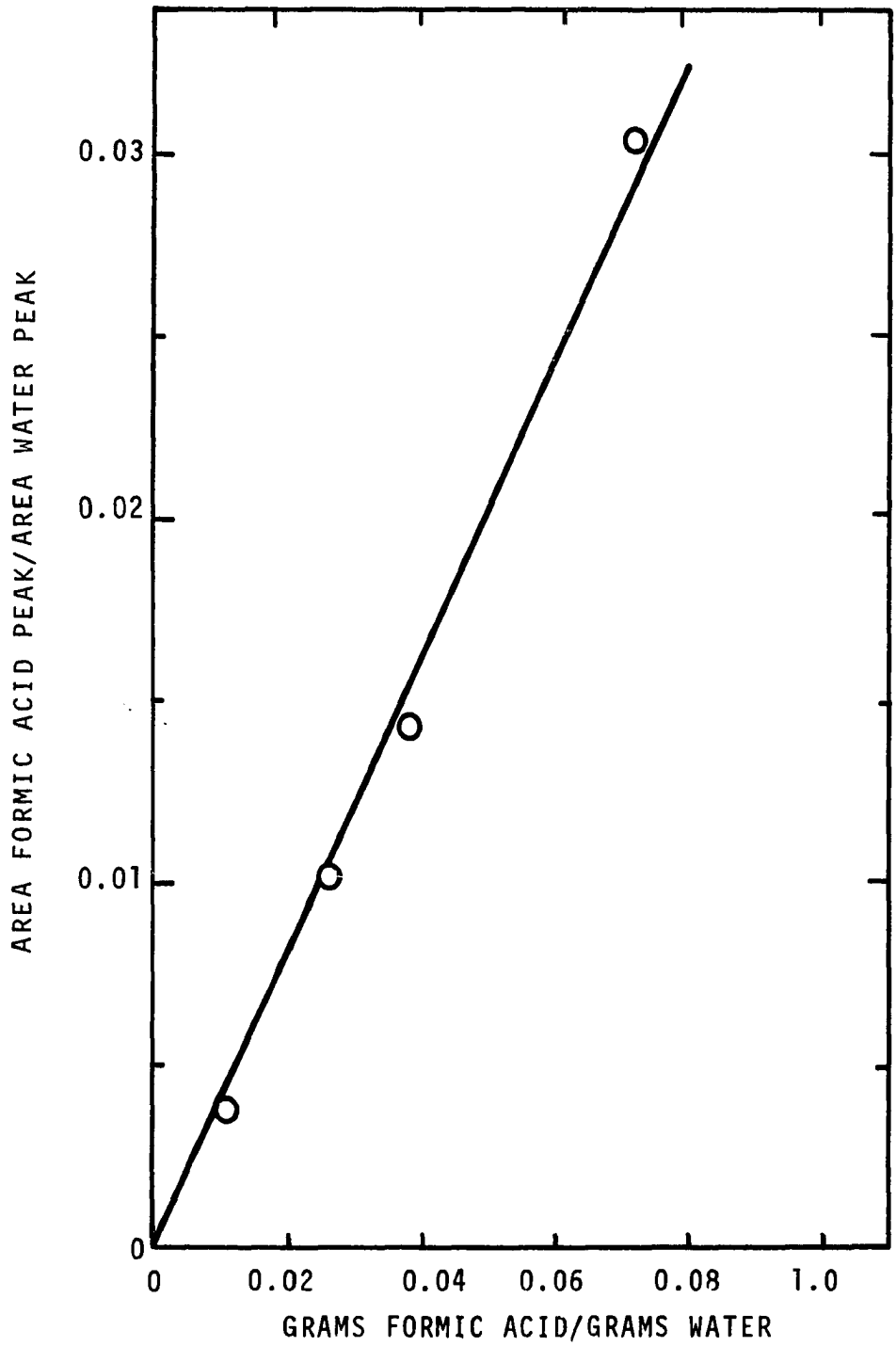

Figure 36. Chromatographic Calibration Curve for Formic Acid.

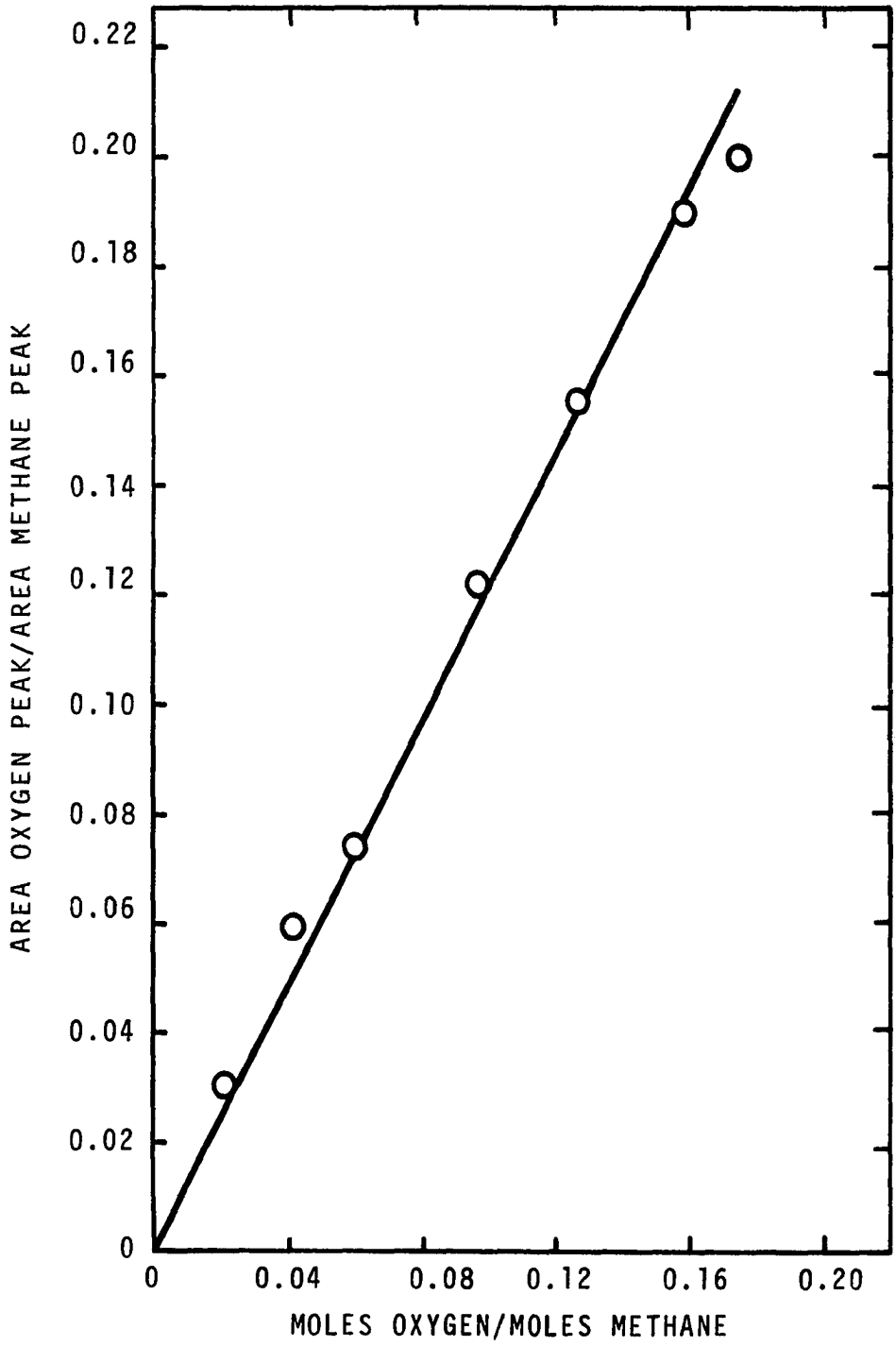

Figure 37. Chromatographic Calibration Curve for Oxygen.

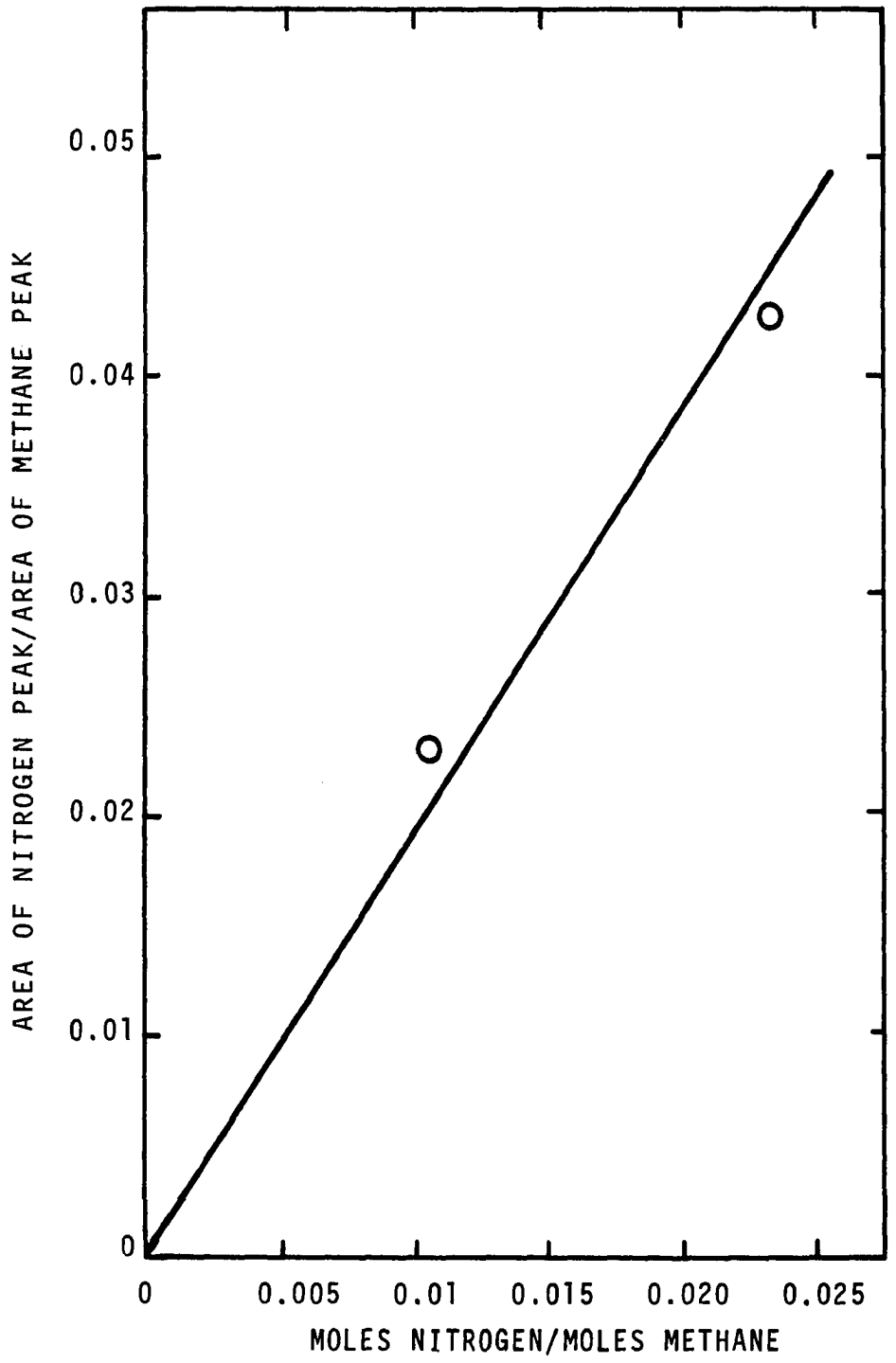

Figure 38. Chromatographic Calibration Curve for Nitrogen.

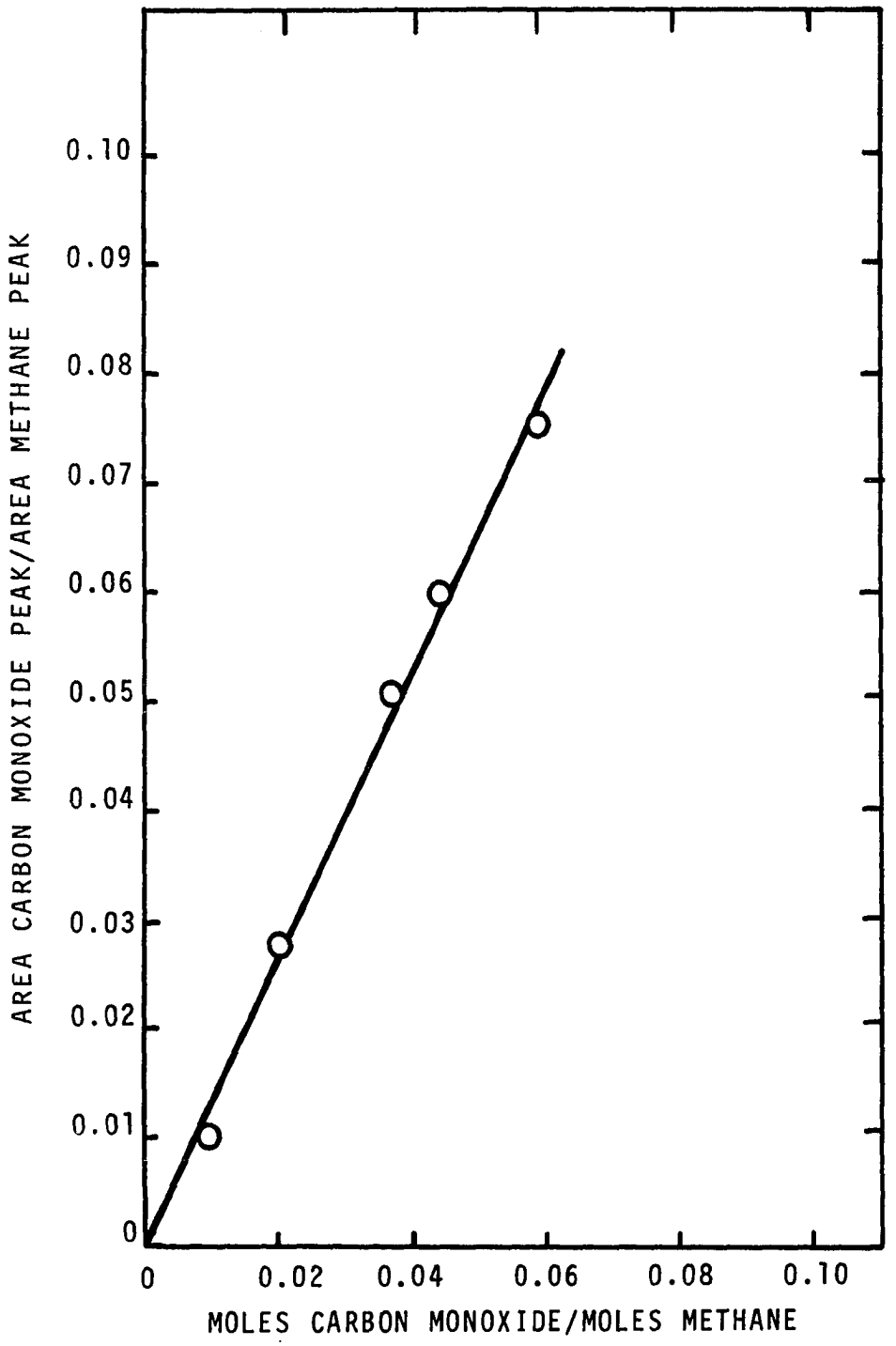

Figure 39. Chromatographic Calibration Curve for Carbon Monoxide.

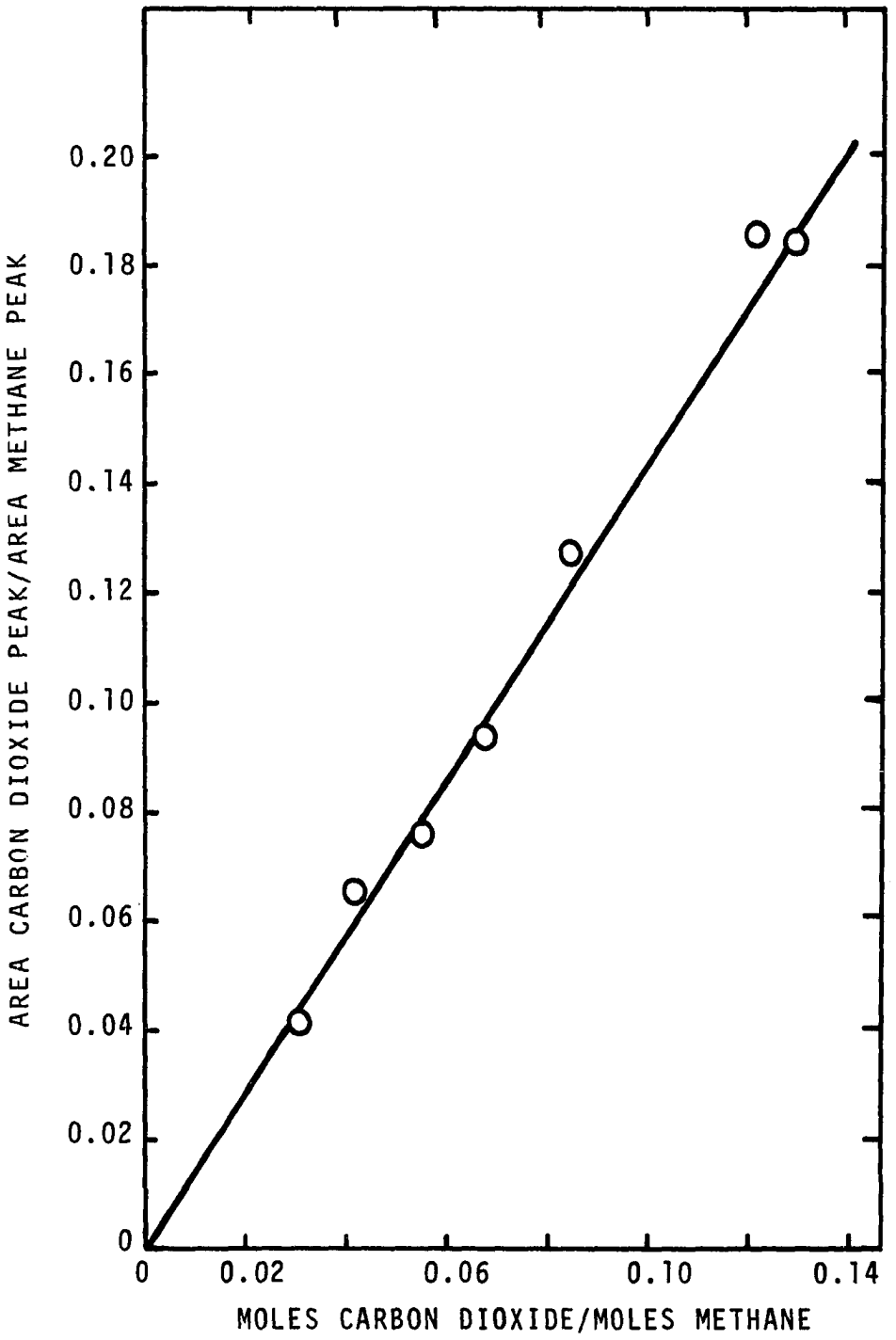

Figure 40. Chromatographic Calibration Curve for Carbon Dioxide.

APPENDIX C

EQUATIONS FOR COMPUTER ANALYSIS

On the following pages is an abbreviated computer listing showing the equations used in the computer analysis. These equations, developed in Chapter VIII, were used to calculate the radical concentrations and the differential changes in the molecular concentrations. Specific values for the rate constants for all reactions, the method for calculation of the initial concentrations for all chemical species, and the integration technique are discussed in Chapter VIII.

```
C
C      DERY TERMS ARE THE DERIVATIVES OF THE CONCENTRATION EQUATIONS
C         FOR THE FOLLOWING MOLECULES, RESPECTIVELY:
C
C       1     O2        OXYGEN
C       2     HCHO      FORMALDEHYDE
C       3     MEOOH     METHYL HYDROPEROXIDE
C       4     H2O2      HYDROGEN PEROXIDE
C       5     CO        CARBON MONOXIDE
C       6     CO2       CARBON DIOXIDE
C       7     CH3OH     METHANOL
C       8     HCOOH     FORMIC ACID
C       9     MF        METHYL FORMATE
C      10     C2H6      ETHANE
C      11     H2O       WATER
C      12     CH4       METHANE
C
C      THE FOLLOWING ARE THE RADICALS USED:
C
C             CH3       METHYL RADICAL
C             CH3O      METHOXY RADICAL
C             HCO       FORMYL RADICAL
C             CH3OO     METHYL PEROXY RADICAL
C             OH        HYDROXYL RADICAL
C             HO2       HYDROPEROXY RADICAL
C             COOH      FORMIC RADICAL
C
C
      IMPLICIT REAL*4(K,M)
      DIMENSION Y(12),DERY(12)
      W0   = K0*CH4*O2
      W4A  = K4A*HCHO*O2
      MEOOH=((K3*CH4+K3A*HCHO)*CH3OO+KM4*CH3O*OH)/(K4+KM3*CH3+KM3A*HCO)
```

```
      A = K9*CH4+K7*HCHO+K6*O2+KM9*H2O+KM9A*H2O2
      C = K2+K3*CH4+KM1+K3A*HCHO
      T = K4*MEOOH
      BA = T+2.*KM11B*CH3OH*HCHO+KM12B*MF+KM11A*HCHO**2+KM11D*H2O2*HCHO
      BB = W4A+KM11*H2O2*CO+KM12A*HCOOH+KM12B*MF+KM11A*HCHO**2
      BC = K5C*CH4+O2*(K6A+K6B)+KM7*CH3OH+KM7A*H2O+KM7B*H2O2
     1 + KM3A*MEOOH+KM7C*HCOOH
      BD = T+2.*K4B*H2O2+KM12*CH3OH+KM12A*HCOOH
      BE = K5A*CH4+HCHO*(K7A+KM2)+K10*H2O2+CO2*(KM6B+KM8)+K8A*CO
     1 + CH3OH*(KM10A+K9)
      BF = W0+W4A+H2O2*(2.*KM11C*O2+KM11*CO+KM11D*HCHO)
      BG = K5B*CH4+HCHO*(K7B+KM6)+CO*(K8+KM6A)+KM10*H2O+K9A*CH3OH
      BL = W0+KM12*CH3OH+2.*KM12C*C2H6
      BM = KM3*MEOOH+K1*O2+KM5*CH3OH+KM5A*H2O+H2O2*(KM5B+K10A)
     1 + KM5C*HCHO+KM5D*HCOOH
      DA = BL+CH4*(K3*CH3OO+K5*CH3O+K5A*OH+K5B*HO2+K5C*HCO+K5D*COOH)
     1 + KM1*CH3OO+KM10A*CH3OH*OH
      DB = BM+KM0*HO2+K12*OH+2.*K12C*CH3
      DC = BA+CH3OH*(KM5*CH3+KM7*HCO+K9*OH+K9A*HO2)+KM6*HO2*HCHO
      DD = A+HCO*(K11A+K12B)+KM4*OH+2.*K11B*CH3O+K11D*HO2
      DE = BB+HO2*(K7B*HCHO+KM6A*CO)+OH*(K7A*HCHO+KM6B*CO2)
     1 + HCHO*(K7*CH3O+KM5C*CH3+K3A*CH3OO+K7C*COOH)
      DF = BC+CH3O*(K11A+K12B)+HO2*(K11+KM4A)+K12A*OH
      DG = CH3*(K1*O2+KM3*MEOOH)+KM2*OH*HCHO+KM3A*MEOOH*HCO
      DH = BD+CH3*(KM5A*H2O+K10A*H2O2)+HCO*(K6B*O2+KM7A*H2O)+K2*CH3OO
     1 + HO2*(K8*CO+KM10*H2O)+KM8A*COOH+KM9*CH3O*H2O
      DI = BE+KM4*CH3O+2.*KM4B*OH+K12*CH3+K12A*HCO
      DJ = BF+CH3O*(K6*O2+KM9A*H2O2)+HCO*(K6A*O2+KM7B*H2O2)
     1 + OH*(K10*H2O2+KM8*CO2)+KM5B*CH3*H2O2
      DK = BG+2.*K11C*HO2+KM0*CH3+HCO*(KM4A+K11)+K11D*CH3O
      CH3   = DA/DB
      CH3O  = DC/DD
      HCO   = DE/DF
```

```
32          CH3OO = DG/C
33          OH    = DH/DI
34          HO2   = DJ/DK
35          COOH = (K8A*CO*OH+HCOOH*(KM5D*CH3+KM7C*HCO))/(KM8A+K5D*CH4
          1 + K7C*HCHO)
36          DERY(1) = HO2*(KM0*CH3+KM4A*HCO+KM6*HCHO+KM6A*CO+K11C*HO2)
          1 +KM1*CH3OO+KM6B*CO2*OH- (W0+W4A+O2*(K1*CH3+K3*CH3O+HCO*(K5A+K6B)
          2 +KM11C*H2O2))
37          DERY(2) = HCO*(KM3A*MEOOH+KM7*CH3OH+K5C*CH4+KM4A*HO2+KM7A*H2O
          1 + KM7B*H2O2+KM7C*HCOOH)+CH3O*(K6*O2+K11B*CH3O+2.*K11A*HCO
          2 +K11D*HO2)+K2*CH3OO - (W4A+HCHO*(OH*(KM2+K7A)+HO2*(KM6+K7B)
          3 + K7*CH3O+KM5C*CH3+KM11B*CH3OH+2.*KM11A*HCHO+K3A*CH3OO
          4 + K7C*COOH+KM11D*H2O2))
38          DERY(3) = 0.0
39          Y(3) = MEOOH
40          DERY(4) = OH*(KM4B*OH+KM10A*CH3OH)+HO2*(K5B*CH4+K7B*HCHO+K11*HCO
          1 +KM10*H2O+K11C*HO2+K9A*CH3OH+K11D*CH3O) - H2O2*(CH3*(KM5B+K10A)
          2 +KM7B*HCO+KM11*CO+K4B+K10*OH+KM11C*O2+KM9A*CH3O+KM11D*HCHO)
41          DERY(5) = HCO*(K6A*O2+K11*HO2)+KM8*CO2*OH+KM8A*COOH
          1 - CO*(KM11*H2O2+HO2*(K8+KM6A)+K8A*OH)
42          DERY(6) = K6B*HCO*O2+K8*CO*HO2 - CO2*(OH*(KM6B+KM6))
43          DERY(7) = CH3O*(K5*CH4+K7*HCHO+K11B*CH3O+KM9*H2O+KM9A*H2O2)
          1 +CH3*(K12*OH+K10A*H2O2) - CH3OH*(KM5*CH3+KM7*HCO+KM12+KM11B*HCHO
          2 +OH*(K9+KM10A)+K9A*HO2)
44          DERY(8) = K12A*HCO*OH+COOH*(K5D*CH4+K7C*HCHO) - HCOOH*(KM12A
          1 +KM5D*CH3+KM7C*HCO)
45          DERY(9) = K12B*HCO*CH3O - KM12B*MF
46          DERY(10) = K12C*CH3*CH3 - KM12C*C2H6
47          DERY(11) = OH*(K5A*CH4+K7A*HCHO+K10*H2O2+K9*CH3OH)
          1 - H2O*(KM5A*CH3+KM7A*HCO+KM10*HO2+KM9*CH3O)
48          DERY(12) = CH3*(KM0*HO2+KM3*MEOOH+KM5*CH3OH+KM5A*H2O+KM5B*H2O2
          1 +KM5C*HCHO+KM5D*HCOOH) - W0 - CH4*(K3*CH3OO+K3*CH3O+K5A*OH
          2 +K5B*HO2+K5C*HCO+K5D*COOH)
```

APPENDIX D

REACTOR DESIGN

Introduction

High pressure oxidation studies of methane at pressures up to 200,000 psi have been made at the University of Oklahoma since 1963. The high pressure reactor was designed by Lott (60) and was constructed by Autoclave Engineers of Erie, Pennsylvania, using Vascomax 250, an 18 percent nickel maraging steel made by the Vanadium-Alloys Steel Company of Latrobe, Pennsylvania. The duplex vessel was assembled by expanding the outer shell with heat, inserting the cooled inner shell, and allowing the vessel to come to thermal equilibrium. This procedure resulted in an interference fit between the two shells.

In 1966, Hardwicke (42) discovered a leak from the sideport connection at pressures above 100,000 psi. This author had the same problem. Helium detection by mass spectrometry showed that the reactor liner probably was not cracked. An examination of the tip of the high pressure double cone in the sideport, as shown in Figure 41, showed that the cone was not seating straight. It appeared that the

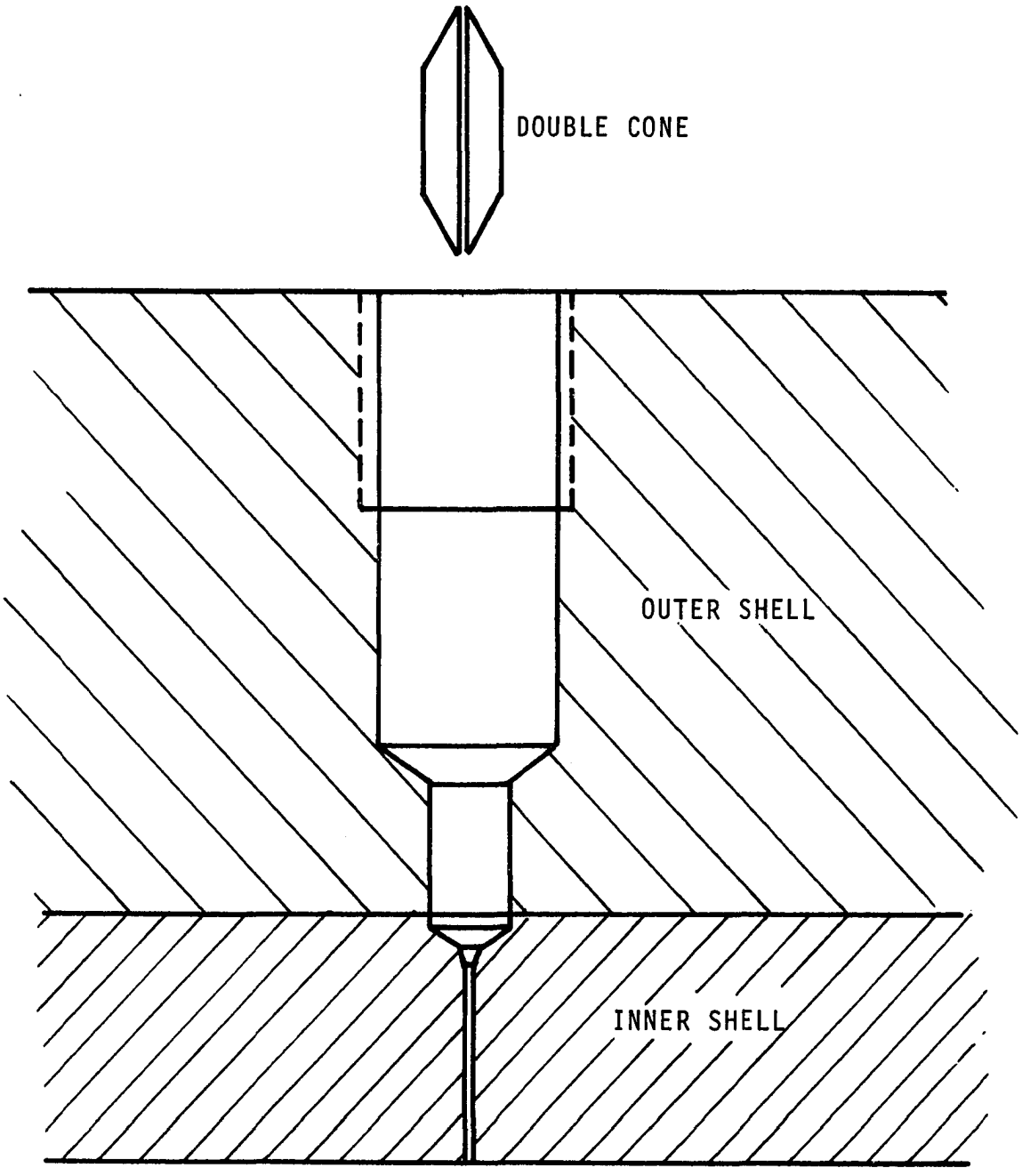

Figure 41. The Sideport Opening with Double Cone. (Reproduced by permission from Autoclave Engineers).

tapered inner liner of the reactor had slipped, despite the 0.027 inch diametral interference. The slippage was further evidenced by the fact that one of the reactor main nuts was frozen in position where the liner had pushed against it.

To eliminate the recurring problems with the sideport connection and for the sake of safety, it was decided to remove the vessel from service and to have it repaired. Based on the following analysis, this author has recommended that a new liner without a sideport entry be installed and that a new bottom plug which contains an inlet for the feed gases through an annulus surrounding the shielded thermocouple be fabricated. To date, these major revisions have not been completed because of funding limitations.

Reactor Design

It was decided that the finished cylinder should have the same dimensions as the original cylinder. The original end closures could then be used, with the only modification being a new bottom plug. Since the original design (60) was reported in British units, this analysis will be likewise.

The reactor, shown in Figure 42, is a duplex vessel with an outside diameter of 12 inches, inside diameter of 2 inches, and diameter of 5 inches at the interference junction. The outer shell, which is to be salvaged from the old reactor, was fabricated from Vascomax 250, an 18 percent nickel maraging steel, made by the Vanadium-Alloys Steel Company (now called

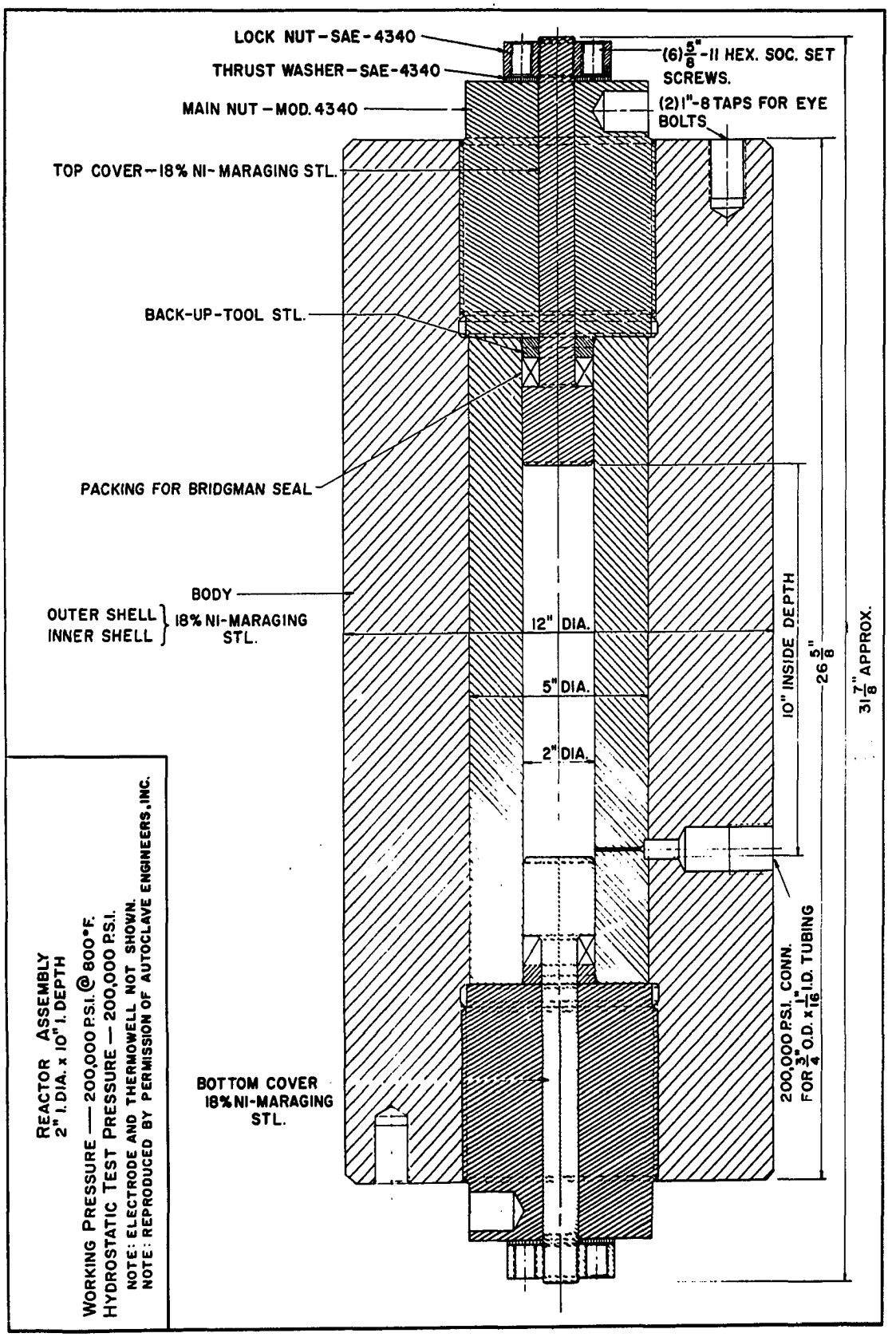

Figure 42. Details of 200,000 psi Reactor [from Lott (60) reproduced by permission].

Vasco, A Teledyne Company) of Latrobe, Pennsylvania. This shell originally had a 1-11/64 inch hole, reduced to 9/16 inch.

The material for the inner shell must have both high strength and corrosion resistance since at operating conditions the reactor may contain as much as 8 mole percent water vapor. Unfortunately, most steels that have good corrosion resistance have low yield strengths. As a compromise, Republic HP 9-4-30 steel, made by the Republic Steel Corporation of Cleveland, Ohio, was selected for use in these calculations. It has fair corrosion resistance and a reasonably high yield strength.

The physical properties of the materials for both the outer and inner shells are listed in Table 7.

The inner liner for the reactor must be thick enough to prevent the internal pressure from extruding part of the liner through the old sideport opening in the outer shell. A drawing of the sideport opening with the new inner liner in place is shown below in Figure 43. The required thickness of the inner liner, x, can be found as a function of internal pressure by balancing the force trying to extrude a plug of steel outward with the force holding it in place. The force exerted outward is

$$F = P_i A \qquad \text{(D-1)}$$

TABLE 7

PHYSICAL PROPERTIES OF CONSTRUCTION MATERIALS

(References 3, 75, 92)

		Vascomax 250	Republic HP 9-4-30
Ultimate Tensile Strength, psi	(RT)	261,000	237,000
	(400°F)	250,000	229,000
	(800°F)	225,000	180,000
0.2 % Yield Strength, psi	(RT)	251,000	214,000
	(400°F)	238,000	208,000
		211,000	178,000
Modulus of Elasticity,		6.5x10^{6}	28.6x10^{6}
Poisson's Ratio		.30	0.29
Hardness, Rockwell "C		53	45-47
Coefficient of Therma in/in/°F		:10^{-6}	*5.7x10^{-6}
Thermal Conductivity, b		180	160
Elongation, percent (RT)		12	14
Reduction of Area, percent (RT)		61	52

*For the temperature range -100° to 78°F.

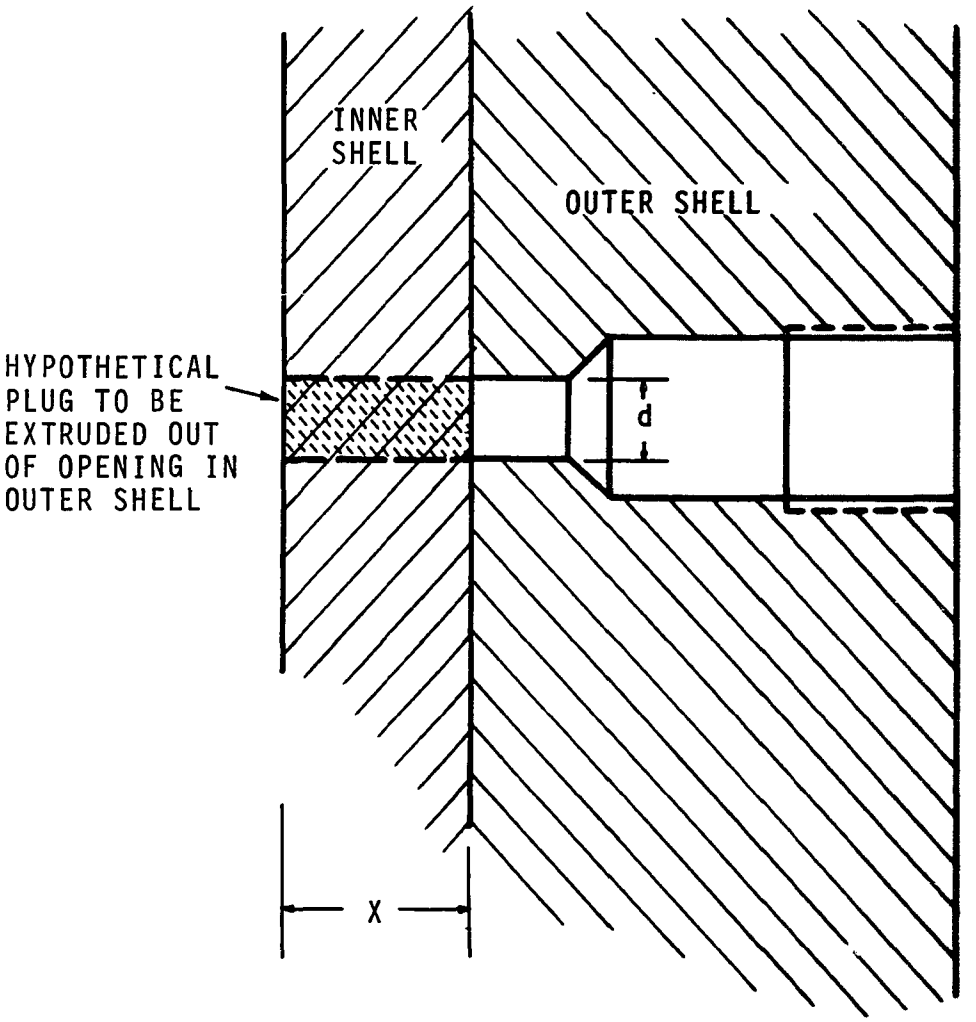

Figure 43. The Sideport Opening with the New Inner Liner.

TABLE 7

PHYSICAL PROPERTIES OF CONSTRUCTION MATERIALS

(References 3, 75, 92)

		Vascomax 250	Republic HP 9-4-30
Ultimate Tensile Strength, psi	(RT)	261,000	237,000
	(400°F)	250,000	229,000
	(800°F)	225,000	180,000
0.2 % Yield Strength, psi	(RT)	251,000	214,000
	(400°F)	238,000	208,000
	(800°F)	211,000	178,000
Modulus of Elasticity, psi		26.5×10^6	28.6×10^6
Poisson's Ratio		0.30	0.29
Hardness, Rockwell "C"		50-53	45-47
Coefficient of Thermal Expansion in/in/°F		5.6×10^{-6}	$*5.7 \times 10^{-6}$
Thermal Conductivity, Btu/hr-ft^2(°F/in)		180	160
Elongation, percent (RT)		12	14
Reduction of Area, percent (RT)		61	52

*For the temperature range -100° to 78°F.

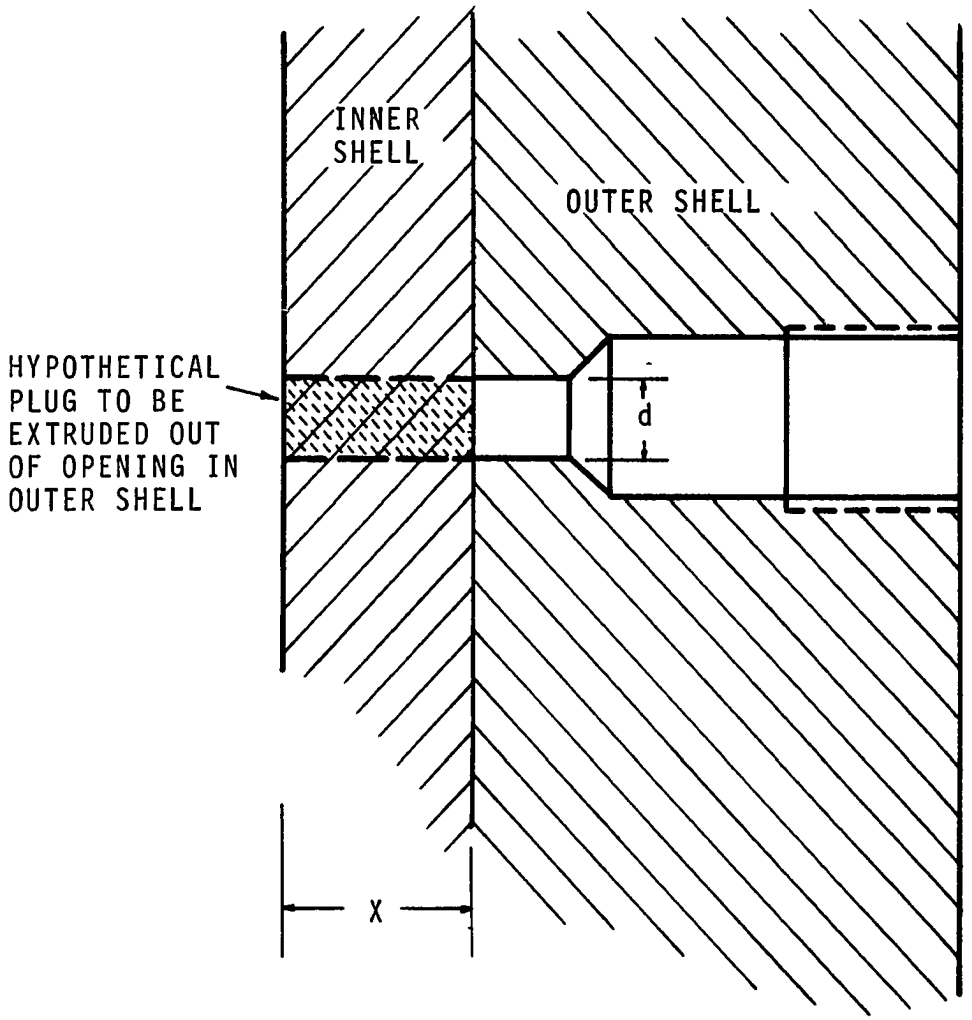

Figure 43. The Sideport Opening with the New Inner Liner.

where A is the end area of the plug being extruded outward and P_i is the internal pressure. The force holding the steel in place is

$$F = \gamma \sigma_y A' \qquad \text{(D-2)}$$

where A' is the lateral area of the plug, σ_y is the yield strength of the material, and γ is the fraction of the yield strength available in shear. Equating the forces in Equations D-1 and D-2 and substituting for the end and lateral areas, the minimum thickness of the shell is found to be

$$x = P_i d/4\gamma\sigma_y \qquad \text{(D-3)}$$

where d is the diameter of the opening in the outer shell at the interface. Using a value of $\gamma = 0.6$

$$x = \frac{(200{,}000)(0.563)}{(4)(0.6)(178{,}000)} = 0.264 \text{ inch}$$

Since an inner shell with a thickness of 1.5 inches is being considered, no extrusion of the inner shell is anticipated.

The Lame equations (56) can be used to calculate the radial, tangential, and axial stresses in a simple, thick-walled cylinder. For any point a distance, r, from the axis, the radial, tangential and axial stresses (σ_r, σ_t, σ_z) are

$$\sigma_r = \frac{P_i - P_o K^2 - (r_o/r)^2 (P_i - P_o)}{K^2 - 1} \qquad \text{(D-4)}$$

$$\sigma_t = \frac{P_i - P_o K^2 + (r_o/r)^2 (P_i - P_o)}{K^2 - 1} \qquad \text{(D-5)}$$

$$\sigma_z = \frac{P_i - P_o K^2}{K^2 - 1} \qquad \text{(D-6)}$$

where P_i, P_o are the internal and external pressures; r, r_i, r_o are a radius, internal radius, and external radius, respectively; and K is the diameter ratio of the cylinder ($2r_o/2r_i$). These equations apply as long as the material of construction remains in the elastic state.

Several theories have been presented to define the limit of elastic behavior for construction materials. According to Comings (23), the Distortion Energy Theory of Mise (65) fits high strength steel most accurately. The Mise theory states that the material has reached the limit of elastic action when the maximum shear stress reaches a point defined by

$$\tau_y = \frac{\sigma_y}{\sqrt{3}} \qquad \text{(D-7)}$$

where τ_y is the maximum shear stress. The shear stress at any point is equal to

$$\tau = 1/2\ (\sigma_t - \sigma_r) \qquad \text{(D-8)}$$

Manning (63) showed that for an optimum stress distribution in a compound cylinder with shells made of identical materials, each component shell should be geometrically similar; that is, having equal ratios of outer to inner diameters.

Pugh (78) found that Manning's results should be modified if different materials are considered for the various shells, so that

$$k_n = \left(\frac{\sigma_{yn}}{\sigma_{yn+1}}\right)^{1/2} k_{n+1} \qquad \text{(D-9)}$$

where k_n is the diameter ratio of component shell n.

It has been shown (63) that, neglecting thermal gradients in the vessel wall, the maximum allowable pressure drop for an elastic monoblock vessel is

$$\Delta P = P_i - P_o = \frac{\sigma_y (K^2-1)}{\sqrt{3}\ K^2} \qquad \text{(D-10)}$$

Similarly, the maximum allowable pressure drop across any completely elastic compound cylinder is

$$\Delta P = \frac{2\sigma_y}{\sqrt{3}} \frac{(K^2-1)}{K^2} \qquad \text{(D-11)}$$

The term pressure drop refers to the difference in pressure across either a component shell of a completed cylinder or a complete cylinder.

In the present application the maximum pressure drop for elastic action in a monoblock cylinder of the same size as the original vessel and made from HP 9-4-30 steel is found from Equation D-10 to be

$$\Delta P = \frac{178{,}000\ (6^2-1)}{\sqrt{3}\ (6^2)} = 100{,}000 \text{ psi}$$

while the corresponding pressure drop allowed in any compound cylinder of the same size made entirely from HP 9-4-30 is 200,000 psi.

Equation D-10 can be used for the individual shells of the completed vessel. The maximum allowable pressure drop across the inner liner is

$$\Delta P_1 = \frac{178{,}000\ (2.5^2 - 1)}{\sqrt{3}\ (2.5)^2} = 86{,}400 \text{ psi}$$

Correspondingly the maximum pressure drop that can be carried by the Vascomax 250 outer shell is

$$\Delta P_2 = \frac{211{,}000\ (2.4^2 - 1)}{\sqrt{3}\ (2.4)^2} = 100{,}700 \text{ psi}$$

Then, still neglecting thermal gradients, the maximum pressure drop possible across the completed compound vessel and still have elastic behavior is

$$\Delta P_T = 86{,}400 + 100{,}700 = 187{,}100 \text{ psi}$$

Therefore, if the external pressure is considered negligible, the internal pressure is limited to 187,100 psi unless plastic deformation is allowed.

The overstrain pressure, P_{os}, or the pressure at which a vessel is completely plastic and ready to burst, was found by Manning (63) to be

$$P_{os} = \frac{2}{\sqrt{3}} \sigma_y \ln (K) \qquad \text{(D-12)}$$

In this application, considering a cylinder built entirely of HP 9-4-30, the overstrain pressure is

$$P_{os} = \frac{2}{\sqrt{3}} (178{,}000) \ln (6) = 400{,}100 \text{ psi}$$

At pressures above the maximum elastic operating pressure and below the overstrain pressure, the vessel wall is in a plastic state.

Whalley (97) has shown the effect of temperature gradients in a vessel wall. The allowable elastic pressure drop across a compound cylinder made of "m" geometrically similar shells was found to be

$$P = \frac{m(k^2-1)}{k^2} \left[\frac{\sigma_y}{\sqrt{3}} + \frac{1}{2} \beta \left\{\frac{k^2}{m(k^2-1)} - \frac{1}{2(m) \ln(k)}\right\}\right] \qquad \text{(D-13)}$$

with $$\beta = \alpha E \Delta T/(1 - \nu) \qquad \text{(D-14)}$$

and $$\Delta T = T_i - T_o \qquad \text{(D-15)}$$

where α is the coefficient of thermal expansion, E is the modulus of elasticity, T_i and T_o are the internal and external temperatures, ν is Poisson's ratio, and β is the thermal stress term.

At this point, knowledge of the temperature distribution through the wall is necessary. A rigorous description of the wall temperature distribution is difficult due to the many variables involved. However, it is possible to bracket the inside wall temperature by making several simplifying assumptions.

Since the temperature distribution is needed only in the stressed center section of the vessel, end effects are neglected. Then, assuming that thermal radiation from the internal heater can be neglected, it can be found that the inner wall temperature must be bracketed by the measured gas temperature as an upper limit and by a lower limit set by pure conduction through a stagnant gas layer. It was calculated that this lower limit is less than 1°F below the upper limit, meaning that the inside wall temperature approximately equals the measured gas temperature.

Once the inside wall temperature is known, the steady state temperature at any point in the wall can be found from the logarithmic temperature distribution in the cylinder, assuming that the slight geometrical discontinuity of the sideport opening can be ignored. Assuming an inside wall temperature of 600°F and an outside wall temperature of 460°F as reasonable values during an experimental run, the temperature at the shell interface can be found to be 528°F.

The possibility exists that the inner wall will be hotter than the measured gas temperature due to radiation effects from the internal heater. However, as shown in Equation D-14, a hotter inner surface will increase the thermal stress term, which decreases the required pressure stress term for a given pressure level. Since this vessel must be designed for the worst possible case, increasing the inner wall

temperature, to a point, will only reduce the wall stress and may thus be ignored.

Using the calculated value of 528°F for the interface temperature, the β term for each component shell can be calculated from Equation D-14 to be

$$\beta_1 = \frac{(5.7 \times 10^{-6})(28.6 \times 10^{6})(600 - 528)}{(1 - 0.29)} = 16{,}600 \text{ psi}$$

$$\beta_2 = \frac{(5.6 \times 10^{-6})(26.5 \times 10^{6})(528 - 460)}{(1 - 0.3)} = 14{,}400 \text{ psi}$$

The total thermal stress term is

$$\beta = 16{,}600 + 14{,}400 = 31{,}000 \text{ psi}$$

Then from Equation D-13 the maximum pressure drop allowed for an elastic wall, considering both thermal gradients at normal operating conditions and dissimilar materials in the shells,

$$P_{max} = \frac{(2.5)^2-1}{(2.5)^2}\left[\frac{178{,}000}{\sqrt{3}} + \frac{1}{2}(16{,}600)\frac{2.5^2}{2(2.5^2-1)} - \frac{1}{2(2)\ln(2.5)}\right]$$

$$+ \frac{(2.4)^2-1}{(2.4)^2}\left[\frac{211{,}000}{\sqrt{3}} + \frac{1}{2}(14{,}400)\frac{2.4^2}{2(2.4^2-1)} - \frac{1}{2(2)\ln(2.4)}\right]$$

$$= 191{,}500 \text{ psi}$$

Manning (63) found that the optimum amount of shrink fit interference for a compound cylinder of "m" geometrically similar shells can be expressed as

$$\delta = \frac{2\Delta P}{mE} \qquad \text{(D-16)}$$

where δ is the radial interference, expressed in inches of shrinkage per inch of diameter. Whalley and Morris (98) derived a similar equation that considered thermal stresses

$$\delta = 2(\Delta P - \tfrac{1}{2}\beta)/mE \qquad \text{(D-17)}$$

Equation D-17 can be used to obtain an estimate of the minimum shrinkage required in the present application.

$$\delta = \frac{2[200{,}000 - \frac{1}{2}(31{,}000)]}{2(26.5 \times 10^{6})} = 6.97 \times 10^{-3} \text{ inch/inch}$$

At a 2.5 inch radius, the interference is 0.0174 inch or 0.0348 inch diametral interference. To obtain this much shrinkage, the temperature rise necessary in the outer shell is approximately

$$\Delta T_s = \frac{0.0174}{2.5\ (5.6 \times 10^{-6})} = 1240°F$$

Since the maraging steel has a specified aging temperature of 900°F, which cannot be exceeded, this calculated temperature difference is not acceptable.

The physical configuration of the equipment is such that at elevated temperatures and pressures, it is impossible for negative temperature gradients (outer wall at higher temperature than inner wall) to exist in the vessel wall. Therefore, the worst possible operating conditions for the vessel occur when the vessel is under maximum pressure and constant wall temperature. Thus, the rest of the design will neglect thermal stresses.

The maximum amount of shrinkage that is possible without destroying the mechanical properties of the materials is obtained by cooling the inner shell to about -100°F and heating the outer shell to 900°F. This maximum diametral interference is then

$$(\delta xd) = 5(5.6x10^{-6})(900-70) + 5(5.7x10^{-6})(70-[-100])$$
$$= 0.0281 \text{ inch}$$

The calculated 0.0281 inch interference can be accomplished only if heat shrinking is accompanied by tapering the interface. If the interface is not tapered, a clearance of about 0.010 inch is needed for assembly, resulting in a maximum interference of about 0.018 inch. The following calculations are based on a diametral interference of 0.027 inch, slightly less than the maximum with a tapered interface.

A general equation has been derived by this author describing the relationship between the shrink fit interference and the residual contact pressure between shells of different materials in a completed compound cylinder. This equation states that

$$\delta = \frac{k_{n+1}^2 P'_n (1+\nu_{n+1}) + P'_n (1-\nu_{n+1}) - 2k_{n+1}^2 P'_{n+1}}{E_{n+1} (k_{n+1}^2 - 1)}$$
$$- \frac{2P'_{n-1} - k_n^2 P'_n (1-\nu_n) - P'_n (1+\nu_n)}{E_n (k_n^2 - 1)} \qquad \text{(D-18)}$$

where P'_n is the residual contact pressure remaining between shells n and n+1 when the vessel is unloaded. Equation D-18 can be solved to find the residual contact pressure caused by a known shell interference. In this application

$$P'_n = \frac{0.027\ (28.6 \times 10^6)(26.5 \times 10^6)(2.5^2 - 1)(2.4^2 - 1)}{(5.0)\left[\begin{array}{l}[2.4^2(1+0.29)+(1-0.29)](26.5 \times 10^6)(2.5^2-1) \\ +\ [2.5^2(1-0.3)+1+0.3](28.6 \times 10^6)(2.4^2-1)\end{array}\right]}$$

$$= 53{,}700 \text{ psi}$$

Manning (63) showed that the contact pressure can be found from

$$P_n = P'_n - \sigma_{rn} \qquad \text{(D-19)}$$

where P_n is the contact pressure under loaded conditions on the outside of shell n at radius b_n, and σ_{rn} is the radial stress at radius b, calculated from Equation D-4, in a monoblock vessel the same size and under the same loaded conditions as the compound cylinder. The contact pressure is then calculated from Equation D-19 to be

$$P_n = 53{,}700 - \frac{200{,}000}{(6^2 - 1)}\left(1 - \left[\frac{6}{2.5}\right]^2\right) = 80{,}900 \text{ psi}$$

The contact pressure between the shells may also be calculated from Manning's equation (63)

$$P_n = P_i - n\Delta P/m \qquad \text{(D-20)}$$

However, this equation assumes constant material properties in the shells and assumes that the optimum shrink fit interference between the shells is used. The ideal contact pressure at the interface in this application can be calculated from Equation D-20 to be

$$P_n = 200{,}000 - 1(200{,}000)/2 = 100{,}000 \text{ psi}$$

and compared to the value of 80,900 psi found using different materials and a non-optimum shrink fit interference.

From earlier calculations it is evident that even with an optimum shrink fit interference, the vessel will not remain entirely elastic at design pressure without the assistance of thermal stresses. The amount of inelastic strain produced by the internal pressure can be calculated (87) from

$$\Delta P = \frac{\sigma_y}{\sqrt{3}} \left[\frac{r_o^2 - r_e^2}{r_o^2} + 2 \ln (r_e/r_i)\right] \qquad \text{(D-21)}$$

where r_e is the radius of inelastic strain. Then from Equation D-21 the radius of inelastic strain is calculated to be

$$r_e \approx 1.227 \text{ inch}$$

The depth of inelastic strain is 0.227 inch into the 1.5 inch thick inner liner. This amount of plastic deformation may be produced prior to actual usage by the process of autofrettage, which will leave a residual compressive stress at the center of the vessel.

The shear stress, the equivalent monoblock shear stress, and the residual shear stress distributions have been calculated at different points as shown in Table 8 and plotted in Figure 44. Figure 45 shows the same data plotted as a fraction of the maximum shear stress. The calculations are based on walls with no thermal gradients. Higher stresses at elevated pressures could only be caused by negative thermal gradients, i.e., with the outer surface hotter than the inner, and with the inner surface at 800°F. This type of temperature distribution cannot be produced with the heating arrangement now available.

The tangential stress distribution in the cylinder has been calculated from Equation D-5 and plotted in Figure 46, with Figure 47 showing the same data plotted as a fraction of the yield strength. The calculations were made considering the worst case of operation, that of 200,000 psi internal pressure and a constant temperature of 800°F in the wall.

Conclusions and Recommendations

The reactor can be fabricated from a Republic HP 9-4-30 inner liner and a Vascomax 250 outer shell. Autofrettage will be necessary if the vessel is to be operated at 800°F and 200,000 psi.

The Vascomax 250 shell is part of the original reactor. This reactor should be bored to an inner diameter of $5.15^{+0.05}_{-0.03}$ inches and stress relieved. The inner surface should then be

TABLE 8

SUMMARY OF DATA FOR FIGURES 44 AND 45*

r/r_i	$\tau \times 10^{-3}$ psi	$\tau_e \times 10^{-3}$ psi	$\tau_{Rn} \times 10^{-3}$ psi
Inner Cylinder			
1.00	103.00	205.70	-102.70
1.23	103.00	146.40	- 43.40
1.25	91.80	131.80	- 40.00
1.50	63.80	91.30	- 27.50
2.00	35.90	51.40	- 15.50
2.50	23.00	32.90	- 9.90
Outer Cylinder			
2.50	96.10	32.90	62.20
3.00	66.80	22.80	44.00
4.00	37.50	12.90	24.60
5.00	24.00	8.23	15.73
6.00	16.70	5.72	10.98

*τ shear stress in cylinder under load

τ_e shear stress in an equivalent monoblock cylinder

τ_{Rn} residual shear stress

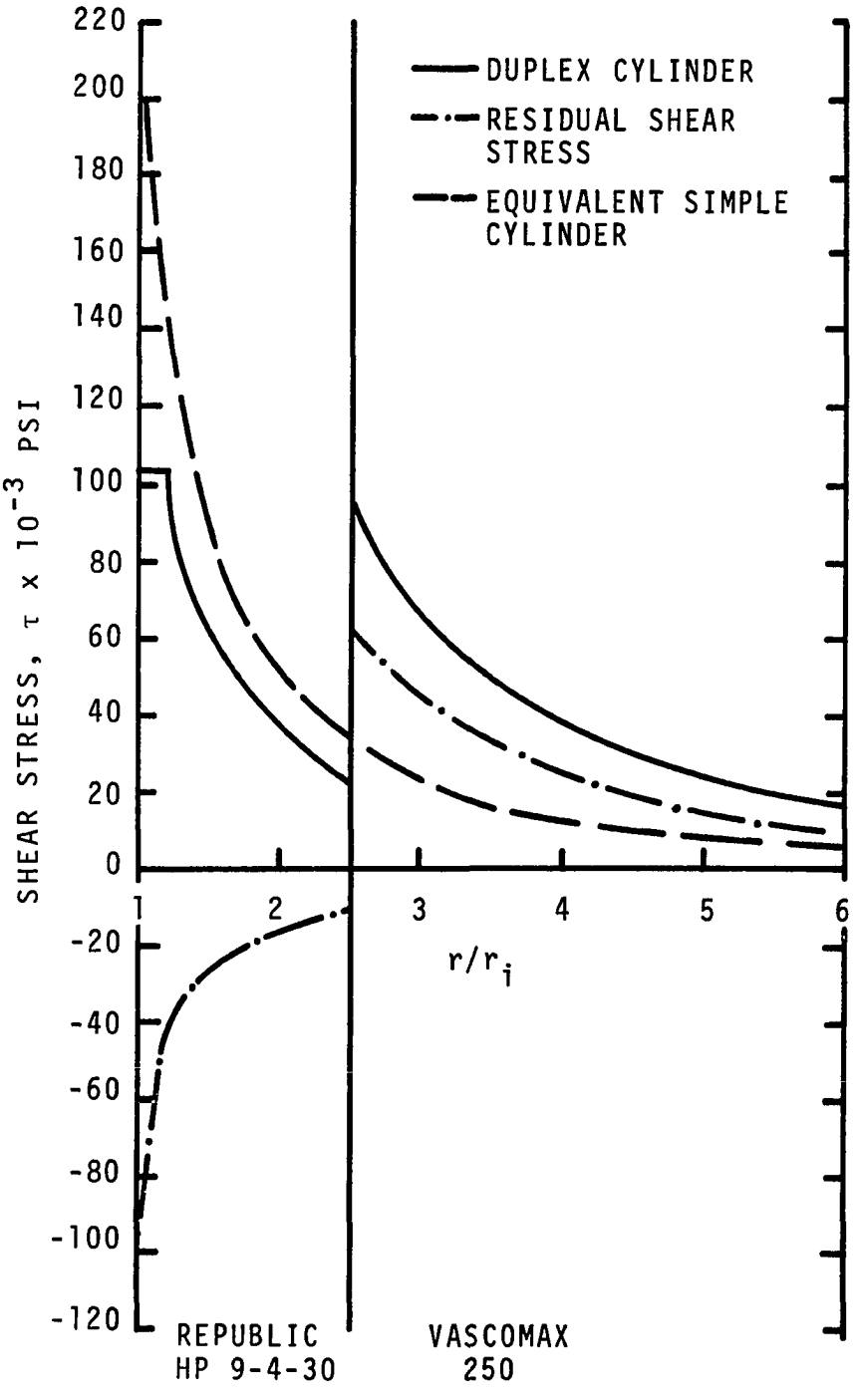

Figure 44. The Shear Stress Distribution in the Completed Vessel.

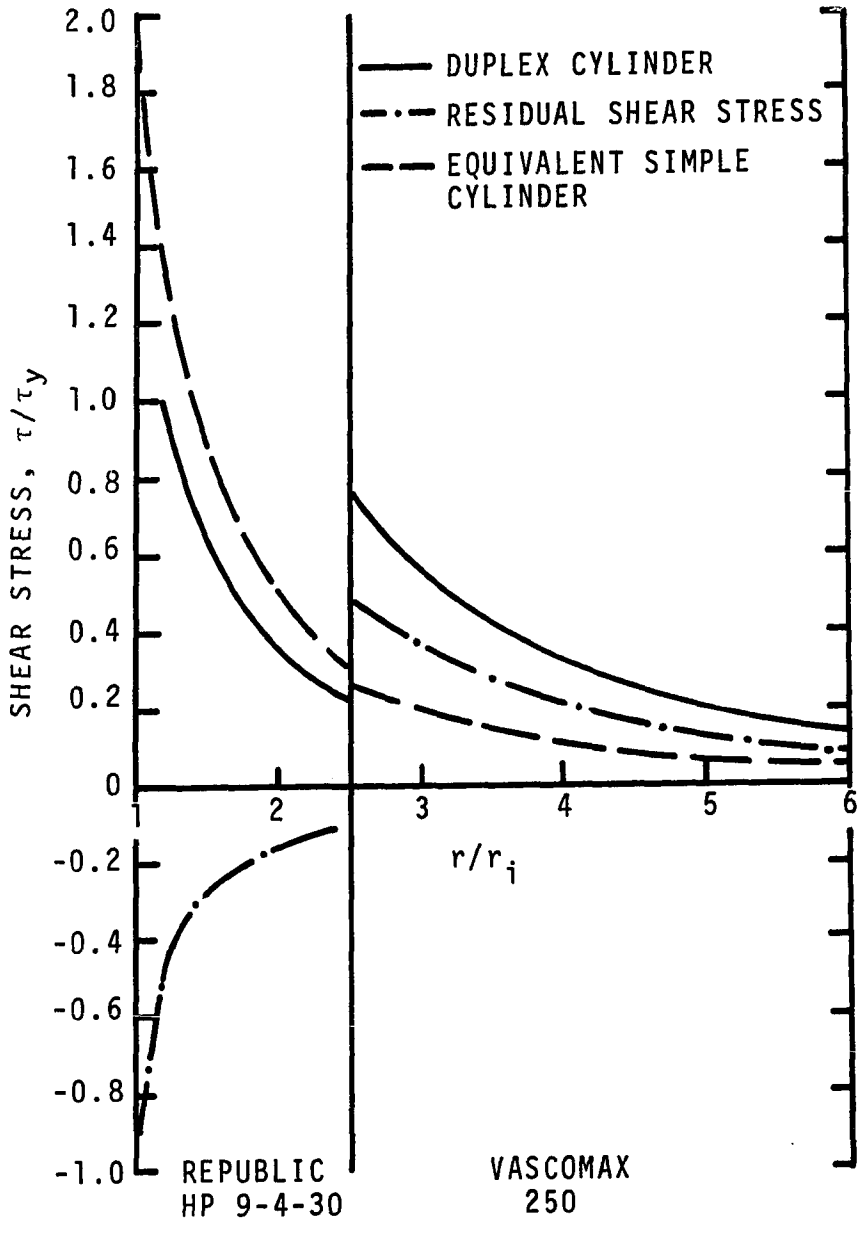

Figure 45. The Reduced Shear Stress Distribution in the Completed Vessel.

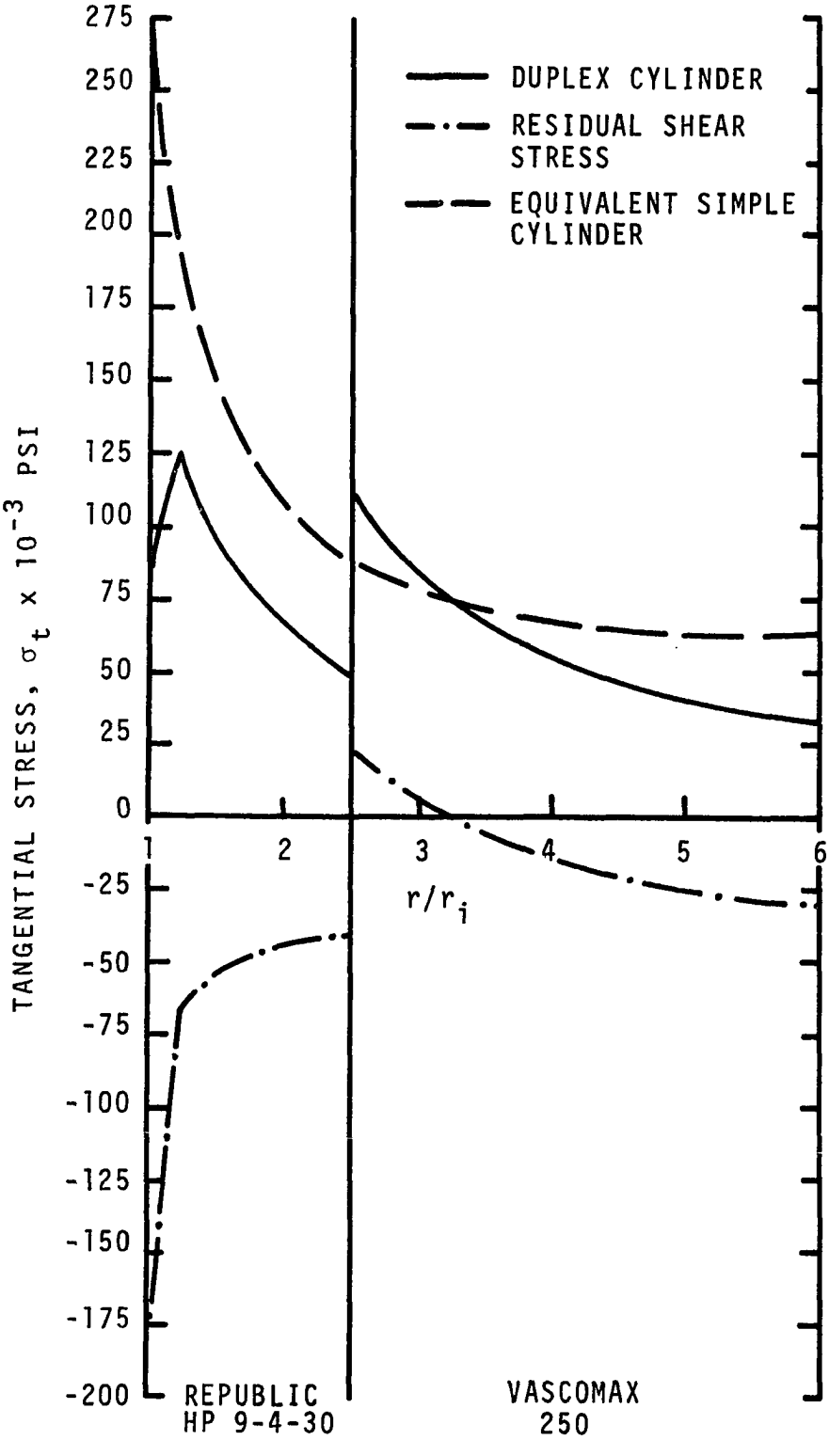

Figure 46. The Tangential Stress Distribution in the Completed Vessel.

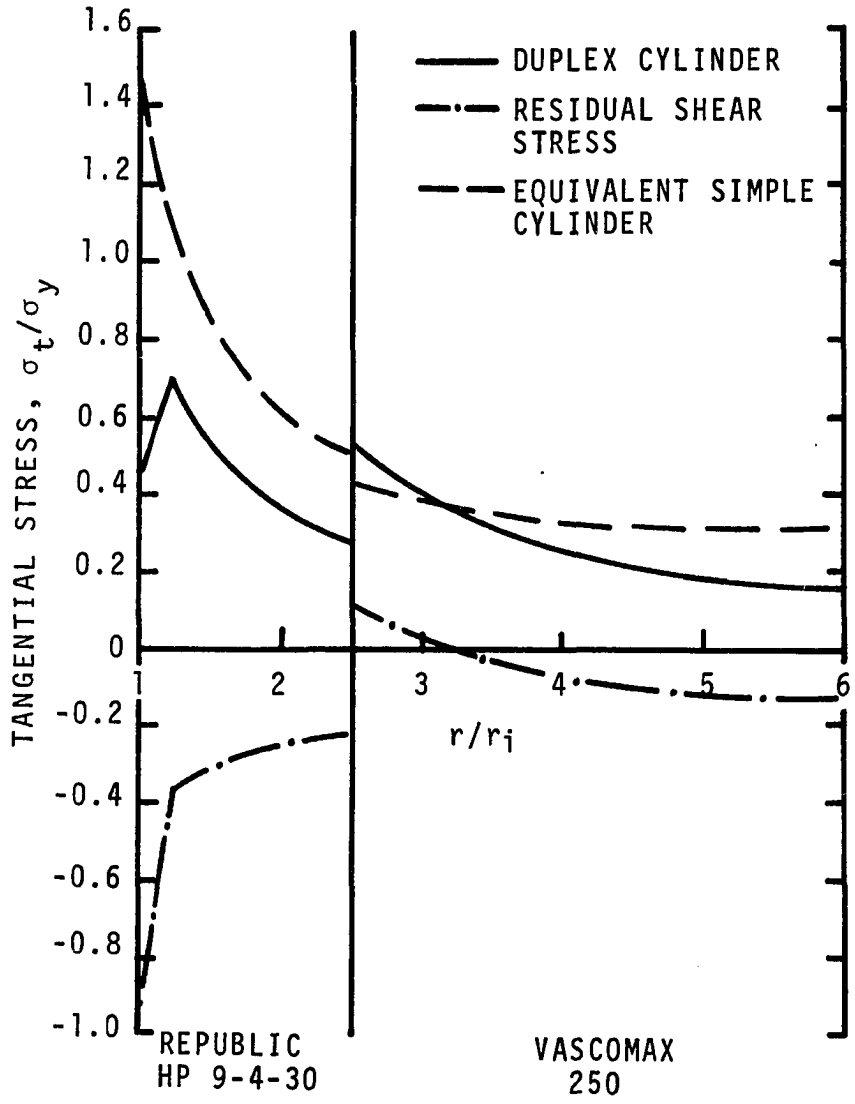

Figure 47. The Reduced Tangential Stress Distribution in the Completed Vessel.

tapered 1/8 inch per foot. The Republic HP 9-4-30 inner shell should be bored to an inner diameter of $1.98\ ^{+0.01}_{-0.00}$ inches. The inner shell's outer surface should be tapered 1/8 inch per foot and ground so that the diameter of the larger end is $0.027\ ^{+0.000}_{-0.002}$ inch greater than the diameter of the larger opening of the outer shell.

The outer shell should be heated to a uniform temperature of 900°F while the inner shell is to be cooled in liquid nitrogen to a temperature of -100°F or colder. The inner cylinder is then to be dropped into the outer cylinder with a positive stop. After the assembled reactor has cooled, the inner bore should be honed to a diameter of $2.00\ ^{+0.002}_{-0.000}$ inches.

The sideport opening in the outer shell should be plugged to protect the inner liner from being scarred or damaged. The plug should also be machined flush with the outside contour of the reactor.

APPENDIX E

SUMMARY OF EXPERIMENTAL DATA

TABLE 9

EXPERIMENTAL PARAMETERS*

Run	Pressure atm-abs	Temperature °C	Residence Time Minutes	Liquid Formed-grams	Methane Conversion Percent	Oxygen Conversion Percent	Material Balance gm/gm
3***	6463	230	0	0.9497	0.27	5.55	1.008
4	7048	270	15	1.2551	0.76	12.71	1.007
5	7007	282	15	6.1902	0.65	23.44	1.005
9	1918	300	30	1.6128	0.93	14.10	1.000
10	2177	290	30	0.4831	0.37	5.38	1.001
11**	1823	310	30	5.3558	5.07	50.78	0.993
14	3401	270	30	1.5129	1.02	16.99	1.007
15***	1823	270	30	0.4858	0.92	11.74	1.006
17**	1687	305	30	4.2462	2.06	24.72	1.007
18	1810	280	30	0.6507	0.78	11.56	1.006
19	1810	290	15	0.2441	0.35	3.70	1.004
20	1850	290	60	0.5141	0.50	5.53	1.006
21	1687	290	0	0.1530	0.50	5.07	1.002

*Runs 9 through 21 were taken in conjunction with Dr. N. Tripathy.

**Non-isothermal runs.

***Below zone of reaction.

TABLE 10

TOTAL OUTLET COMPOSITION, MOLE PERCENT

Run	CH_4	O_2	N_2	CO	C_2H_6	CO_2	H_2O	CH_3OH	HCHO	FA*	Acet*	EtOH*
3***	91.84	6.85	0.57	0.02	0.11	0.19	0.40	0.01	0.01	--	--	--
4	91.16	6.88	0.65	--	0.10	0.69	0.50	0.02	trace	--	--	--
5	91.16	5.08	0.60	--	0.12	0.38	2.49	0.17	trace	--	--	--
9	88.31	7.48	2.24	0.42	--	0.40	1.11	0.04	trace	--	trace	trace
10	89.44	8.23	1.58	--	0.14	0.30	0.31	--	--	--	--	--
11**	85.40	4.67	0.45	1.25	3.18	2.05	1.75	1.20	--	--	trace	0.05
14	92.37	5.57	0.40	0.07	--	0.83	0.74	0.01	trace	0.01	--	--
15***	92.36	5.97	0.43	0.12	0.15	0.65	0.31	0.01	trace	--	trace	--
17**	90.00	6.25	0.42	0.01	0.26	0.63	1.49	0.89	0.01	--	trace	0.03
18	89.94	6.43	2.38	0.15	0.09	0.57	0.44	trace	--	--	--	--
19	92.08	6.90	0.43	0.17	0.14	0.10	0.18	--	trace	--	--	--
20	93.67	4.96	0.49	0.32	0.11	0.09	0.35	0.01	trace	--	trace	--
21	92.46	6.52	0.37	0.08	0.19	0.28	0.10	trace	trace	--	trace	--

*FA = formic acid; Acet = acetone; EtOH = ethanol.

**Non-isothermal runs.

***Below zone of reaction.

TABLE 11

YIELD AS PERCENT OF REACTED METHANE

Run	Methane Conversion Percent	CH_3OH	HCHO	FA*	Acetone	EtOH*	CO	CO_2
3***	0.266	4.24	0.21	--	--	--	10.53	85.02
4	0.755	2.15	0.13	--	--	--	--	97.72
5	0.649	30.20	0.61	--	--	--	--	69.19
9	0.932	4.42	0.29	--	0.18	0.15	49.24	45.72
10	0.369	--	--	--	--	--	--	100.00
11**	5.072	25.33	--	--	trace	2.03	27.60	45.04
14	1.020	1.36	0.04	1.10	--	--	7.48	90.02
15***	0.921	0.78	0.03	--	0.38	--	15.51	83.30
17**	2.058	55.00	0.30	--	1.45	3.65	0.83	38.77
18	0.778	0.58	--	--	--	--	21.16	78.26
19	0.346	--	0.09	--	--	--	62.02	37.89
20	0.500	2.75	0.15	--	0.09	--	74.89	22.12
21	0.502	0.47	0.08	--	trace	--	23.00	76.45

*FA = formic acid; EtOH = ethanol

**Non-isothermal runs.

***Below zone of reaction.